

Technische Universität Dresden

Fakultät Umweltwissenschaften

Pollution-induced community tolerance in freshwater biofilms – from molecular mechanisms to loss of community functions

Dissertation zur Erlangung des akademischen Grades

Doctor rerum naturalium (Dr. rer. nat.)

Vorgelegt von: Stefan Lips

Geburtsdatum: 20.08.1988

Geburtsort: Brandenburg an der Havel

Gutachter Prof. Dr. Markus Weitere, Technische Universität Dresden

Gutachter Prof. Dr. Sergi Cortes Sabater, Universitat de Girona

Gutachter Dr. Ahmed Tlili, Eawag Switzerland

Übereinstimmungserklärung:

Die Übereinstimmung dieses Exemplars mit dem Original der Dissertation zum
Thema:

**Pollution-induced community tolerance in freshwater biofilms – from
molecular mechanisms to loss of community functions**

wird hiermit bestätigt.

Leipzig, 26.01.2023

Ort, Datum

Stefan Lips

Unterschrift (Vorname Name)

Abstract

Introduction: Exposure to herbicides poses a threat to aquatic biofilms by affecting their community structure, physiology and function. These changes render biofilms to become more tolerant, but on the downside community tolerance has ecologic costs. A concept that addresses induced community tolerance to a pollutant (PICT) was introduced by Blanck and Wängberg (1988). The basic principle of the concept is that microbial communities undergo pollution-induced succession when exposed to a pollutant over a long period of time, which changes communities structurally and functionally and enhancing tolerance to the pollutant exposure. However, the mechanisms of tolerance and the ecologic consequences were hardly studied up to date. This thesis addresses the structural and functional changes in biofilm communities and applies modern molecular methods to unravel molecular tolerance mechanisms.

Methods: Two different freshwater biofilm communities were cultivated for a period of five weeks, with one of the communities being contaminated with 4 $\mu\text{g L}^{-1}$ diuron. Subsequently, the communities were characterized for structural and functional differences, especially focusing on their crucial role of photosynthesis. The community structure of the autotrophs was assessed using HPLC-based pigment analysis and their functional alterations were investigated using Imaging-PAM fluorometry to study photosynthesis and community oxygen profiling to determine net primary production. Then, the molecular fingerprints of the communities were measured with meta-transcriptomics (RNA-Seq) and GC-based community metabolomics approaches and analyzed with respect to changes in their molecular functions. The communities were acute exposed to diuron for one hour in a dose-response design, to reveal a potential PICT and uncover related adaptation to diuron exposure. The combination of apical and molecular methods in a dose-response design enabled the linkage of functional effects of diuron exposure and underlying molecular mechanisms based on a sensitivity analysis.

Results/Discussion: Chronic exposure to diuron impaired freshwater biofilms in their biomass accrual. The contaminated communities particularly lost autotrophic biomass, reflected by the decrease in specific chlorophyll a content. This loss was associated with a change in the molecular fingerprint of the communities, which substantiates

structural and physiological changes. The decline in autotrophic biomass could be due to a primary loss of sensitive autotrophic organisms caused by the selection of better adapted species in the course of chronic exposure. Related to this hypothesis, an increase in diuron tolerance has been detected in the contaminated communities and molecular mechanisms facilitating tolerance have been found. It was shown that genes of the photosystem, reductive-pentose phosphate cycle and arginine metabolism were differentially expressed among the communities and that an increased amount of potential antioxidant degradation products was found in the contaminated communities. This led to the hypothesis that contaminated communities may have adapted to oxidative stress, making them less sensitive to diuron exposure. Moreover, the photosynthetic light harvesting complex was altered and the photoprotective xanthophyll cycle was increased in the contaminated communities. Despite these adaptation strategies, the loss of autotrophic biomass has been shown to impair primary production. This impairment persisted even under repeated short-term exposure, so that the tolerance mechanisms cannot safeguard primary production as a key function in aquatic systems.

Table of content

Abstract	i
Table of figures	vi
Table of tables	vii
Glossary on the different perspectives on function	vii
List of abbreviations	viii
Danksagung	ix
1. The effect of chemicals on organisms and their functions	1
1.1 Welcome to the anthropocene	1
1.2 From cellular stress responses to ecosystem resilience	3
1.2.1 The individual pursuit for homeostasis	3
1.2.2 Stability from diversity	5
1.3 Community ecotoxicology - a step forward in monitoring the effects of chemical pollution?	6
1.4 Functional ecotoxicological assessment of microbial communities	9
1.5 Molecular tools – the key to a mechanistic understanding of stressor effects from a functional perspective in microbial communities?	12
2. Aims and Hypothesis	14
2.1 Research question	14
2.2 Hypothesis and outline	15
2.3 Experimental approach & concept	16
2.3.1 Aquatic freshwater biofilms as model community	16
2.3.2 Diuron as model herbicide	17
2.3.3 Experimental design	18
3. Structural and physiological changes in microbial communities after chronic exposure - PICT and altered functional capacity	21
3.1 Introduction	21
3.2 Methods	23
3.2.1 Biofilm cultivation	23
3.2.2 Dry weight and autotrophic index	23
3.2.4 Pigment analysis of periphyton	23
3.2.4.1 <i>In-vivo</i> pigment analysis for community characterization	24

3.2.4.2 <i>In-vivo</i> pigment analysis based on Imaging-PAM fluorometry	24
3.2.4.3 <i>In-vivo</i> pigment fluorescence for tolerance detection.....	26
3.2.4.4 <i>Ex-vivo</i> pigment analysis by high-pressure liquid-chromatography	27
3.2.5 Community oxygen metabolism measurements	28
3.3 Results and discussion	29
3.3.1 Comparison of the structural community parameters	29
3.3.2 Photosynthetic activity and primary production of the communities after selection phase	33
3.3.3 Acquisition of photosynthetic tolerance	34
3.3.4 Primary production at exposure conditions.....	36
3.3.5 Tolerance detection in primary production.....	37
3.4 Summary and Conclusion	40
4. Community gene expression analysis by meta-transcriptomics	41
4.1 Introduction to meta-transcriptomics	41
4.2. Methods	43
4.2.1 Sampling and RNA extraction.....	43
4.2.2 RNA sequencing analysis.....	44
4.2.3 Data assembly and processing.....	45
4.2.4 Prioritization of contigs and annotation	47
4.2.5 Sensitivity analysis of biological processes	48
4.3 Results and discussion	48
4.3.1 Characterization of the meta-transcriptomic fingerprints	49
4.3.2 Insights into community stress response mechanisms using trend analysis (DRomic's).....	51
4.3.3 Response pattern in the isoform PS genes	63
4.5 Summary and conclusion.....	65
5. Community metabolome analysis	66
5.1 Introduction to community metabolomics	66
5.2 Methods	68
5.2.1 Sampling, metabolite extraction and derivatisation.....	68
5.2.2 GC-TOF-MS analysis	69
5.2.3 Data processing and statistical analysis	69
5.3 Results and discussion	70
5.3.1 Characterization of the metabolic fingerprints	70

5.3.2 Difference in the metabolic fingerprints	71
5.3.3 Differential metabolic responses of the communities to short-term exposure of diuron	73
5.4 Summary and conclusion	78
6. Synthesis	79
6.1 Approaches and challenges for linking molecular data to functional measurements	79
6.2 Methods	83
6.2.1 Summary on the data	83
6.2.2 Aggregation of molecular data to index values (TELI and MELI)	83
6.2.3 Functional annotation of contigs and metabolites using KEGG	83
6.3 Results and discussion	85
6.3.1 Results of aggregation techniques	85
6.3.2 Sensitivity analysis of the different molecular approaches and endpoints	86
6.3.3 Mechanistic view of the molecular stress responses based on KEGG functions	89
6.4 Consolidation of the results – holistic interpretation and discussion	93
6.4.1 Adaptation to chronic diuron exposure - from molecular changes to community effects	93
6.4.2 Assessment of the ecological costs of Pollution-induced community tolerance based on primary production	94
6.5 Outlook	97
Appendix	99
References	109
Thesis publications and manuscripts	122

Table of figures

Figure 1 Simplified graph on the physiological state of a cell in response to environmental change.	4
Figure 2 Schematic representation of the emergent levels of function	11
Figure 3 Workflow on the outlined steps in this thesis	16
Figure 4 Schematic representation of photosystem II	18
Figure 5 Graphical representation of the experimental design and the PICT concept	20
Figure 6 Relative community composition based on in-vivo pigment analysis.....	29
Figure 7 Principal component analysis (PCA) of the relative pigment content.....	32
Figure 8 Inhibition of the photochemical quantum yield of photosystem II	35
Figure 9 Inhibition of the net primary production normalized to chlorophyll a	38
Figure 10 Principal component analysis based on the rlog transformed meta-transcriptome fingerprints	50
Figure 11 Heatmap of the GO-processes related to the carbohydrate and fatty acid metabolism	56
Figure 12 Heatmap of the GO-processes related to the acetyl-CoA metabolism, glyoxylate cycle and ATP synthesis coupled electron transport	57
Figure 13 Schematic representation of the expression of genes involved in the photosynthetic apparatus.....	59
Figure 14 Heatmap of the GO processes related to amino acid metabolism	61
Figure 15 Heatmap of the pooled photosynthethic GO processes.....	62
Figure 16 Boxplot of the cross-reference gene expression analysis between the communities of the contigs related to photosynthesis	64
Figure 17 Principal component analysis of the metabolic fingerprints	71
Figure 18 Venn diagramm of the 190 metabolites of the final alignment	73
Figure 19 Boxplot of the normalized peak area of the metabolites TA and LAL	74
Figure 20 Boxplot of the normalized peak area of the metabolites GL and PA	76
Figure 21 Global cumulative sensitivity distribution of the contigs, metabolites and inhibition of the photosynthetic yield	89
Figure 22 Cumulative sensitivity distribution of molecular KEGG functions	92

Table of tables

Table 1 Settings of HPLC pigment analysis.	28
Table 2 Results of the community oxygen profiling	39
Table 3 Results of the sensitivity analysis of the GO processes	52
Table 4 Summary on data collected in the physiological and molecular analysis	83
Table 5 Example of the hierarchical classification system of KEGG	84

Glossary on the different perspectives on function

Perspective	Description	Terminology for this thesis	Measuring Parameter
Process*	Measurable flux of matter or energy.	<ul style="list-style-type: none"> ecologic function community function molecular function 	O ₂
Role*	A characteristic of a community that indicates the presence of a function.	<ul style="list-style-type: none"> functional trait KEGG function functional genomics 	Chl _a , PS-genes
Service*	The transmitted value of one or more process(es) for downstream systems.	<ul style="list-style-type: none"> not used 	-
Functioning*	The interaction of different processes for the good of an overall system (e.g. organism, community).	<ul style="list-style-type: none"> community functioning cellular functioning 	I-PAM
Function	Arises from the fusion of process and functioning: A measurable flow of matter or energy that maintains the wellbeing of a system (see Chapter 1.4 for a precise definition).		

* With reference to “*Function and “functioning” in ecology: what does it mean?*” by Jax (2005).

List of abbreviations

Acronym	Full form
AA	Ascorbic acid
AAL	Arabinonic acid-1,4-lactone
AGP	Anhydro-glycopyranose
ATP	Adenosine triphosphate
BMD	Benchmark dose
Chla	Chlorophyll a
CSD	Cumulative sensitivity distribution
DDT	1,1,1-Trichlor-2,2-bis(4-chlorophenyl)ethan (insecticide)
DHA	Dehydroascorbic acid
DW	Dry weight
EC _x	Effect concentration affecting x % of the studied parameter
EPS	Extracellular polymeric substances
GAP	Glycerolaldopyranosid
GC-TOF MS	Gas chromatography coupled to time-of-flight mass spectrometer
GO	Gene Ontology (http://geneontology.org)
GL	Glycerol
HC _x	Hazardous concentration to x % of species
HPLC	High-pressure liquid-chromatography system
KEGG	Kyoto Encyclopedia of Genes and Genomes (https://www.kegg.jp/kegg/)
LAL	Lyxonic acid-1,4-lactone
MELI	Metabolic effect level index
MoA	Mode of action
MRC _x	Molecular regulation concentration
NADPH	Nicotinamide adenine dinucleotide phosphate
NCBI	National Center for Biotechnology Information
NPP	Net primary production
NOTEL	No observed transcriptional effect level
OMICs	e.g. Genomics, Metagenomics, Transcriptomics, Proteomics, Metabolomics, Phenomics
PA	Phosphoric acid
PAM	Pulse-amplitude modulation
PC	Principal component
PICT	Pollution-induced community tolerance
PSI & II	Photosystem I and II
ROS	Reactive oxygen species
RPM	Revolutions per minute
RPP	Reductive pentose-phosphate cycle
TA	Threonic acid
TELI	Transcriptional effect level index
Q _A	Plastoquinone Q _A
Zn	Zinc

Danksagung

Diese Dissertation ist, obgleich des Namens auf der Titelseite, natürlich keine Einzelleistung, sondern das geistige Produkt der Zusammenarbeit vieler Kollegen und Freunde. Im Folgenden möchte ich daher deren Beitrag zu dieser Arbeit herausstellen und entsprechend würdigen.

Mechthild Schmitt-Jansen möchte ich für ihre jahrelange Beratung und Betreuung, die Einarbeitung in das Forschungsthema, die Anregungen und Korrekturen dieser Arbeit und die Unterstützung im Dissertationsprozess danken.

Markus Weitere danke ich für seine universitäre Betreuung und dem IP ‚Healthy Aquatic Ecosystems‘ für die Finanzierung meiner Promotion.

Peggy Wellner, Silke Aulhorn und Janet Krüger bin ich zu tiefem Dank im Hinblick auf ihre großartige Laborunterstützung bei der Analyse der Pigmentzusammensetzung und des Metaboloms verpflichtet.

Floriane Larras hat mit ihrem DRomics Tool entscheidend zu dem Erfolg dieser Arbeit beigetragen und mich durch ihre Arbeit am Transkriptom Datensatz zu tiefergehenden Analysen inspiriert. Daher gebührt ihr ein großer Dank und ich hoffe, unser gemeinsames Paper zu diesem Thema wird nicht das Letzte sein.

Matthias Bernt danke ich für seine bioinformatische Unterstützung mit dem EVE Cluster des UFZ, wodurch mir die umfassende Analyse des Transkriptom Datensatzes ermöglicht wurde.

Stephan Schreiber danke ich für die umfassende Hilfe bei der Transkriptomsequenzierung und den stetigen Rat.

Afolarin Olaposi Ogungbemi bin ich für seine Ratschläge und die sprachliche Korrektur der Dissertation dankbar.

Zu guter Letzt möchte ich mich bei meinen langjährigen Kollegen aus der BIOTOX und insbesondere bei Christoph Rummel, Bastian Polst, David Leuthold und Riccardo Massei bedanken, welche mir immer mit einem schnellen Rat zur Seite standen.

1. The effect of chemicals on organisms and their functions

1.1 Welcome to the Anthropocene

Since that moment mankind detached from its ecological niche, they have triggered a tremendous ecological transformation. In the course of this transformation, a mass extinction episode was initiated unparalleled for 65 million years (Ceballos et al., 2015). In the very beginning it was just the hunger for new sources of protein (Sandom et al., 2014) or the loss of habitat due to the spread of agriculture and settlements (agricultural revolution) which put the ecosystems under stress. With the onset of industrialization human activity has triggered new stressors such as climate change, eutrophication or chemical pollution, which have exacerbated the problem that mankind poses to ecosystems. The recognition of the disastrous human environmental footprint is reflected in the concept of Planetary Boundaries (Rockström et al., 2009). This concept aims to define a safe operating space for safeguarding global functioning. The authors identified nine environmental boundaries that, if exceeded, “will trigger non-linear, abrupt environmental change within continental- to planetary-scale systems”.

Among those boundaries chemical pollution is considered in the category “Novel entities”, which was defined by Steffen et al. (2015) as “new substances, new forms of existing substances and modified life forms that have the potential for unwanted geophysical and/or biological effects”. Today, about 350'000 chemicals and mixtures are registered on the global markets, while many chemicals remain publicly unknown because they are claimed as confidential (over 50'000) or ambiguously described (up to 70'000) (Wang et al., 2020). Many of these chemicals eventually end up in the environment, unless they were intentionally applied there anyway such as many plant protection products. According to a report of the Federal Office of Consumer Protection and Food Safety (BVL), domestic sales of plant protection products remained on a consistently high level in 2021. The sales of active substances were mostly herbicides (16114 tons) and, to a lesser extent, fungicides (9699 tons) and insecticides (1995 tons). In the wake of chemical pollution, a number of negative effects on animal populations have been identified, such as the decline of raptors by DDT (Porter & Wiemeyer, 1969) and diclofenac (Oaks et al., 2004), disruption of the sex ratio in fish by ethinylestradiol (Purdom et al., 1994) and molluscs by tributyltin (Bettin et al., 1996) or the acute toxicity of 6PPD-quinone for salmon fish (Tian et al., 2021). This overview

illustrates the diversity of environmental impacts of chemicals, and thus assessing the planetary boundaries of novel entities requires a number of control variables. Persson et al. (2022) discussed several variables to control the unwanted impact of novel entities, based on production volume, trends in release or monitoring of unwanted impacts. They concluded that all control variables have an essential role in assessing the integrity of the biosphere, but the safe operating range is exceeded even “when annual production and releases increase at a pace that outstrips the global capacity for assessment and monitoring”. Hence, there are two priorities for dealing with the complexity of chemical pollution, I) production and release of novel entities to the environment needs to be reduced and II) efficient monitoring of environmental impacts must be ensured. Addressing the latter aspect requires consideration of the biological and chemical complexity. Release of chemicals to the environment initiates the formation of mixtures, which may have effects even if individual chemicals occur below critical thresholds (Walter et al., 2002). Managing mixtures requires incorporation of mixture toxicity into legislation (Kortenkamp et al., 2019), testing (real-life) chemical mixtures to humans and wildlife (Drakvik et al., 2020), and approaches to assess potential risks from environmental mixtures, like prediction of toxicity (based on read-across approaches) or effect-directed analysis (Brack et al., 2018).

However, chemical complexity is only half the battle. In nature, no species lives in isolation and the diversity of species and their sensitivity must be considered when looking at chemical pollution (biological complexity). Against this background, an expansion of current ecotoxicological testing from a single species to more complex and interacting communities is essential. Community ecotoxicology offers insights into pollution from an ecologic perspective by including species abundance, diversity and interactions as emerging properties beyond population-based analysis (Clements & Rohr, 2009). Thus, indirect effects of interactions (e.g. loss of prey or interspecific competition) are included in the assessment and improved protection of ecological integrity can be ensured. Tlili et al. (2016) proposed the Pollution-induced community tolerance (PICT) concept introduced by Blanck and Wängberg (1988) (see **Chapter 1.3**) as a diagnostic tool for ecologically relevant risk assessment of chemical pollution. However, further standardization, validation and development of more advanced (molecular) endpoints is needed to enable retrospective risk assessment of chemicals based on PICT.

1.2 From cellular stress responses to ecosystem resilience

1.2.1 The individual pursuit for homeostasis

Organisms strive for **homeostasis**, the stable state of optimal physical and chemical condition that ensures the most efficient functioning of cellular processes. This desired optimal state is rarely reached under natural fluctuation conditions and the physiological state of the cell is more likely to oscillate around the idealized optimal state. The oscillation within certain pre-set limits can be defined as the homeostatic range (Davies, 2016). Organisms respond to any deviation from homeostasis by regulation, acclimation and adaptation (Borowitzka, 2018) which is shown schematically in **Figure 1**. The process of **regulation** represents the activation or deactivation of already existing cell structures during environmental fluctuations (e.g. the light-harvesting complex of photoautotrophic organisms) (Giordano, 2013). Regulation starts immediately after an environmental change occurs. It does not require substantial changes in cell metabolism, so this process is particularly relevant for setting the homeostatic range. If an environmental condition exceeds the homeostatic range, an organism faces macromolecular damages associated with a metabolic imbalance, which can be defined as a physiological state of **stress**. During stress, the biotic potential is reduced and resources are shifted from somatic growth to cellular stress responses and acclimation processes. The **cellular stress response** covers a universal set of functions to defend against macromolecular damage caused by environmental change. Involved functions, such as cell cycle control, repair or removal of damaged proteins or stabilization of DNA, aim to stabilize the physiological state temporarily (Kültz, 2005). Their action represents a non-specific response to the environmental stimulus. The processes of cellular stress response and **acclimation** overlap, however, acclimation involves a modification of the macromolecular structure to return to homeostasis. Thus, acclimation leads to transcription and translation of specific genes to synthesize crucial proteins that adjust cell metabolism to the new environment. If the genetic capacity and the available resources allow establishing homeostasis under the new environmental conditions, stress is relieved. Conversely, **cell death** occurs when the extent of environmental change surpasses the intolerance threshold or the duration of acclimation requires an energy budget that exceeds cellular capacity. The range of self-stabilization up to a maximum environmental change (intolerance) is termed **homeostatic capacity**. Another strategy to face stressful conditions is **avoidance**, for example by forming dormant, stress-resistant non-

reproductive structures. Although there are different types of survival forms, such as endospores, aplanospores or cysts, they all have in common that the organisms have minimal metabolism during the dormancy phase. In this stage they can last for years, without contributing to environmental processes.

Permanent environmental changes give rise to the process of **adaptation**, which consolidates the acclimated state in the genotype. During adaptation, advantageous mutations are selected that allow maintaining homeostasis at low metabolic cost. The selection of advantageous small scale mutations is also defined as **micro-evolution** (Medina et al., 2007). The result of acclimation and adaptation can create a favorable metabolic state called **hormesis** (Agathokleous et al., 2021), but also increase costs from altered metabolic processes (Medina et al., 2007).

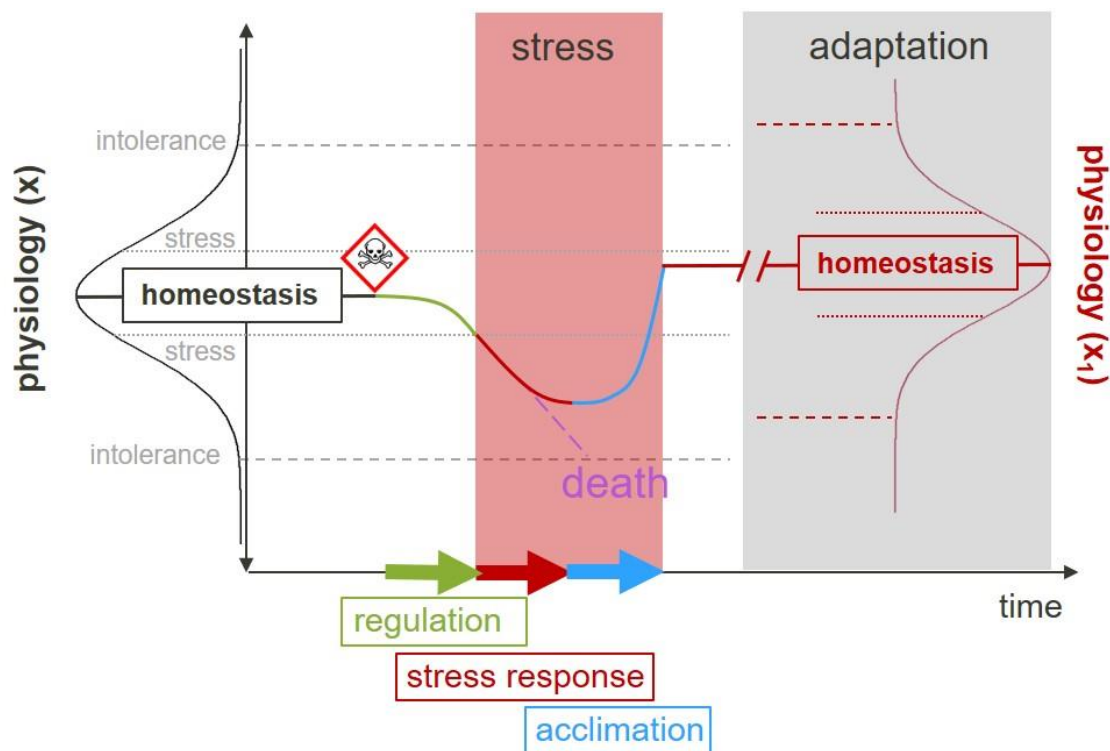


Figure 1 Simplified graph on the physiological state of a cell in response to environmental change (adapted from Borowitzka (2018)). The physiological optimum of a cell as a function of an environmental variable x is shown on y-axis and hypothetical thresholds for stress and intolerance are plotted with a dashed line. The skull pictogram marks an environmental stimulus (e.g. toxic exposure) upon which the cellular homeostasis starts declining. A cascade of cellular responses is triggered, which can be divided into regulation, stress response and acclimation. The moment the cellular state moves beyond homeostatic range of regulation a stress situation is initiated (red area). After acclimation, homeostasis is re-established in the new environmental situation, and if the environmental stimulus persists, adaptation can occur (gray area), consolidating the acclimated state in the genotype.

1.2.2 Stability from diversity

Environmental communities are shaped by the coexistence of different species in space and time. Coexistence has been conceptualized by a scaling into nested levels of biological organization, ranging from populations to communities. A **population** is defined as a group of organisms of the same genotype on a given location. Genetic differences of small scales can exist both within and between populations at different sites. Genetic variance within species of the same population (intraspecific variation) stabilizes against environmental fluctuations, as there is higher chance of individual members of the population performing better under altered conditions. A **community** is an association of populations at the same temporal and geographic scale, which co-exist due to differences in their niche and other external factors. The niche arises from the integration of all physiological requirements of an organism to the prevailing conditions. The populations within a community are intertwined in a complex network that includes interactions ranging from competition to mutualism. Compared to populations, communities show a higher stability, as they have additional genetic variance between species (interspecific variation). Intraspecific and interspecific variation can be summarised as genetic diversity, which is a cornerstone of biodiversity. High genetic diversity in communities is ensured by environmental factors and interactions such as predator-prey relationships, as these dampen the dominance efforts of individual species (McCann, 2000). McCann (2000) further argues that the loss of biodiversity increases the strength of interaction between remaining species, making a community more vulnerable to disturbance.

On a higher level of abstraction, genetic diversity converges into shared metabolic pathways, which themselves contribute to community or ecosystem functions (see **chapter 1.4**). This is illustrated by the frequently observed phenomenon that the composition of functional genes remains relatively stable across comparable environments, while the taxonomical composition of the communities varies considerably (e.g. Louca et al., 2016). This stability in the functional composition arises from **functional redundancy** of a diverse set of species within the community, which is greater on basal functions with thermodynamically favorable pathways such as respiration (Louca et al., 2018). Naeem (1998) postulated functional redundancy as a critical feature of ecosystems and paved the way for the **insurance hypothesis** (Yachi & Loreau, 1999). The authors proved that biodiversity stabilizes (eco-) systems against declines in their functioning. Their modeling approach showed that diversity has two

main effects, such as I) a reduction in the temporal variance of a function (buffering), and II) an increase in the temporal mean of a function (stimulation).

Both, functional redundancy and the insurance hypothesis are important aspects in microbial community ecotoxicology, as they form the basis of the concept of 'Pollution-induced Community Tolerance' (PICT) of Blanck and Wängberg (1988), which is outlined in **chapter 1.3**.

1.3 Community ecotoxicology - a step forward in monitoring the effects of chemical pollution?

A community is more than the sum of its individual populations, as it includes interactions at different trophic levels. From an ecotoxicological perspective, communities reveal indirect effects that cannot be derived from the sum of the sensitivities of the individual populations to a chemical exposure. This has been illustrated by McClellan et al. (2008), who showed that chronic effects of the herbicide diuron at the community level could not be predicted from tests with individual algal species. Due to the combination of ecological complexity and ecological relevance, community ecotoxicology remains an important and challenging field of science (Clements & Rohr, 2009). A possible simplification of the experimental effort while maintaining ecological complexity is to focus on the ecotoxicology of microbial communities such as biofilms (Guasch et al., 2016; Sabater et al., 2007). The key advantage of microbial communities is the combination of genetic diversity and short generation time of the microbes. Therefore, focusing on microbial communities allows the investigation of a regulatory, acclimation and adaptation processes with respect to their potential to affect community structure and function on acute and chronic scale.

In this thesis aquatic freshwater biofilms were used as model microbial communities, to tackle the aspects of structural and functional effects of chronic herbicide exposure (**chapter 1.4**) and unravel adaptation mechanisms (**chapter 1.2.1**). Aquatic biofilms can cover a wide range of phyla, such as unicellular microalgae, bacteria, archaea, fungi, and protozoa that share a delimited habitat on submerged surfaces. Attachment to surfaces is facilitated by a matrix of extracellular polymeric substances (EPS) excreted by algae and bacteria. Their diversity and ubiquitous occurrence makes

aquatic biofilms a hotspot of biogeochemical cycles that brings along a wide array of ecological functions ranging from respiration of organic matter, primary production or nutrient retention (Battin et al., 2016). However, microbial communities are often regarded as black-box systems with constant process rates (Allison & Martiny, 2008). In contrast, the authors' meta-study showed that microbial community composition is sensitive to changes in environmental parameters and recovery from disturbances can take up to years.

The sensitivity of members of a community to a chemical can vary by several orders of magnitude, implying that exposure to a pollutant will affect the organisms differently. Chronic exposure to a chemical therefore triggers the process of toxicant-induced succession (Blanck, 2002). This process shapes the structural and physiological characteristics of a community by selecting for adapted species. A trait that arises from adaptations is tolerance, which can be quantified according to the concept of 'Pollution-induced Community Tolerance' (PICT) introduced by Blanck and Wängberg (1988). However, community tolerance is no absolute measure, instead it becomes evident by comparing it with a reference value. Therefore, demonstrating PICT requires a short-term exposure of a chronically exposed and a reference community (with the respective stressor) as well as an integrative measurement reflecting the physiological state in the communities (Blanck, 2002). This approach implies that a community is more tolerant and thus better adapted if it can tolerate a higher amount of toxicant while maintaining its functional state. The author summarized common metabolic endpoints for the quantification of PICT, including the photosynthetic yield (e.g. ^{14}C -carbonate incorporation or pulse-amplitude modulated fluorescence analysis) and proxies of secondary production like nucleic acid or protein biosynthesis (e.g. ^3H -thymidine or ^3H -leucine incorporation). So far the PICT-concept was tested for biofilm communities in the context of tolerance augmentation along environmental pollution gradients (Pesce et al., 2010; Rotter et al., 2011), co-tolerance development under multiple stressor conditions (Schmitt-Jansen et al., 2016), restoration of community sensitivity after pollution (Dorigo, Bérard, Bouchez, et al., 2010; Rotter et al., 2011; Tlili et al., 2020) and to explore the molecular mechanisms of tolerance by analyzing target genes of a toxicant (Eriksson, Clarke, et al., 2009).

An increase in tolerance of a community has three different mechanisms (Blanck & Wängberg, 1988; Grant, 2002): I) the replacement of species, II) replacement of individuals of a species and III) adaptation of the individuals (see **chapter 1.2.1**).

Factors I) and II) have been referred to as ‘genetic erosion’ (van Straalen & Timmermans, 2002), and, given a high functional redundancy in biofilms that can compensate these genetic losses it remains to be demonstrated that the insurance hypothesis applies (see **chapter 1.2.2**) and chemical-induced loss of the most sensitive species does not affect community functions as proposed by Tlili et al. (2016). Following this suggestion PICT should on the one hand strengthen a community and its ecological functions against future chemical exposure, but on the other hand could come along with community costs (I & II) and individual costs (III) may reduce the ecological functions of biofilms (Pesce et al., 2010). Mouneyrac et al. (2011) summarized individual costs into I) redistribution of energy from somatic growth and reproduction towards tolerance mechanisms (Calow, 1991), II) adverse genetic mutations and alterations of protein functions (Taylor & Feyereisen, 1996), and III) reduced adaptability of the community to future environmental conditions (Meyer & Di Giulio, 2003).

Given the potential ecological costs of PICT, the tolerance trait of a community needs to be measured in conjunction with integrated functional parameters like net primary production or changes in biomass to enable conclusions on the role of PICT for community functioning (see **chapter 1.4**). To prove the assumption that PICT stabilizes the ecological functions of a community under repeated exposure, the functional assessment should be carried out in a reference approach.

1.4 Functional ecotoxicological assessment of microbial communities

The protection of structure as a proxy for ecological functions is a central dogma of ecological risk assessment. Thus, water quality assessment in the Water Framework Directive (2000/60/EC), Annex V utilizes ecological indicators, which are mainly based on structural parameters like species composition, abundance and biomass. Structural parameters imply many advantages like their cost-effective examination, however these parameters lack diagnostic power in microbial communities, for several reasons:

I) By January 2022 a number of 21'739 prokaryotes were documented in the "List of Prokaryotic names with Standing in Nomenclature" (Parte et al., 2020), which seems like a drop in the ocean compared to the estimated microbial diversity of one trillion species (Locey & Lennon, 2016). The sheer number of unknown prokaryotes and the lack of knowledge on the indicator value of already known species often limits the assessment of water quality based on microbial composition and is restricted to eukaryotic microbial organisms. Thus, the biological quality component of microphytobenthos has so far been the only microbial component for water quality assessment.

II) Microbes can switch their metabolism to dormancy rendering their presence less important for ongoing processes.

As the structural assessment comes to its limits, functional analysis of microbial systems might pose an alternative approach for the impact assessment of a stressor. Functional indicators respond fast and consistent across taxa. Their significance was illustrated with respect to the general ecological status of river ecosystems (Feio et al., 2010; Young et al., 2008) and specifically to chemical pollution (Johnston et al., 2015; McMahon et al., 2012; Peters et al., 2013). In addition, functional assessment provides an integrated ecological insight into the effect of chemical pollution, an aspect that can be addressed in taxonomic analysis only in conjunction with functional traits (Krause et al., 2014).

Structure and function are tightly bond entities which emerge from each other. **Structure** resembles a static physical information (e.g. genes or organisms), which can be seen as proxy of function with limited capacity to predict the realized extent of a function. During dormancy, for example, bacteria switch off their function while they still contribute to genetic structures (e.g. the metagenome). For this reason, structural

and functional measurements have different significance, with the latter being closely related to the physiological state of an organism, a community or ecosystem. Function has been interpreted in various ways and Jax (2005) identified four major notions of the term ‘function’ from an ecological perspective, as I) ‘process’ or interaction between two objects, II) ‘functioning’ of a system (e.g. an organism) as the result of a multitude of processes and interactions, III) ‘role’ within a system and IV) ‘service’ of a system for practical (anthropogenic) use. This multifaceted interpretation of functions is also evident in the **glossary**. The interpretation of a function as a process and service for a superordinate system is in line with this dissertation, although different levels (from molecular to ecosystem) can be considered in this context. To account for the different levels, Farnsworth et al. (2017) proposed a universal definition of function:

“A biological function is a process enacted by a biological system A at emergent level n which influences one or more processes of a system B at level $n+1$, of which A is a component part.” (Farnsworth et al., 2017, p. 1370)

In that sense function is a dynamic variable (e.g. flux) with a specific impact on biological entities of higher levels. The authors refer to ‘emergent levels’ as nested structures of biological organization, which scales from molecules to ecosystems. With regard to functional redundancy, potentially several components of a system can support a function. Here, the concept of “functional equivalence classes” can be applied, although it was originally intended for biochemical networks (Auletta et al., 2008).

“The concept of equivalence class ... [is] a pure functional biological category, where different operations are considered functionally equivalent if they produce the same outcome for some functional purpose (the goal).” (Auletta et al., 2008, p. 1164)

Accordingly, a functional equivalence class accounts for functional redundancy (see **chapter 1.2.2**) by grouping a set of processes that have the same effect with respect to a defined outcome. Functional equivalence classes may differ on lower emergent levels, but converge at a higher level into biogeochemical cycles. This functional redundancy has to be incorporated in the definition of Farnsworth et al. (2017) to address the increasing redundancy in upscaling. Moreover, to operationalize the concept of function in ecotoxicology, a flow of matter or energy arising from a function must be measurable. Accordingly, the flow of information (e.g. transcription,

translation) cannot be included. Adapting the definition of Farnsworth et al. provides a basis for understanding function in this thesis.

“A function arises from the activity of one or more processes enacted by a biological system A at emergent level n producing an equivalent flux of matter and energy which is essential for one or more processes of a system B at level n+1, of which A is a component part.”

According to this definition, a function is characterized by a process rate; if this is missing, only a functional trait remains (such as the role of a gene in functional genomics). The essentiality of the process of system A (e.g. the performance of photosynthesis) emphasizes the importance of the function for the dependent system B, thus creating the basis for complex ecological hierarchies.

As structure comprises a hierarchical organization also function spans all levels of biological organization. In terms of the above definition of functions, this applies from the molecular to the ecosystem level (Farnsworth et al., 2017). In order to clarify the emergent level, the terms molecular, community or ecosystem function are used in this work. Thus, the energy conversion into ATP and NADPH via the light-dependent reaction resembles a molecular function and, building on this, primary production of a community resembles a community function (see **Figure 2** for an example for primary production).

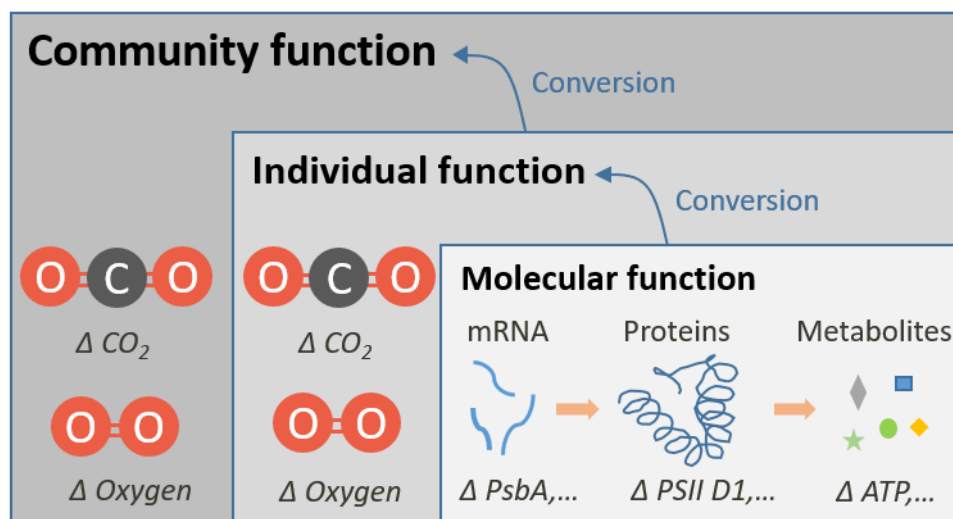


Figure 2 Schematic representation of the emergent levels of function exemplified for primary production. The molecular function has a multitude of potential endpoints that converge in their output to oxygen and carbon dioxide as quantifiers for the process rate on apical functional levels.

However, a quantitative extrapolation among different emergent levels remains a major challenge, because the interaction of the components is largely unclear and concepts for aggregation are lacking. Thus, the scope of a functional measure is limited to the emergent level it was measured and only qualitative extrapolation (e.g. using sensitivity or correlation) is applicable. Due to the nested organizational principle of functions, reasons for a decline in functions must first be examined at the respective lower levels. Thus, at the molecular level, both individual and community functions can be studied, although molecular approaches for biofilm communities are still largely unexplored. In this thesis the functional impact of chronic diuron exposure on biofilm communities was examined, and the molecular function was addressed by exploring the functional role of responsive genes and metabolites in these communities.

1.5 Molecular tools – the key to a mechanistic understanding of stressor effects from a functional perspective in microbial communities?

In-vivo studies form the basis of ecotoxicology, as they provide essential data to ensure ecologic relevance. However, the results of *in-vivo* tests are not always conclusive for understanding underlying mechanisms, as they resemble a highly aggregated response. Especially with microbial communities, *in-vivo* studies mostly fail to unravel complex changes in community structure and their physiological state. Expanding the focus to sub-cellular regulation using integrative molecular methods promises a more differentiated insight. Molecular tools addressing the pools of ribonucleic acids (transcriptomics), proteins (proteomics) and metabolites (metabolomics) in a comprehensive manner, collectively referred to as OMICs or functional genomics, have become a crucial resource for the mechanistic understanding of chemical effects and provide a molecular functional perspective on stress responses of organisms (see **chapter 1.4**). However, a mechanistic understanding requires I) a suitable experimental design and II) anchoring of the molecular regulation into an apical effect (e.g. changes in phenotype or function).

With respect to I), a paradigm shift from the traditional comparison of two conditions (hypothesis testing) to a gradual exposure design (Smetanová et al., 2015) is needed. The combination of OMICs and a dose-response design can provide causality by correlating molecular regulation and gradually increasing exposure concentrations of

a chemical. This approach strengthens mechanistic understanding, especially when it is combined with pathway analysis (e.g. Larras et al., 2018).

Regarding II), the integration and extrapolation of molecular regulation towards organismal or even community effects remain a major challenge of OMICs-technologies. Molecular processes form a complex network wherein regulatory changes can be disproportionate and non-linear compared to a highly aggregated apical effect. A review by Stitt and Gibon (2014) illustrates this discrepancy with respect to gene expression and protein activity. The authors argued that biological activity of proteins is modified by several factors such as the average half-life of RNA, alternative splicing, proteolysis, assembly into complexes, post-translational modifications and levels of substrates and effectors. Moreover, biomolecules can have multiple physiological roles in the organism and interpretation depends on the physiological state. Thus, OMICs-techniques are particularly diagnostic for toxic effects when being anchored to phenotypic or apical functional parameters such as changes in cell size or primary production (Grossmann et al., 2012; Sans-Piché et al., 2010; Viant, 2007) or even grounded on ecological concepts such as pollution-induced community tolerance. Anchoring provides a second level of causality to prove that regulation leads to changes in phenotype or function.

Expanding the focus of OMICs-techniques to functional analysis has great opportunities but also challenges. On the one hand OMICs-techniques allow a qualitative, multifaceted assessment of biomolecules such as genes or proteins associated with functions, but on the other hand they fail to capture functions quantitatively. Thus, OMICs can be used to explore the functional diversity of a community (Dopheide et al., 2015; Störmer et al., 2013), link functional diversity to the chemical fingerprints (Fasching et al., 2020) or derive relative activity of functional genes (Hultman et al., 2015). These examples demonstrate that OMICs can comprehensively predict the presence and activity of functions. However, a review of Strzepek et al. (2021) highlights the inability of molecular methods to estimate process rates in the coming decades based on the currently available approaches and simultaneously underlines the central role of functional measurements to provide projections of global change.

2. Aims and Hypothesis

2.1 Research question

Chemical pollution is a major environmental concern, but the consequences on the biological level of communities, or ecosystems are still barely understood (Köhler & Triebkorn, 2013). Communities are an important piece of the puzzle of chemical effects assessments, as they integrate natural complexity and thereby provide a perspective on higher-level impacts (e.g. ecosystem services). Reducing biological complexity to single species and analyzing their responses on a biochemical or molecular level can improve mechanistic understanding and specificity, while expanding complexity brings ecological relevance but often lacks mechanistic explanations (Clements & Rohr, 2009). This dissertation therefore combines ecological relevance of the community approach and the mechanistic power of molecular methods to unravel the effect of chronic chemical exposure from both perspectives.

To address the ecologic perspective, natural microbial communities (freshwater biofilms) were exposed to a model herbicide of environmental concern (see **chapter 2.3.2** for herbicide selection). Biofilms can be regarded as early warning systems for chemical pollution (Sabater et al., 2007). Chronic exposure of biofilms was shown to initiate 'Pollution-Induced Community Tolerance' (PICT) in laboratory experiments (Corcoll et al., 2019; McClellan et al., 2008) and along environmental pollution gradients (Pesce et al., 2010; Rotter et al., 2011). Before PICT is detectable, biofilm communities undergo adaptation and selection processes (see **chapter 1.2**). The induction of community tolerance was postulated to have a stabilizing effect on community functions (Tlili et al., 2016). However, even genetically inherited tolerance by micro-evolution can have fitness cost from altered physiological processes (Medina et al., 2007), and the significance of PICT for periphyton functions remains to be demonstrated. Therefore, the aim of this thesis is to identify the adaptive mechanisms of biofilm communities resulting in PICT and to assess whether PICT supports an important community function, namely net primary production.

2.2 Hypothesis and outline

Related to the above mentioned aims of this thesis, the following hypotheses are addressed:

H1 Chronic exposure affects communities in structure resulting in PICT towards diuron.

H2 Induced community tolerance following chronic exposure (PICT) imposes costs that impact key ecological functions.

H3 Functional measures on molecular scale facilitate the identification of adaptation mechanisms that maintain homeostasis under diuron exposure conditions and form the basis for PICT.

For a graphical outline of this work, see **Figure 3**. The individual chapters include the following focal points:

The consequences of chronic diuron exposure for community structure are discussed in **chapter 3**. This chapter particularly addresses the autotrophic part of the biofilm communities, by focusing on changes in photosynthetic pigments, photosynthesis and primary production. These parameters are evaluated with regard to the physiology, tolerance and function of the biofilm communities in the ecologic context.

Adaptation to a stressor can be identified in the molecular fingerprint of the organisms that compose a community. Modern molecular tools such as meta-transcriptomics promise mechanistic insights into stressor action, however, they are rarely applied to complex natural communities. **Chapter 4** examines the molecular adaptation of communities with and without chronic exposure from the perspective of gene expression and explores responsive genes based on their functional traits.

Chapter 5 advances towards the realized adaptation, by analyzing the consequence of adaptation in the community metabolome. This chapter specifically addresses the question of which tolerance mechanisms were induced in the course of chronic exposure.

Chapter 6 integrates the results of the previous chapters into a sensitivity-based synthesis. This synthesis examines the strength of the different methods with respect to mechanistic understanding of the pollutant effects and PICT, places the molecular

effects in a functional context with the communities and summarizes the results of all chapters into a final conclusion.

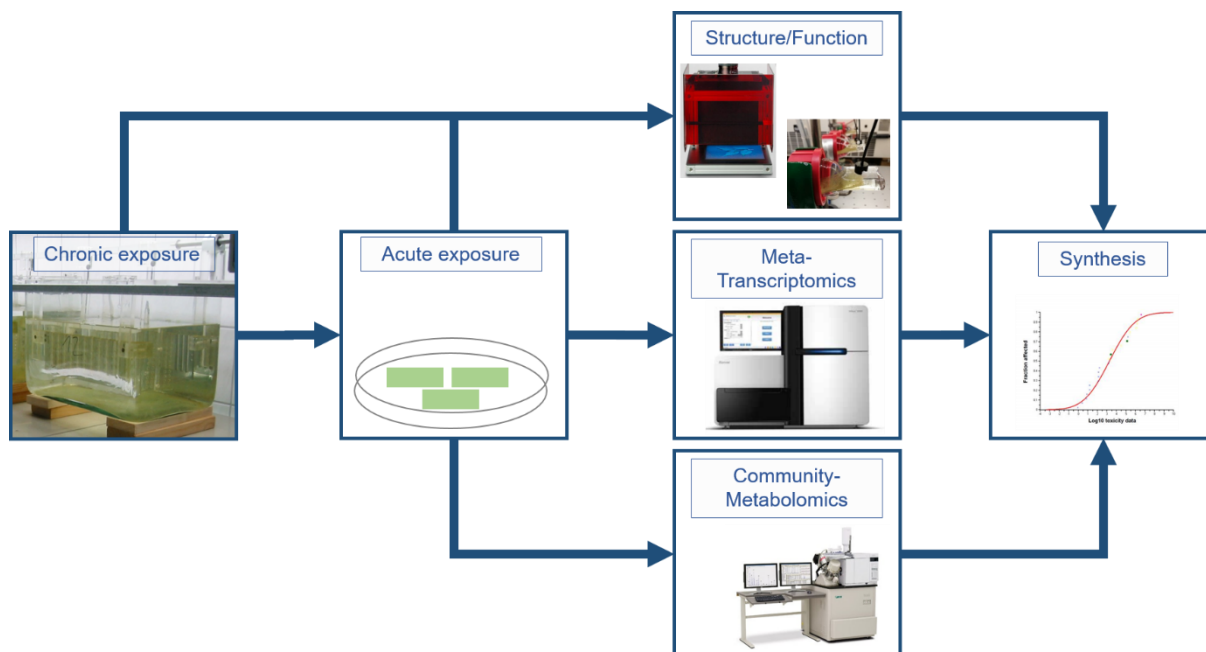


Figure 3 Workflow on the outlined steps in this thesis. A detailed illustration on the cultivation and sampling is presented in *Figure 5*.

2.3 Experimental approach & concept

2.3.1 Aquatic freshwater biofilms as model community

To address the outlined questions and hypotheses, a microcosm experiment covering different exposure scenarios of freshwater biofilm communities was chosen. Freshwater biofilms were selected as model community for their high content of autotrophic organisms and their significant contribution to primary production. To approximate the natural complexity of biofilms, the communities were cultivated from a natural inoculum of a local stream. Thus, the communities comprised a variety of species with different sensitivities to herbicides. In this thesis, all organisms embedded in the EPS matrix are considered to be part of the biofilm (see **chapter 1.3**). To specifically address the autotrophs within the biofilm community, the term periphyton is used. Biofilms are treated as one functional entity, which implies an integrating perspective on the biological processes taking place in the biofilm (similar to a supra-organism). As a result, processes carried out by a subfraction of biofilm species are attributed to the entire biofilm entity. In line with this perspective, selection of adapted species and intrinsic adaptation to contaminant exposure also converge to a joint

adaptive response, rendering the biofilm more tolerant. For this reason, the term adaptation in the following includes both selection and adaptation processes, which were defined in **chapter 1.2.1**.

2.3.2 Diuron as model herbicide

Herbicides have gained an increasing importance in worldwide crop production (Gianessi, 2013), especially when combined with genetically modified herbicide-tolerant crops (Bonny, 2016). Due to their ubiquitous use, herbicides burden aquatic ecosystems where they are commonly found (Malaj et al., 2014; Villeneuve et al., 2011). Among them, the phenylurea herbicide diuron (3-(3,4-dichlorophenyl)-1,1-dimethylurea) takes a prominent role. The herbicide is partially banned in the European Union and listed in Annex II of Directive 2008/105/EC on Priority Substances and Certain Other Pollutants. However, diuron was among the 13 substances commonly found in European rivers with environmental concentration of 1 to 1000 ng L⁻¹ (Busch et al., 2016) indicating a potential hazard of diuron exposure in aquatic systems. This assumption is supported by studies of the French river Morcille, which receives a constant load of diuron from local vine farming. The local biofilms adapted to diuron pollution, which is indicated by increased tolerance (Dorigo et al., 2007; Pesce et al., 2010). For the above mentioned reasons, diuron was selected as model herbicide for the present thesis.

This herbicide is a potent photosystem inhibitor, which displaces the plastoquinone Q_B at the D1 protein (gene *psbA*) in the Photosystem II reaction center (Battaglino et al., 2021). The binding interrupts the electron transfer from Q_A to Q_B (**Figure 4**) and thus the downstream synthesis of ATP and NADPH. The inhibition triggers increased chlorophyll fluorescence and favors the formation of reactive oxygen species (ROS) by transferring electrons to O₂ (Krieger-Liszkay & Rutherford, 1998; Rutherford & Krieger-Liszkay, 2001).

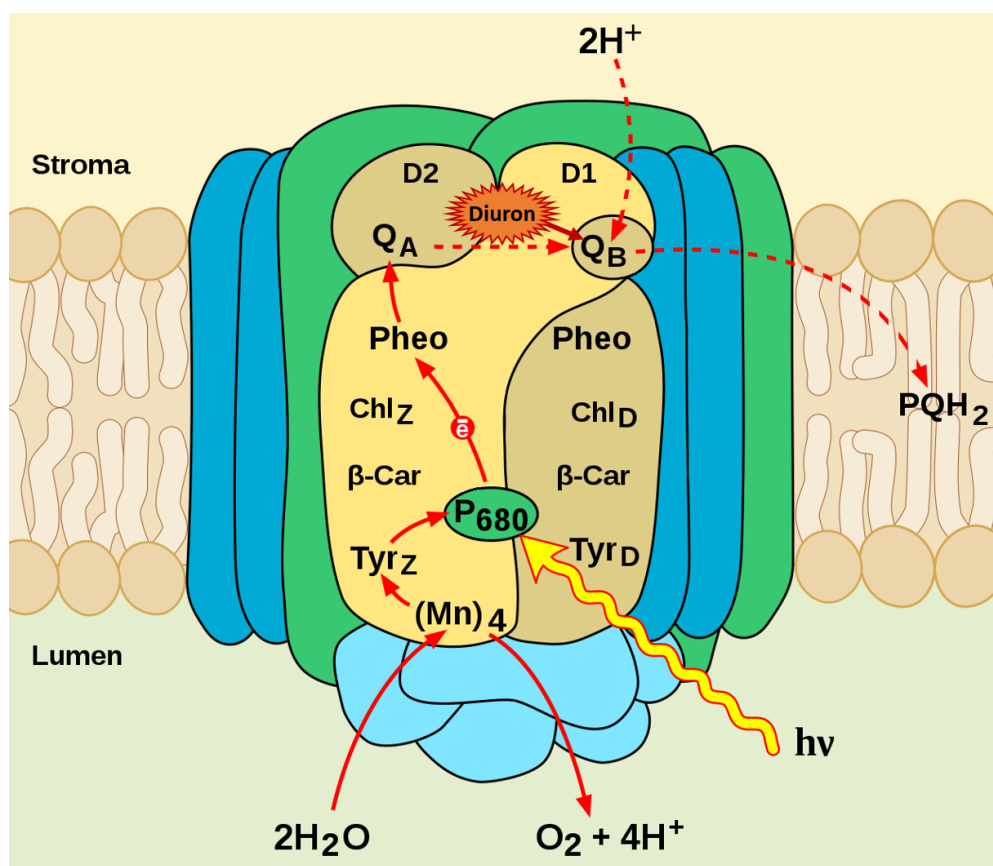


Figure 4 Schematic representation of photosystem II: The electron flow is indicated by arrows and the receptor of the diuron molecule on the D1 protein is located where Q_B is highlighted. The dashed lines represent the molecular actions blocked by diuron. Adapted from: Kaidor, CC BY-SA 4.0 <<https://creativecommons.org/licenses/by-sa/4.0/>>, Wikimedia Commons

2.3.3 Experimental design

The mechanistic analysis as well as management of chemical pollution requires effect thresholds as markers for unwanted adverse effects. Such thresholds can be determined by gradient exposure such as a dose-response analysis. Especially when working with destructive snapshot methods such as omics-technologies, where continuous measurement of *in-vivo* responses is impossible, gradient analysis can provide a suitable method for mechanistic understanding (see **chapter 1.5**). Focusing on response patterns along driver gradients rather than exploring differences among treatment groups can capture non-linear cellular responses and help to determine causality between observed responses (Kreyling et al., 2018). In contrast, replicated designs test the difference between limited numbers of groups (e.g. exposure concentrations), which allows quantification of statistical variation.

According to the PICT-methodology, this experiment was divided in two phases, a selection phase with replicated design and a detection phase with gradient design (**Figure 5**). The selection phase comprises the cultivation and chronic exposure of half of the biofilm cultures. Chronic exposure was designed to model a polluted site, where a contaminated community is formed by pollution induced succession. In contrast, the other half of the microcosms was not polluted, thus creating a reference community. Cultivation was carried out under constant conditions (**Annex 1**), whereas the medium (water from a nearby river) was exchanged weekly to guarantee sufficient supply of nutrients and a diverse set of inoculating organisms.

In the detection phase, contaminated and reference communities were short-term exposed to the selecting stressor, using a dose-response design. This gradient exposure ranged from 0.0001 to 100 $\mu\text{g L}^{-1}$ diuron and was designed to range from no measurable effects to a maximum inhibition of the photosystem. The acute exposure should reveal an altered stress response of the two communities due to the different exposure histories of the communities. In the detection phase, communities were exposed for 1 h, which was proven sufficient for diuron to reach the target site (< 5 min) in biofilms (Morin et al., 2018). Upon the arrival at the target-receptor, a multistage toxicodynamic process is initiated, covering early (primary) and late stage (secondary) effects. By limiting the exposure time to 1 hour, the primary effects of diuron were addressed.

This multi-phased exposure design addresses adaptation by comparing the acclimatory responses of the two communities. In this experiment, the acclimation effort of the reference communities corresponds to the non-adapted response which is assumed to be MoA specific. Contrary, the contaminated community refers to the adapted response. However, specific adaptations only become apparent in the difference between the acclimation responses of these two communities. Therefore, in this thesis, **any difference in response between communities is referred to as adaptation and it is assumed to have a genetic background.**

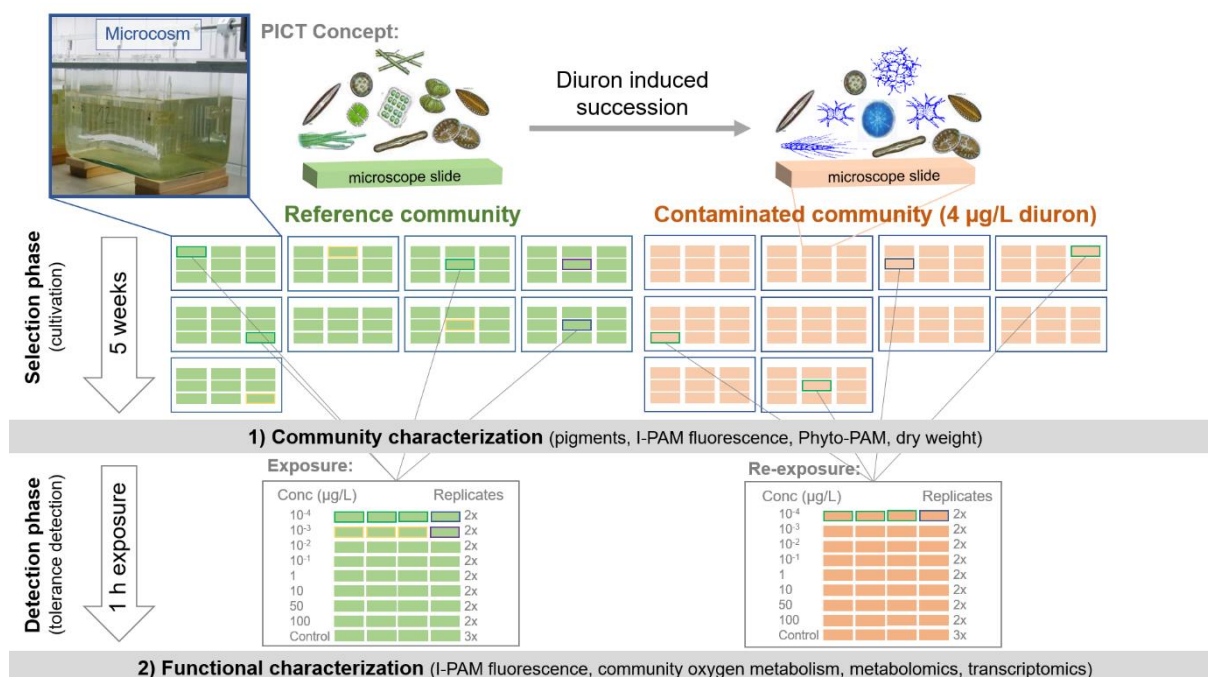


Figure 5 Graphical representation of the experimental design and the PICT concept. The first panel shows the selection phase, in which half of the microcosms were contaminated with 4 µg L⁻¹ diuron. The second panel illustrates the detection phase, where both communities were challenged with a diuron concentration gradient. The sampling procedure is explained in the center of the lower panel.

3. Structural and physiological changes in microbial communities after chronic exposure - PICT and altered functional capacity

3.1 Introduction

Pollution induced community tolerance (PICT) is a tool to infer chemical-induced alterations in a microbial community that translate into tolerance (Blanck & Wängberg, 1988). But before PICT is detectable, biofilms undergo adaptation and selection processes induced by chronic exposure. These processes bring about structural and physiological changes, which finally translate into the function a community supports in an ecological context. Tolerance is usually addressed by assessing an integrative physiological or functional parameter, such as photosynthetic yield (McClellan et al., 2008), b-glucosidase activity (Corcoll et al., 2014), respiration (Tiili et al., 2011) or primary and secondary production (Blanck, 2002) in acute short-term exposure experiments. Ideally, the selection of this integrating metabolic parameter should correspond to the MoA of the respective chemical, as this provides the highest sensitivity for the tolerance detection. Increased tolerance may stabilize a physiological or functional parameter against chemical stress (Tiili et al., 2016), but as noted above, PICT is also associated with structural changes. However, structural changes can be associated with costs and therefore reduce the net output of a community function.

Community structure is determined by taxonomic composition of biofilms, or by a proxy such as a genetic or biochemical fingerprint. The tools for assessing structural community changes vary in effort and significance and range from classical taxonomic analyses to chemotaxonomy and genetic methods. Porsbring et al. (2007) suggested HPLC-based chemotaxonomy of community pigment profiles as robust measure to assess community shifts after toxic exposure. This method combines two major advantages, such as the quantification of the autotrophic part of the community by chlorophyll a, which is a highly conserved component of the photosystem of a vast majority of microalgal species and the qualitative assessment of the community composition based on marker pigments. Marker pigments such as chlorophyll b, fucoxanthin or divinyl chlorophyll a' have evolved in distinct algal lineages, as a consequence of endosymbiosis (Jeffrey et al., 2011) and can be used to estimate community composition quantitatively. However, concentrations of pigments and pigment ratios are also altered in response to environmental factors, such as changes in light, temperature or even chemical stressors (Schlüter et al., 2000; Southerland &

Lewitus, 2004). This alteration must be addressed by controlled experimental conditions or adequate referencing so that pigment analysis as a surrogate for shifts in community structure is indicative for stressor effects. When appropriate referencing is considered, the sensitivity of pigments to environmental factors can become a valuable asset that can be used to characterize the physiological state of autotrophic organisms. This potential was used, for example, to investigate the effects of polycyclic aromatic hydrocarbons on phytoplankton (Southerland & Lewitus, 2004).

Community functions of biofilms are determined by the metabolic processes of their taxonomic components (see **chapter 1.4**). An essential function of freshwater biofilms is primary production (Battin et al., 2016), which is particularly significant in well-illuminated streams as it relies on the process of photosynthesis. Chronic exposure to agricultural herbicides can pose a risk to this function (Pesce et al., 2022) and thus to overall ecological functioning. Photosynthetic pigments can also facilitate the analysis of photosynthetic processes by means of *in-vivo* fluorescence. Here, fluorescence is used as marker for the efficiency of photochemistry by pulse-amplitude-modulation technique (Schreiber et al., 1986). This fluorescence data is converted into the photosynthetic yield, a direct measure of photosynthetic functioning. Photosynthesis-related endpoints like the photosynthetic yield and chlorophyll a have been shown to be sensitive in detecting chronically exposed biofilms (e.g. Ricart et al., 2009). A direct proxy of oxygenic photosynthesis is the monitoring of dissolved oxygen as a waste product of the process. In conjunction with community respiration, oxygen metabolism is a useful estimate of primary production and trophic conditions in the community.

The structural and functional characterization of biofilms undergoing chronic diuron exposure has a long tradition (McClellan et al., 2008; Molander & Blanck, 1992; Pesce et al., 2006; Pesce et al., 2010; Ricart et al., 2009; Tlili et al., 2010; Tlili et al., 2008). In many of these studies PICT was proven, however implications for community functions like primary production have hardly been studied. This chapter examines the structural and functional changes associated with chronic diuron exposure, with particular attention to the role of tolerance in stabilizing community functioning and addresses hypothesis H1 and H2 from the overall hypothesis of this thesis (**Chapter 2**). The following questions will be specifically addressed.

- I) Is there a toxicant-induced succession in the structure of chronically exposed communities?

- II) Does chronic exposure alter physiological processes related to the function of primary production?
- III) Does chronic exposure affect primary production and does tolerance stabilizes this function against repeated exposure?

3.2 Methods

3.2.1 Biofilm cultivation

Cultivation and chronic exposure of periphyton was performed for five weeks in 20 L glass microcosms. The inoculum was taken from a local stream (see **Annex 1** for more details). Periphyton was grown on microscope glass slides as artificial substrate for five weeks and half of the microcosms were contaminated with $4 \mu\text{g L}^{-1}$ diuron, starting from the second week of cultivation. The addition of diuron should induce the growth of contaminated communities, whereas the uncontaminated microcosms represent the reference communities. The inoculum and exposure concentration of diuron were renewed by weekly water exchange. A monitoring of the diuron chronic exposure confirmed a mean concentration of $3.4 \pm 1.0 \mu\text{g L}^{-1}$ before and $4.0 \pm 0.9 \mu\text{g L}^{-1}$ after the diuron addition (see **Annex 13 A**). Before tolerance analysis, periphyton slides from parallel microcosms were used for an initial characterization of the communities.

3.2.2 Dry weight and autotrophic index

The dry weight was analyzed from each community using 57 replicates each. The communities were snap-frozen in liquid nitrogen and freeze dried for 24 hours. The biofilm was scrapped off the glass surface and weighed immediately. The dry weight was used to calculate the autotrophic index, a ratio of chlorophyll a and dry weight that indicates the relative abundance of autotrophic species in biofilms.

3.2.4 Pigment analysis of periphyton

A non-invasive pigment assessment (*in-vivo*) was conducted using the multi-wavelength pulse-amplitude modulation technique (PAM), and an *ex-vivo* analysis was compiled using a high-pressure liquid-chromatography system (HPLC).

3.2.4.1 *In-vivo* pigment analysis for community characterization

A fiber chlorophyll fluorometer PHYTO-PAM equipped with an Emitter Detector Fiberoptics Unit PHYTO-EDF (Heinz WALZ GmbH, Effeltrich, Germany) was used to analyze the periphyton component of the biofilms. The emitter-detector features four different LED excitation wavelengths (435, 500, 550 and 630 nm) and one actinic light source (660 nm) for simultaneous excitation and deconvolution of algae groups. The (default) reference excitation spectra of the species *Anacystis nidulans*, *Ankistrodesmus braunii* and *Phaeodactylum tricornutum* was used for deconvolution between cyanobacteria, chlorophytes and diatoms. Those algae groups differ substantially in the absorbance spectra of their antenna pigments. Thus, the total fluorescence was deconvoluted into relative portions of phytoplankton groups. A quantification of deconvoluted fluorescence to chlorophyll concentrations (as marker of biomass) is inappropriate for a multi-species community, as the fluorescence method is not specific to chlorophyll, but rather a measure of the concentration of all antenna pigments that participate to energy transfer. Therefore, chlorophyll conversion requires specific calibration factors covering the relative chlorophyll content of a reference species.

Algal class composition of the reference and contaminated community was analyzed on 19 slides each. Periphyton was dark-acclimated for three minutes and acclimated to the measurement light for one minute. Then, the automatic gain control was performed and a measuring frequency of 32 (PAR: 20 $\mu\text{mol m}^{-2}\text{s}^{-1}$) was used. The fiber-optic sensor (\varnothing 4 mm) was positioned within a distance of 1 to 2 mm above the biofilm surface and pigment fluorescence was determined at three points across each slide

3.2.4.2 *In-vivo* pigment analysis based on Imaging-PAM fluorometry

The photochemical quantum yield of photosystem II (PS II) in periphyton was measured with an Imaging-PAM M-series chlorophyll fluorometer equipped with LED-Array illumination unit (IMAG-MAX/L, 450 nm, WALZ GmbH, Effeltrich, Germany) and a CCD camera (IMAG-K6, WALZ GmbH, Effeltrich, Germany). The method is based on pulse-amplitude modulation (PAM) (Schreiber et al., 1986), which measures light utilization of the available PS II acceptor pool by fluorescence emission. Due to the discovery of the dark-light induction effect, called the "Kautsky effect" (Kautsky, 1931),

the yield analysis can be performed at different physiological states. The authors found that after dark acclimation, the PS II must rearrange the electron-accepting reaction centers and the transport chain for photochemical quenching, and during this process incident light quanta are re-emitted as fluorescence. The dark-adapted state is characterized by a fully oxidized acceptor quinone (Q_A) and the absence of a proton gradient in the thylakoids, which maximizes photochemical quenching (Schreiber, 2004). The photochemical quantum yield after dark acclimation is termed 'optimal quantum yield' ($\Phi_{II \max}$), which was defined by Genty et al. (1989) as [1].

$$\Phi_{II \max} = \frac{(F_m - F_0)}{F_m} \quad [1]$$

F₀ is defined as base fluorescence intensity of chlorophyll at a low, non-actinic measuring light. F_m is the maximum fluorescence induced by a saturation pulse. This pulse is a short but strong flash of light (PAR > 1250 $\mu\text{mol m}^{-2}\text{s}^{-1}$) that completely reduces Q_A, but at the same time is too short for photochemical metabolization (Maxwell & Johnson, 2000). Thus, the pulse is emitted as fluorescence, which is a proxy for the maximum quantum yield of the energy conversion in PS II. From these parameters, $\Phi_{II \max}$ can be defined as a (relative) measure of the maximal quantum yield of PS II. In this experiment $\Phi_{II \max}$ was estimated after five minutes of dark acclimation.

During the illumination state, photochemical quantum yield is lowered due to closed reaction centers (the electron acceptor plastoquinone Q_A is "occupied") and by stimulated heat release (increased non-photochemical quenching). This yield is termed 'effective quantum yield' (Φ_{II}) and is defined by Genty et al. (1989) as [2].

$$\Phi_{II} = \frac{(F_m' - F)}{F_m'} \quad [2]$$

Thus, Φ_{II} measures the proportion of the light absorbed by chlorophyll for photochemistry. The parameters are very similar to [1], where F is the chlorophyll fluorescence under actinic illumination of 111 $\mu\text{mol m}^{-2}\text{s}^{-1}$ in this study (the state of reduced electron acceptor quinones). Again, F_m' is maximal fluorescence yield after the application of a saturation pulse, but under illuminated conditions. In summary, Φ_{II} measures the fraction of light effectively used by chlorophyll of PS II for photochemistry. The biofilms were acclimated to light for 5 minutes, before the Φ_{II} measurement started.

3.2.4.3 *In-vivo* pigment fluorescence for tolerance detection

Both photochemical quantum yields were measured twice, after the selection phase of reference conditions or chronic exposure (t_0) and after the acute exposure (t_{1h}) in order to reveal a potential PICT. The acute exposure was performed for 1h in a concentration gradient ranging from 0.0001 to 100 $\mu\text{g L}^{-1}$ (dilution factor 10). The slides were placed in 500 mL petri dishes containing equilibrated diuron solution and controls were triplicated, the exposed samples duplicated. The exposure conditions were consistent to the selection phase using a phytotron (MultitronPro, IFORS, Einsbach, Germany). Diuron exposure concentrations of the detection phase were monitored by LC-MS/MS (see **Annex 13 B**). The exposure concentrations 0.0001 and 0.001 $\mu\text{g L}^{-1}$ were superposed by the background concentration of diuron and showed additional high variation. The dosing required DMSO as solvent and the spiked amount was kept below 0.25%, which is supposed not to cause effects to biofilms (McClellan et al., 2008).

The relative inhibition of the PSII yield was calculated by comparing both measurements according to:

$$\text{Inhibition (\%)} = 100 - \frac{100 * \Phi_{t1h}}{\Phi_{t0}} \quad [3]$$

The inhibition data was modelled using a four-parameter log-logistic function [4] of the R package 'drc' version v3.0-1 (Ritz et al. 2015).

$$f(x) = c + \frac{d - c}{1 + e^{b * (\log(x) - \log(e))}} \quad [4]$$

The parameters c and d were fixed and determine the minimum (0) and maximum (100) range of the model, b is the slope and e is the model inflection point. The inflection point corresponds to the half-maximum inhibitory concentration (in case of fixation of the parameters c and d to 0 and 100, respectively) (EC_{50}).

Moreover, a benchmark dose (BMD) was calculated for the inhibition of the photosynthetic yield of each community using the automatized dose-response modelling R package 'DRomics' version 2.2 (Larras et al., 2018; Muller et al., 2021). A BMD represents the concentration that causes an effect different from the control, taking into account the residual standard deviation of the fitted dose-response model.

For increasing the significance of the BMD, a multiplication factor can be used for the residual standard deviation. In this thesis a factor of 1 was applied.

3.2.4.4 *Ex-vivo* pigment analysis by high-pressure liquid-chromatography

The pigment composition of 12 slides of the contaminated and 21 slides from reference communities was analyzed. The pigments were extracted and analyzed according to a modified protocol of Woitke et al. (1994). Periphyton was scraped off the slides, filtered onto a glass microfiber filter (LABSOLUTE, 1.20 µm, 47 mm), placed in 90 % acetone, sonicated for four minutes at 56 °C and subsequently frozen at - 80 °C for 10 h. The extracts were filtered (Spartan 13/0.2 RC, Schleicher & Schuell, Dassel, Germany) and the extraction was repeated on the residual biomass. The extracts were analyzed on a high-pressure liquid chromatography system (HPLC BIO-TEK Kontron) equipped with a C18 RP column (Knauer; Superspher; 250 x 4 mm) coupled to a diode array detector. The injection volume was 30 µL, the flow rate 1 mL and the quantification of the pigments was performed at 430 nm. A polarity gradient from the polar IPR eluent to acetone:acetonitrile was applied along the 34-minute run (see **Table 1** for more information). Identification and quantification of pigments was performed using the reference standards chlorophyll a, chlorophyll b, β-β-carotene, chlorophyll c2, alloxanthin, lutein, echinenone, monadoxanthin, neoxanthin, fucoxanthin and zeaxanthin (DHI LAB Products, Denmark). To overcome retention time shifts, a relative retention time with respect to chlorophyll a was calculated, which facilitated pigment alignment across the different samples. The repeated extractions were aggregated (in peak area and quantified concentration) in the aligned data and normalized to the chlorophyll a content of the sample (as proxy of biomass). The aggregated and normalized peak area data was subjected to a principal component analysis with `prcomp()` including the center and scaling option and visualized using the 'factoextra' R package v1.0.7 (Kassambara & Mundt, 2017). The quantified pigment content was used for ratio calculation of marker pigments (see **Annex 12**). In addition, the chlorophyll-a content was used to calculate the autotrophy index. To this end, the quantified chlorophyll a content was divided by dry weight.

Table 1 Settings of HPLC pigment analysis.

Parameter	Settings			
Eluent A (8.316 g ammonium acetate, 1.62 g tetrabutylammonium acetate, 216 mL water (HPLC-grade), 384 mL methanol, 1400 mL acetonitrile)	Time [min]	Eluent A	Eluent B	Eluent C
	1	100 %	-	-
	2.5	50 %	50 %	-
	9.5	25 %	70 %	5 %
	15.5	-	59 %	41 %
	20.5	-	29 %	71 %
Eluent B (10 % acetone, 90 % acetonitrile)	25.5	-	-	100 %
	34	Acquisition Off		
Eluent C (80 % acetone, 20 % acetonitrile)				
Runtime	40 min			
Injection volume	30 µL			
Flow rate	1 mL min ⁻¹			
Temperature	25 °C			
DAD Channel for integration	430/5			

3.2.5 Community oxygen metabolism measurements

Community oxygen metabolism was measured in 40 mL custom-made borosilicate glass containers. The containers were placed in an incubator (MultitronPro, IFORS, Einsbach, Germany) at 200 RPM and a biphasic illumination regime. During the first phase light was switched off for six hours (dark phase), afterwards biofilms were illuminated at 150 μ mol m⁻² s⁻¹ for two hours (light phase). Dissolved oxygen concentrations were monitored every minute by an optical oxygen meter (FSO2-C4, Pyroscience, Germany) and contactless oxygen sensor spots (OXSP5, Pyroscience, Germany), which were glued to the inner surface of the glass container. Alterations in water temperature were compensated by a temperature probe (TSUB21-NC, Pyroscience, Germany). The containers were filled with sterile-filtered river water which was spiked with 0.01, 10, 100 μ g diuron L⁻¹ or was left unpolluted. The containers were filled below water surface to avoid air pockets. The obtained data was converted to absolute oxygen values by multiplying the chamber volume to carbon equivalents by the atomic mass factor 0.375 and converted to carbon turnover rates by the R function diff(). The factor derives from the stoichiometric ratio of oxygen and carbon in photosynthesis and aerobic respiration. A lag phase of one hour in the dark phase and 30 minutes in the light phase was chosen to guarantee a linear trend in the measurements. All values beyond the lag phase were averaged, and measurements during the dark phase determined community respiration (Resp) in the same way the

light phase represented net primary production (NPP). The ratio of respiration and net primary production reflects the productivity of the community and can be considered an indicator of autotrophy. The parameters Resp and NPP represent the net functional output of the community, whereas normalization to biomass units (e.g. dry weight or chlorophyll a content) captures specific oxygen metabolism. Normalization accounts for chronic effects on biomass and facilitates uncovering potential tolerance benefits.

3.3 Results and discussion

3.3.1 Comparison of the structural community parameters

Structural parameters indicated a clear difference between reference and contaminated communities after four weeks of exposure. Biomass (dry weight) was significantly reduced ($p < 0.001$) to $2.2 \pm 0.7 \text{ mg cm}^{-2}$ in the contaminated community, compared to $3.3 \pm 1 \text{ mg cm}^{-2}$ in the reference. The deconvolution of the multi-wavelength *in-vivo* pigment fluorescence analysis into algal classes indicated a significant shift in contaminated periphyton with an increase in chlorophytes ($p < 0.05$) and decrease in diatoms ($p < 0.001$) (**Figure 6**). The relative abundance of cyanobacteria remained unchanged.

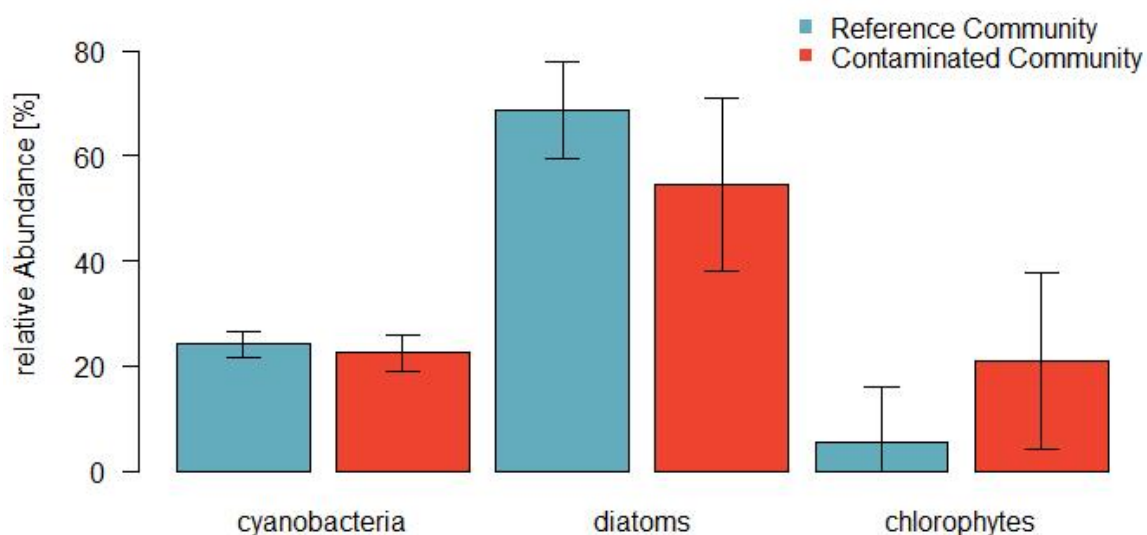


Figure 6 Relative community composition based on *in-vivo* pigment analysis by PHYTO-PAM fluorescence measurements after 5 weeks of exposure to diuron.

The HPLC pigment analysis revealed 17 pigments, whereas 13 could be identified based on reference substances. The most essential photosynthetic pigment, chlorophyll a, showed a significant difference ($p < 0.001$) among the communities with $3.5 \pm 1.9 \mu\text{g cm}^{-2}$ in the reference and $1.0 \pm 0.5 \mu\text{g cm}^{-2}$ in the contaminated one. The specific chlorophyll a content matched this decline ($p < 0.001$) with $5.2 \pm 3.4 \text{ ng mg}^{-1}$ DW in the reference and $2.1 \pm 1.3 \text{ ng mg}^{-1}$ DW in the contaminated community. This reduction indicates a general loss of autotrophic biomass from the biofilm community as a result of chronic exposure. Other studies have shown that low doses of diuron of $1 \mu\text{g L}^{-1}$ can also induce the chlorophyll a content or biomass, which indicates a hormesis effect or a 'shade-adaptation' (Ricart et al., 2009; Tlili et al., 2008). During shade-adaptation, an increased amount of chlorophyll is observed in the cells, which is interpreted as a compensatory mechanism for the diuron effect. A hormetic response was also observed by Molander and Blanck (1992), who found a stimulation of marine periphyton at diuron concentrations below PICT was initiated. Based on the reduction of chlorophyll a and biomass it can be concluded that in this study the intensity of the stressor during chronic exposure may have exceeded the cellular threshold for hormesis or shade-adaptation and triggered a toxicant-induced selection of species in the biofilm.

Moreover, a principal component analysis of the normalized pigment data revealed a toxicant-induced pigment pattern (**Figure 7**). The first three components explained 69 % of the variance and the community pattern was very distinct on these components. The first principal component explained about 33 % of the variance in the data and was mainly constructed from the pigments echinenone, beta-carotene, chlorophyll b, lutein, neoxanthin, zeaxanthin and two unknown pigments. The pigments lutein, chlorophyll b and neoxanthin are predominantly found in the green lineage of algae and lutein is a particular marker pigment of chlorophytes (**Annex 12**). A significant increase ($p < 0.01$) in the lutein:chl a ratio from 1.8 %_{Chla} in the reference to 3.4%_{Chla} in the contaminated community was observed. Also the chlorophyll b:a ratio increased in a similar manner, albeit the increase (4.9 %_{Chla} to 8.5 %_{Chla}) was not significant. In agreement with the *in-vivo* pigment analysis, PC1 shows an increase in green algae content that occurred in response to chronic exposure. The pigments chlorophyllide a, fucoxanthin, chlorophyll-c2 and diadinoxanthin significantly contributed to the second principal component. The latter three pigments occur preferentially in diatoms, with fucoxanthin and diadinoxanthin as marker pigments for

this group of algae. For this reason, PC2 is considered to be relevant in indicating changes in the diatom fraction in the community. A slight reduction in the fucoxanthin:chl a and diadinoxanthin:chl a ratio was observed in the reference community (34 %Chla and 6 %Chla) towards the contaminated community (32 %Chla and 5 %Chla). Thus, chronic exposure reduced relative diatom abundance in the contaminated community. In accordance to these findings previous microcosm experiments demonstrated that chronic exposure to diuron at environmental realistic concentrations (0.08 to 2 $\mu\text{g L}^{-1}$) can affect the photoautotrophic composition of the community by lowering the diatom abundance and their biovolume (McClellan et al., 2008; Ricart et al., 2009). Even short pulses of 48 hours of diuron at 13 $\mu\text{g L}^{-1}$ were shown to affect the diatom abundance by inducing diatom mortality up to 79 % (Proia et al., 2011).

The third PC explained 12.3 % of the variance and was dominated by the pigments neoxanthin, violaxanthin, chlorophyll-b, zeaxanthin and the unknown carotenoid. The violaxanthin:chl a ratio differed significantly ($p < 0.001$) between the communities, with 2.5 %Chla in the reference and 3.6 %Chla in the contaminated community. No difference was found for neoxanthin and zeaxanthin. However, the loading vector of zeaxanthin and violaxanthin points in opposing directions, suggesting a counteracting effect in these pigments. The pigments violaxanthin and zeaxanthin are the main pigments of the xanthophyll cycle, which is one of the most important photoprotection mechanisms in green algae and vascular plants (Goss & Jakob, 2010). Violaxanthin is located nearest to the special chlorophyll a in the reaction center of the antenna and only violaxanthin is able to transfer a photon to the special chlorophyll a (Baker, 2008). The conversion of violaxanthin to zeaxanthin minimizes the amount of energy reaching the reaction center and stimulates energy dissipation within the light- harvesting antenna proteins through non-photochemical quenching. The xanthophyll cycle contains two conversion steps that convert violaxanthin to zeaxanthin via ascorbate as co-substrate (Hager, 1969). The violaxanthin:zeaxanthin ratio (normalized to chl a) in the communities indicates a higher amount of violaxanthin in the contaminated community (1.5) compared to reference (0.9). The increased amount of violaxanthin (**Annex 8**) in the contaminated community could indicate an improved energetic balancing mechanism between the absorption of light and the impaired electron transport (Latowski et al., 2011).

The results based on HPLC-based analysis of community pigment profiles confirmed toxicant-induced shifts in the autotrophic composition of biofilms on a qualitative and quantitative basis. Moreover, the pigment pools involved in the xanthophyll cycle revealed information on the physiological status of the photosystem (Latowski et al., 2011), indicating that the contaminated community has adapted to the chronic diuron exposure. This confirms the findings of Porsbring et al. (2007), who found that community pigment profiling is able to distinguish between different communities with a resolution similar to microscopic species counting, and demonstrated the added value of pigments for gaining insights into physiological status of a community. The authors observed changes in the proportions of diadinoxanthin and diatoxanthin related to diatom xanthophyll cycle, after igarol (another PSII) inhibitor was applied. Unfortunately, diatoxanthin was not identified in this thesis and the exploration of the xanthophyll cycle in diatoms remains a future perspective.

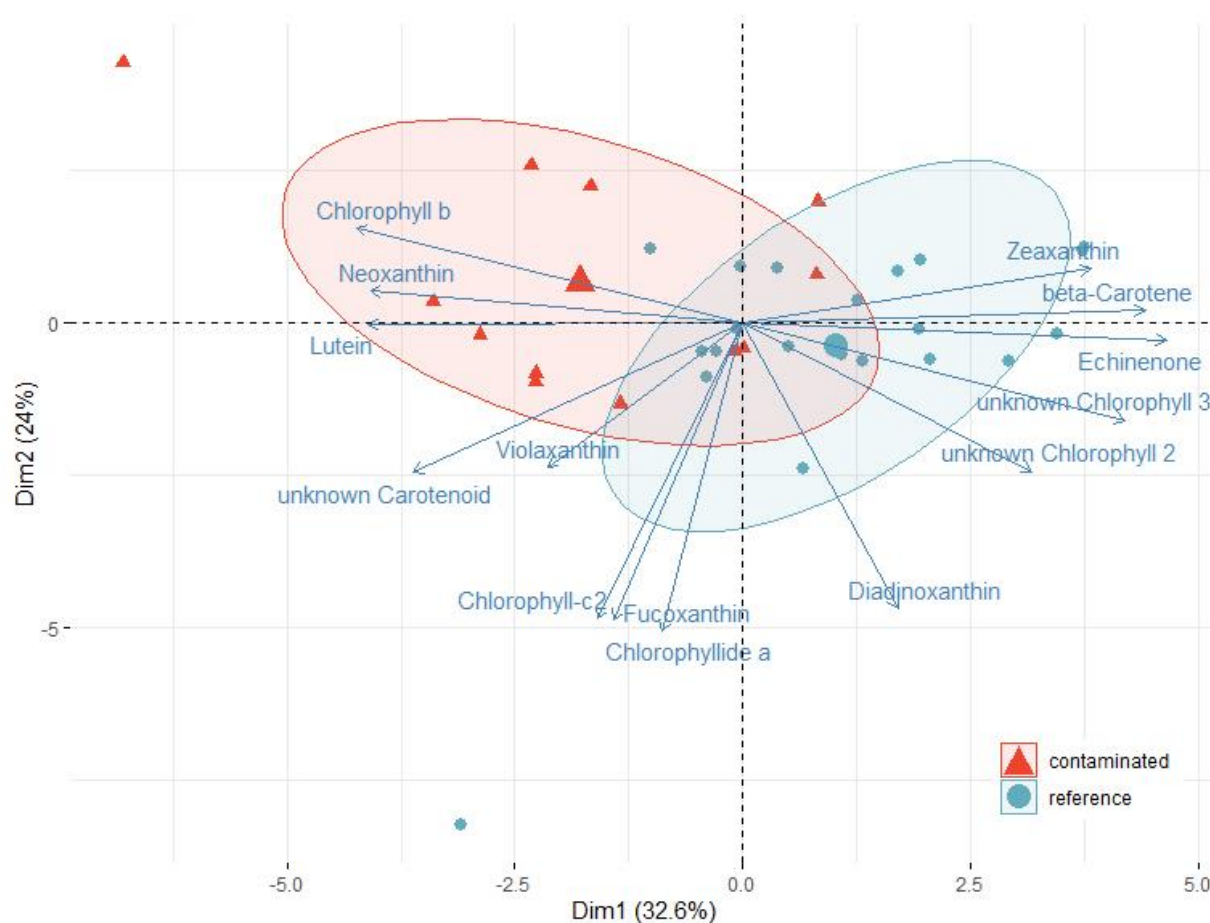


Figure 7 Principal component analysis of the pigment content (normalized to chl a). The PCA scores of the samples are plotted by circles (reference) and triangles (contaminated) and the loadings (arrows) indicate how strongly each pigment affects the principal components.

3.3.2 Photosynthetic activity and primary production of the communities after selection phase

The optimal quantum yield ($\Phi_{II\ max}$) of the reference communities ranged at 0.46 ± 0.04 , whereas the level of the contaminated communities was significantly ($p < 0.001$) lower at 0.36 ± 0.06 . The effective quantum yield (Φ_{II}) under illumination conditions also differed ($p < 0.001$) with 0.27 ± 0.03 for the reference and 0.23 ± 0.02 for contaminated community. In both states the yield of the contaminated communities was 20 % percent below the reference communities, indicating an adverse effect of chronic diuron exposure on the photosynthetic capacity. $\Phi_{II\ max}$ is determined by physiological conditions and taxonomic identity, but a value of ~ 0.8 for healthy plant leaves (Schreiber, 2004), ~ 0.6 for the green algae culture *S. vacuolatus* and 0.4 to 0.3 for autotrophic biofilms can be assumed (Tlili et al., 2020), thus the measured $\Phi_{II\ max}$ values, found in this study are characteristic for biofilms.

Under laboratory conditions, there is a linear correlation between the Φ_{II} and CO_2 assimilation (Fryer et al., 1998; Sjollema et al., 2014) or algal growth rate (Magnusson et al., 2008). However, $\Phi_{II\ max}$ and Φ_{II} are relative measures of light conversion that do not allow any quantifiable prediction on primary production. For more detailed assessments of the function of the communities in primary production, oxygen metabolism was measured in gas-tight containers. As described in **chapter 3.2.5**, the oxygen data was analyzed with respect to the net output of the communities (e.g. $Resp_{tot}$ or NPP_{tot}) and normalized to dry weight (NPP_{DW}) or chlorophyll ($NPP_{chl a}$). Normalization accounted for chronic effects on biomass and facilitated uncovering potential tolerance effects.

Overall respiration of the communities was comparable, while normalization to biomass (dry weight) revealed twice as much respiration in the contaminated community (**Table 2**, initial measurements). A similar result was found for NPP_{tot} , where the reference community had a slightly higher rate of $287.2\ \mu g_C\ cm^{-2}\ d^{-1}$ compared to $266.1\ \mu g_C\ cm^{-2}\ d^{-1}$. Normalization of NPP_{tot} resulted in a higher specific NPP of the contaminated community of 140 % for NPP_{DW} and 120 % for $NPP_{chl a}$ higher compared to the reference community. The $NPP:Resp.$ ratio showed a higher autotrophy of 24.5 in the reference compared to 17.9 in the contaminated community. In summary, both NPP_{tot} and $NPP:Resp$ ratio were higher in the reference community, suggesting a decrease in autotrophy in the contaminated community. The increase of NPP_{DW} and NPP_{Chla} in the contaminated community may indicate the acquisition of

tolerance at the expense of overall productivity. However, a causal relationship between the tolerance gained after chronic exposure and primary production can only be established under re-exposure to diuron, which is assessed in the following section.

3.3.3 Acquisition of photosynthetic tolerance

A short-term exposure to diuron of 1 h (detection phase) was performed to investigate tolerance to diuron originating from the selection phase. The quantification of tolerance was performed using an endpoint close to the MoA of diuron by measuring the inhibition of the photochemical quantum yield of PS II. Towards this end, a gradient of diuron concentrations ranging from 0.001 to 100 $\mu\text{g L}^{-1}$ was applied to the communities. The diuron concentration causing 50 percent inhibition in $\Phi_{\text{II max}}$ was 44 $\mu\text{g L}^{-1}$ in the contaminated and 15 $\mu\text{g L}^{-1}$ in reference communities (**Figure 8**). The confidence intervals of both curves diverged at 6 $\mu\text{g L}^{-1}$, and a significant difference of the EC_{50} values is demonstrated. The benchmark dose-1SD (BMD) for the inhibition of $\Phi_{\text{II max}}$ derived by 'DRomics' revealed a diuron threshold of 1.8 $\mu\text{g L}^{-1}$ for the reference and 4.4 $\mu\text{g L}^{-1}$ for the contaminated communities. This threshold expresses the concentration at which the treatment effect becomes distinguishable compared to the control, based on one standard deviation as the confidence interval. This shows that the contaminated communities required at least 4 $\mu\text{g L}^{-1}$ diuron for showing an effect, which corresponds to the diuron level they were exposed during chronic exposure. The 100 $\mu\text{g L}^{-1}$ diuron treatment caused inhibition of $\Phi_{\text{II max}}$ up to 74 % and Φ_{II} of 90 %. The PS II includes a fraction of unconnected Q_A plastoquinones that were shown to be insensitive to diuron (Lavergne & Briantais, 1996), thus no inhibition is possible. In contrast to $\Phi_{\text{II max}}$, the inhibition of Φ_{II} does not differ between communities, indicating that no tolerance induction has taken place. This result is discussed with regard to possible measurement errors in F_m and F_m' the following section.

The threefold increase in the diuron tolerance threshold in the $\Phi_{\text{II max}}$ of the contaminated communities underpins the development of PICT. A similar increase of diuron tolerance was documented in a comparable setting using $\Phi_{\text{II max}}$ (Tlili et al., 2010) and Φ_{II} (McClellan et al., 2008). A much higher tolerance was detected in a contaminated river ($\Phi_{\text{II max}}$ EC_{50} up to 500 $\mu\text{g L}^{-1}$), however there was no uncontaminated reference biofilm grown for comparison (Pesce et al., 2010). The high tolerance in natural streams might result from the continuous inoculation with a diverse

set of species, while in microcosm studies the inoculum is renewed to a much lesser extent. Thus less species potentially more tolerant are available during the process of toxicant-induced succession.

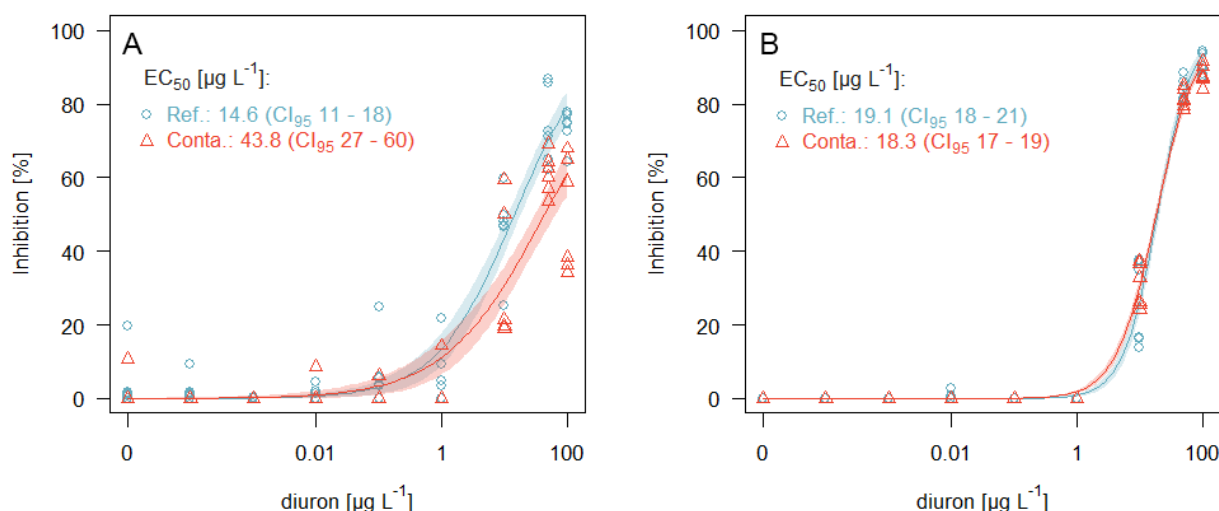


Figure 8 Inhibition of the photochemical quantum yield of photosystem II after 1 h of diuron exposure. **A)** Inhibition of optimal quantum yield ($\Phi_{II \max}$) of dark-adapted biofilms and **B)** effective quantum yield (Φ_{II}) at constant illumination. The x axis is displayed on log scale. The models were computed with a confidence level of 95 % and the CI is provided in brackets.

Both yields have different significance for determining tolerance based on the physiological state they cover. Diuron tolerance manifested in optimal quantum yield ($\Phi_{II \max}$), which requires a photosystem adapted to darkness. At this state the photosystem is in resting mode, the electron transport chain has run empty and the primary electron acceptor plastoquinone Q_A is assumed to be fully oxidized (reaction centers ‘open’). In the presence of diuron, electron transfer at plastoquinone Q_A to Q_B is blocked (effect size depends on amount of substance), which affects the Q_A re-oxidation (Schreiber et al., 2007). The basal chlorophyll fluorescence F_0 in the reference communities increased from their initial state (after chronic exposure) to $50 \mu\text{g L}^{-1}$ diuron by a factor of 1.7 and compared to $100 \mu\text{g L}^{-1}$ diuron exposure by 2.5 times. In contrast, F_0 fluorescence in the contaminated communities maximally increased by factor of 1.5 under the same conditions (**Annex 2**). The F_m fluorescence remained largely unaffected by the acute diuron exposure. In conclusion, the contaminated communities may have acquired a tolerance mechanism to maintain the oxidation status of Q_A , resulting in an F_m and F_0 fluorescence after acute exposure

similar to the original values. The general increase of chlorophyll fluorescence (200 to 500 %) at higher diuron concentrations is a typical phenomenon of PSII-specific inhibitors (Schreiber et al., 2007). A study of Kim Tiam et al. (2015) confirms the observed increase in F_0 fluorescence for chronically exposed biofilms, however the authors did not test for a tolerance mechanism using the PICT concept. McClellan et al. (2008) explored the temporal dynamic in the F_0 fluorescence of polluted and unpolluted biofilms, found an increase in F_0 fluorescence in the polluted biofilms from 5 weeks on and related the different F_0 fluorescence to tolerance. Unfortunately, the authors did not show the F_0 fluorescence of the acute exposure in the detection phase, with the result that the F_0 values from **Annex 2** cannot be compared.

In contrast, this indicative quality disappeared with illumination. At illuminated conditions, the plastoquinone Q_A pool is reduced by photochemical electron transfer and, in case the sample is exposed, also by the effect of diuron. Again, F fluorescence of the reference and contaminated communities increased in a similar manner to F_0 . However, compared to the dark-adapted condition, also the maximum fluorescence F_m' intensified after the saturation pulse, particularly in the reference communities (**Annex 4**). At the $100 \mu\text{g L}^{-1}$ diuron treatment F_m' of the reference communities even increased to the initial F_m , which compensated the effect in F_0 and resulted in similar effective quantum yields (Φ_{II}) across the communities. In the physiological normal state, the value of F_m decreases towards F_m' by non-photochemical quenching (like heat dissipation) (Schreiber, 2004). Since the F_m' was not supposed to be influenced by the acute chemical exposure, Φ_{II} was not considered in the tolerance analysis (cf. Schreiber et al., 2007 Fig. 3 C).

3.3.4 Primary production at exposure conditions

The tolerance induction in $\Phi_{II \max}$ in the contaminated community raises the question if primary production as the key function of autotrophs benefits from an improved energy supply under short-term diuron conditions. Towards this end oxygen metabolism of the reference and contaminated communities was monitored at 0.01 , 10 and $100 \mu\text{g L}^{-1}$ diuron exposure and compared to the initial measurement (**chapter 3.3.2**) after the selection phase. Again, the overall and the specific (per biomass unit) oxygen metabolism was examined.

First, community respiration was tracked during a 6 hour dark period (**Table 2**). Overall respiration increased in the reference communities with increasing diuron concentration and remained on a stable level at $10 \mu\text{g L}^{-1}$ and $100 \mu\text{g L}^{-1}$ treatment. In contrast, the respiration of the contaminated communities was already higher than reference in the initial state and only increased at $10 \mu\text{g L}^{-1}$.

Second, community net primary production (NPP) was tracked during a 2 hour light period. NPP_{tot} and NPP_{DW} of the communities showed an increase at $0.01 \mu\text{g L}^{-1}$ and a subsequent concentration dependent decline. Both NPP_{tot} and NPP_{DW} were higher for the reference communities under exposure conditions. The NPP parameters of the contaminated communities ranged between 40 to 90 % of the reference communities and only at $100 \mu\text{g L}^{-1}$ diuron exposure they converged to a similar value. In the $100 \mu\text{g L}^{-1}$ treatment only 3 % of the initial NPP_{tot} was left indicating that photosynthesis of both communities was almost completely inhibited at this concentration. The higher NPP of the reference communities is also evident in the NPP:Resp. productivity ratio, which was always higher in the reference, except when treated with $100 \mu\text{g L}^{-1}$ diuron, which resulted in a similar ratio below 1 in both communities. At the initial state and the $0.01 \mu\text{g L}^{-1}$ treatment, the reference community productivity was more than 20% higher than in the contaminated counterpart and more than 50% at $10 \mu\text{g L}^{-1}$. This indicates an overall higher autotrophy in the reference, which was maintained even under re-exposure to diuron.

In conclusion, tolerance in $\Phi_{\text{II max}}$ did not maintain NPP_{tot} or NPP_{DW} under re-occurring exposure conditions as the NPP parameters of the contaminated community were consistently below the reference. Most striking was the overall NPP loss of the contaminated community at a diuron concentration of $10 \mu\text{g L}^{-1}$. This concentration was still below the respective tolerance threshold of the $\Phi_{\text{II max}}$, but the productivity of the contaminated community was only 40% of the reference.

3.3.5 Tolerance detection in primary production

Normalization of NPP to dry weight may be biased by a variable proportion of autotrophic organisms. Hence, NPP_{tot} was additionally normalized to the chlorophyll a content, which exclusively describes the autotrophic biomass. This normalization revealed that the $\text{NPP}_{\text{chl a}}$ of the contaminated community was higher than in the reference along the entire concentration range of exposure. However, the exposure

time altered the chlorophyll a content, which was determined at the end of exposure. For this reason, the derived $NPP_{chl a}$ for the diuron treatments is biased towards the terminal chlorophyll a amount. Therefore, relative comparisons instead of absolute values were used in the following to derive a general tendency towards tolerance. The lowest diuron treatment slightly stimulated $NPP_{chl a}$ in the reference and contaminated communities to 109 and 115 %, respectively (**Figure 9**). At $10 \mu g L^{-1}$ diuron, 72 % and 62 % inhibition of primary production of reference and contaminated communities was found, and at $100 \mu g L^{-1}$ an inhibition of 90 % was observed. Comparing the inhibitory levels obtained from the optimal quantum yield $\Phi_{II \max}$, a value of $100 \mu g L^{-1}$ diuron is obtained for an equivalent inhibition of 72 % in the reference and $30 \mu g L^{-1}$ for 62 % in the contaminated communities. Hence, community oxygen metabolism was less sensitive than $\Phi_{II \max}$ and the PICT is less pronounced. Moreover, normalization to chlorophyll a was key to the comparability of the communities in terms of tolerance formation.

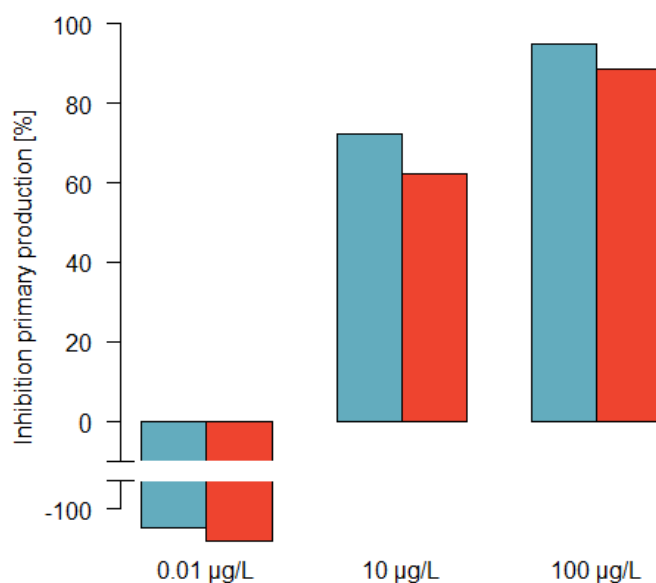


Figure 9 Inhibition of the net primary production normalized to chlorophyll a at different diuron treatments (red contaminated; blue reference communities).

Table 2 Results of the community oxygen profiling in gas-tight containers. The upper part of the table shows respiration and net primary production (NPP) normalized to biomass, which is listed as dry weight (NPP_{DW}) or chlorophyll a (NPP_{Chla}). The lower part with a grey shading displays the unnormalized values. The respiration was monitored for 6 hours and net primary production for 2 hours. For the calculation of the NPP:Resp. ratio the non-normalized values were used.

Parameter		Initial	0.01 µg L ⁻¹	10 µg L ⁻¹	100 µg L ⁻¹
Biomass (DW) normalized	Respiration [µgC mg_{DW}⁻¹ d⁻¹]				
	Reference	3.6	5.2	6.0	6.1
	Contaminated	6.7	5.9	8.8	5.3
	NPP_{DW} [µgC mg_{DW}⁻¹ d⁻¹]				
	Reference	88.3	145.1	34.5	3.4
	Contaminated	120.2	130.9	21.0	3.7
	NPP_{Chla} [µgC µg_{Chla}⁻¹ d⁻¹]				
	Reference	55.8	61.1	15.4*	2.9*
	Contaminated	65.6	76.1	24.8*	7.5*
Non-normalized data	Respiration [µgC cm⁻² d⁻¹]				
	Reference	11.7	17	19.6	19.7
	Contaminated	14.9	13	19.5	11.8
	Net Primary Prod. [µgC cm⁻² d⁻¹]				
	Reference	287.2	471.8	112.2	11.1
	Contaminated	266.1	289.9	46.5	8.1
	Net Primary Prod. / Resp [-]				
	Reference	24.5	27.7	5.7	0.6
	Contaminated	17.9	22.3	2.4	0.7

*Chlorophyll a content was affected by herbicide exposure and the values may be biased.

3.4 Summary and Conclusion

The chronic exposure to 4 $\mu\text{g L}^{-1}$ diuron caused a toxicant-induced succession which was characterized by a general reduction in autotrophic biomass as indicated by the reduced specific chlorophyll-a content and a shift in the autotrophic community composition. Diatoms decreased in abundance and were replaced by green algae. Apart from the structural changes, also functional changes occurred. The contaminated communities differed from the reference communities concerning photosynthesis, as their photosynthetic yields were lowered and the pigment profile revealed a potential mechanism of photo-protection, which might represent an adaptation to chronic diuron exposure. The contaminated communities had lower net primary production rates unless normalized to biomass or chlorophyll a.

The net primary production to respiration ratios showed a lower autotrophy in the contaminated communities, potentially translating to the lower dry weight. The contaminated communities acquired a higher tolerance in the optimal photosynthetic yield, which was three times higher than the reference. This induction is consistent with the higher specific NPP in the contaminated community and suggests that a pollution-induced community tolerance has developed.

The tolerance of the contaminated community did not pay off when exposure to diuron was repeated, as the specific net primary production and the NPP:Resp. ratio was always below the reference community. The depletion of autotrophic species from the contaminated biofilms seems to dominate primary production, and acquired tolerance cannot compensate for this loss of autotrophic function. It can be concluded that the decline in autotrophic biomass and eventually also biodiversity has reduced the insurance effect (buffering against chemical exposure) for the autotrophic function of the contaminated communities. This finding shed light on the "selection process" as a critical aspect of PICT that can influence the ecological functioning of biofilm communities and also increase their vulnerability to future disturbances.

4. Community gene expression analysis by meta-transcriptomics

4.1 Introduction to meta-transcriptomics

As outlined in **chapter 3**, chemical exposure of natural biofilm communities above critical concentration leads to toxicant-induced succession, which can manifest in increased community tolerance. Based on this observation, the 'Pollution-induced community tolerance' concept (PICT) was developed by Blanck and Wängberg (1988) and confirmed by various studies (Blanck, 2002). The mechanisms of tolerance induction are often related to a shift in taxonomic structure in the community and its association with known traits like species sensitivity (Schmitt-Jansen & Altenburger, 2005). Nowadays, sequencing analysis of microbial communities provides an efficient alternative to structurally classify toxicant-induced succession in biofilms. A variety of methods have emerged that either target individual target genes (metabarcoding) such as ribosomal subunits like 16S rRNA or 18S rRNA (Carles et al., 2021; Woese & Fox, 1977), *rbcL* (Hollingsworth et al., 2009; Wolf & Vis, 2020) or examine the entire genome of a community (metagenomics) (Pu et al., 2021; Sanli et al., 2015). However, none of the mentioned approaches provides mechanistic insights into responses of a community to a stimulus, as these approaches use changes in genetic structures as proxies for their effects. Considering dormant members of a community or (rapid) environmental changes these approaches fail in diagnosing effects, nor do they help detecting the variety of cellular processes taking place. Analyzing the activity of a gene (transcription) can fill this gap and provide a readout of the molecular changes in a biological system at a certain point of metabolic activity. In the conventional technique of gene expression analysis, the polymerase chain reaction (PCR), the analysis is limited to a few, pre-selected target genes. However, recent advances in molecular techniques have paved the way for the detection of the full spectrum of active genes (transcriptomics). Parallelization in Next-generation sequencing has revolutionized transcriptomics, introduced application to communities (meta-transcriptomics) and inspired novel applications in the field (Shakya et al., 2019). In other words, meta-transcriptomics represents an integrating analysis across a large number of organisms and as such can represent an average community response for many genes. The technique has been recently applied for several scientific purposes, e.g. to characterize active microbes in a community (Bashiardes et al., 2016; White et al., 2016), study interactions in the human microbiome or plant and bacterial species (Bikel et al., 2015;

Crump et al., 2018) and evaluate the response to toxicants on molecular scale (Bergsveinson et al., 2020; Yang et al., 2019; Yao et al., 2022). The focus has primarily been on the study of the intestinal microbiome, while in recent years more and more attention has been paid to aquatic environmental transcriptomics (Shakya et al., 2019). To facilitate the interpretation of the extensive data in an environmental context, it is an ultimate goal to fully annotate genes in their functional traits. This step would allow the assessment of functional redundancy (see **chapter 1.2.2**) and indicate potential functional changes in a community.

A rather understudied subject are freshwater microbial biofilms, which is the most common life form for microorganisms in the upper- and middle reaches of streams (Battin et al., 2016). Meta-transcriptomics is a promising method to study the ecology of biofilms with respect to their metabolic pathways and trophic interactions. The potential was illustrated in a meta-transcriptomic comparison of sessile and planktonic biofilm communities indicating differences in their physiological states and metabolism, although 16S phylogeny did not reveal a significant difference in the bacterial community (Nakamura et al., 2016). In a study by Yergeau et al. (2012), the 16S composition of the river biofilm community also remained constant, although low concentrations of antibiotics altered the expression of genes associated with important functions of photosynthesis, carbon utilization and N and P metabolism. Unfortunately, the authors did not provide complementary measurements of associated apical functions, implying that an ecological anchoring of their results was not possible. A promising topic for meta-transcriptomics is the analysis of molecular mechanisms of stress regulation and adaptation. A first step in this direction was the study of Eriksson, Antonelli, et al. (2009), who explored the phylogenetic diversity of the *PsbA* - gene, the target protein in photosystem II for several herbicides including Irgarol. The authors assessed PICT after chronic irgarol exposure, which was associated with a decreased taxonomic diversity and lowered *PsbA* diversity, compared to a reference community. A particular mutational signature became evident among the more tolerant communities, which was assigned to diatoms by phylogenetic analysis of *PsbA* from databases. The authors suggest that the chosen mutation confers higher tolerance due to differences in non-conserved amino acids in the so-called PEST region, which favor high turnover of the protein (Eriksson, Clarke, et al., 2009). This study proves that molecular methods bear great potential for elucidating tolerance mechanisms, although they focused on a targeted, pre-selected gene. Extending the focus to meta-

transcriptomics could help identify the adaptation mechanisms underlying PICT. Thus, this work aims at a comprehensive characterization of adaptations to chronic diuron exposure using meta-transcriptomics and pursues a broader analysis of community tolerance mechanisms. Towards this end, the different communities were short-term exposed to a diuron gradient and untargeted ribonucleic acid sequencing (RNA-seq) analysis was used to uncover molecular mechanisms of stress adaptation. With respect to the increased tolerance of the contaminated community and the MoA of the applied herbicide (see **chapter 3.3.3**) a different gene expression pattern of the communities with respect to photosynthetic processes is hypothesized.

4.2. Methods

4.2.1 Sampling and RNA extraction

Biofilms were sampled after short-term exposure to diuron and immediately transferred to RNeasyTM Lysis Solution (Invitrogen, Thermo Fischer Scientific, Inc., Waltham, MA). Biofilms were scraped off the glass surface into a cryovial within 2 minutes and then quenched in liquid nitrogen. The RNA was extracted using the RNeasy Plant Mini Kit (QIAGEN, Inc., Valencia, CA). Contrary to the manufacturers protocol the frozen pellet was transferred into a mortar filled with liquid nitrogen and grinded with a pre-cooled pestle until a fine powder was produced. The tissue powder was transferred into a new 2 ml microcentrifuge tube filled with 450 μ L buffer RLC and vortexed for 10 seconds. Starting at step 4 the RNeasy Plant Mini Kit protocol was followed afterwards. In brief the lysate was cleared from cell debris in the QIAshredder spin column and short nucleic acids were adsorbed and washed in the RNeasy spin column. After the washing steps were completed the RNA was eluted from the column in two steps using 30 μ L and 10 μ L of nuclease free water. The nuclease free water was heated to 60°C, in order to increase desorption efficiency. An aliquot of 30 μ L of the final RNA extract was cleared from DNA impurities which were co-extracted by the RNeasy spin column due to their similar characteristics. The DNA was digested using the Turbo DNA-freeTM Kit (Thermo Fisher Scientific, Inc., Waltham, MA). The rigorous DNase treatment including the optional two-step incubation of the Turbo DNase enzyme was applied. The samples were kept on ice until the 10x Turbo DNase Buffer and the Turbo DNase were added. After DNA digestion the upper, aqueous phase was transferred into a new 1.5 mL safeLock Tube where the RNA got precipitated and washed. In brief, 140 μ L

RNase-free water, 4 μL of 5 mg/mL glycogen, 20 μL 3M sodium acetate and 600 μL of pure ethanol were mixed with each sample. Then the samples were stored at -20°C for 12 hours and centrifuged at 4°C on $16,900 \times g$ for 30 minutes. The supernatant was discarded and the RNA pellet was washed twice. In detail, 500 μL of ice-cold 70 percent ethanol was added, vortexed briefly and centrifuged at 4°C on $16,900 \times g$ for 5 minutes. The supernatant was removed each step and finally the pellet air dried, dissolved in 20 μL RNase-free water and incubated for 8 minutes at 58°C . RNA was quantified on a Qubit 2.0 fluorometer using the Qubit RNA HS Assay kit (Thermo Fisher Scientific). RNA integrity was determined with an Agilent Bioanalyzer using the RNA 6000 Pico Kit (Agilent Technologies, Inc., Santa Clara, CA). Two samples ($0.001 \mu\text{g L}^{-1}$ of the reference and $10 \mu\text{g L}^{-1}$ of the contaminated community) were removed from downstream analysis due to RNA deficits.

4.2.2 RNA sequencing analysis

100 ng total RNA was used for rRNA depletion. Ribosomal RNAs were removed from total RNA using the Ribo-Zero Magnetic Kit (Illumina, San Diego, CA, USA) according to the manufacturer's low input instructions. To improve rRNA depletion, rRNA probes from Ribo-Zero bacteria kit (MRZMB126) and plant kit (MRZPL1224) were combined. A strand-specific library for transcriptome sequencing was prepared using the ScripSeqv2 Kit (Illumina) following the manufacturer's instructions. The library was checked by using the Agilent 2100 Bioanalyzer system with a High Sensitivity DNA Kit (Agilent) according to the manufacturer's instructions. Library concentration was determined by using the Qubit 2.0 instrument using the Quant-iT dsDNA High Sensitivity kit (Thermo Fisher Scientific) according to the manufacturer's instructions.

Single libraries were normalized by equimolar pooling. The library pool was size-selected in a range of 150-600 bp using a preparative agarose gel in combination with MinElute gel extraction kit (Qiagen) according to the manufacturer's protocol. 12 pmol of the library pool were clustered on 7 lanes of an Illumina paired-end flow cell and 2x100 bp were sequenced according to the manufacturer's instructions using the v3 Cluster Generation and SBS Sequencing Kits (Illumina, San Diego, CA, USA) on a HiSeq2000 system.

4.2.3 Data assembly and processing

The assembly of the demultiplexed sequencing data was facilitated by Philippe Veber using Trinity version 2.9.1 and default options (Grabherr et al., 2011). Trinity features three modules: Inchworm, Chrysalis and Butterfly applied sequentially to process large volumes of RNA-Seq reads. The Inchworm module assembles short reads from the sequencing into unique sequences of transcripts. Then, Chrysalis clusters the Inchworm results to similar sequences, representing the full transcriptional complexity for a given sequence. Such a transcript cluster is very loosely referred to as a 'gene'. A de Bruijn graph is constructed for each cluster, which reflects the overlaps between the clustered variants. In a last step, the Butterfly module reconstructs distinct full-length transcripts for spliced isoforms and differentiates transcripts that belong to paralogous genes. Trinity encodes the processing information in the accession number of a contig. For example 'TRINITY_DN16831_c0_g1_i2' (the *psbA* contig) contains information the Trinity read cluster 'TRINITY_DN16831_c0', the gene 'g1', and isoform 'i2'. The combination of read cluster and the corresponding gene results in a unique gene identifier and the isoform number associates gene variants with this identifier. This approach allows Trinity to *de novo* assemble transcriptomes independently of a metagenome template, which is the key to any meta-transcriptome analysis. However, Trinity assembly without reference genomes can produce several contigs even for the same gene (notably in case there are several isoforms). This technical limitation complicates biological interpretation, as several contigs with the same annotation may derive from the same or from different species. For example, a species can have several paralogous *psbA* genes, such as cyanobacteria, which contain up to 5 variants conferring different functional properties the PS (e.g. for light adaptation) (Mulligan et al., 1984; Vrba & Curtis, 1990).

After assembly, the scientific results have in part been computed at the High-Performance Computing (HPC) Cluster EVE, a joint effort of both the Helmholtz Centre for Environmental Research - UFZ (<http://www.ufz.de/>) and the German Centre for Integrative Biodiversity Research (iDiv) Halle-Jena-Leipzig (<http://www.idiv-biodiversity.de/>). The compute environment was set up using conda (conda-forge and bioconda channels) installing DESeq2 v1.34 (Love et al., 2014) and Seqinr v4.2_8 (Charif et al., 2021). The raw counts matrix of each community was imported to R using `DESeqDataSetFromMatrix()`. To enable multivariate statistics on the raw counts data of both communities was merged and transformed to log 2 scale by the `rlog()` command

of 'DESeq2'. This transformation removes the experiment-wide trend of variance over mean.

Furthermore, gene expression was evaluated calculating the ratio between I) a treated sample to its corresponding control (acute effect) and II) a treated sample to the same treatment in the other community (chronic effect). However, ratios do not intuitively reflect a change in gene expression, since, for example, a doubling of gene expression gives an induction of 2 and an equivalent halving gives a reduction of 0.5. To scale the ratios symmetrically, the log2 fold change of the ratio was calculated (Quackenbush, 2002). Based on these considerations, the DESeq() command of the 'DESeq2' package was used, which calculates the log2 fold change while accounting for library size variations (potential initial sample biases) by normalizing the raw data count. The comparison of the diuron effect within a community from I) was achieved using the following formula [5]:

$$\text{Control-referencing} \quad fold\ change_i = \log_2 \left(\frac{N_{T,i}}{N_{0,i}} \right) \quad [5]$$

The expression change of a contig i was formed by dividing the read count (N) of a treatment N_T against the respective read quantity of that contig in the control N_0 . The parameter N_T covered all treatments from 0.0001 to 100 $\mu\text{g L}^{-1}$ and this formula was applied for the reference and the contaminated communities individually. Calculating the log2 fold change based on the respective control N_0 (control-referencing) allows to focus on the effect of the short-term exposure (acute effect). To focus on the difference between community responses as a result of chronic exposure, the following formula [6] was applied:

$$\text{Cross-referencing} \quad fold\ change_i = \log_2 \left(\frac{C_T}{R_T} \right) \quad [6]$$

In this cross-referencing approach, C_T represents a condition in the contaminated community (a control or a treatment of the 0.0001 to 100 $\mu\text{g L}^{-1}$ diuron gradient) and R_T is the same condition in the reference community. Thus, log2 fold change was calculated from the ratio of contaminated to reference community for each treatment.

4.2.4 Prioritization of contigs and annotation

The complexity of the data set with more than three million contigs required a reduction to responsive contigs. To this end the data was filtered and prioritized based on the exposure design of the chronic and acute exposure. This selection was facilitated by principal component analysis (PCA) in the 'vegan' package version 2.5-7 (Oksanen et al., 2013) and dose-response analysis with 'DRomics' using the R package version 2.2 (Muller et al., 2021). PCA was performed by `prcomp()` using the `rlog` data of DESeq2. This analysis facilitated an unsupervised analysis of variance to test whether the exposure conditions induced variance in a systematic manner. The analysis in DRomics was specifically addressed to the short-term exposure. Responsive contigs were identified and sensitivity thresholds derived by estimating dose-response models. To capture the diversity of response trends in gene expression DRomics features linear, Hill, exponential Gauss-probi and log-Gauss-probit models to evaluate monotonic and biphasic responses (Larras et al., 2018). The analysis was carried out by Larras et al. (in prep) by processing the reference and contaminated community data set independently. Specifically, contigs were imported to DRomics with `RNAseqdata()` by selecting the 'rlog' option, filtered with `itemselect()` using a quadratic trend test and an FDR of 10%, and models were fitted with `drcfit()` using the Akaike information criterion (AIC) for model fit selection. In a final step, the BMD was determined using `bmdcalc()`. All BMD values beyond the tested concentration range were replaced by the lowest concentration of $0.0001 \mu\text{g L}^{-1}$.

The responsive and prioritized contigs were annotated using the DIAMOND - high throughput protein alignment tool (Buchfink et al., 2015) on the EVE Cluster (UFZ). DIAMOND makes use of the Non-redundant protein sequences database of NCBI and outputs Reference Sequence (RefSeq) accession numbers for the matched genes and taxonomic identifiers (TaxID) for the respective corresponding species. The RefSeq was used to annotate the sequences using the UniProt protein database (The UniProt Consortium, 2020). Beside information on the protein identity UniProt is also linked to the Gene Ontology (GO) database (The Gene Ontology Consortium, 2021), which contains classified meta-information of genes. The GO classification of a biological process was used as representative of the molecular function in the sensitivity analysis of the contigs for this thesis. The TaxID was used to access the taxonomic classification of the RefSeq gene species in the NCBI taxonomy database (Federhen, 2011).

4.2.5 Sensitivity analysis of biological processes

In a last step the log2 fold change data was filtered for annotated biological processes of the GO classification with BMD's up to the EC₅₀ of photosynthesis inhibition ($\Phi_{II\ max}$), assuming that these processes might reveal molecular adaptations stemming from chronic diuron exposure. Anchoring the analysis of the molecular GO annotation to the apical functional analysis should guarantee that the cells were within homeostatic capacity and exclude apoptosis processes which might occur beyond 50% inhibition of a vital process like photosynthesis. To determine the sensitivity of a biological process, the 25th percentile was calculated from all BMD values of that respective GO process. Only processes with more than four BMDs in one of the two communities were considered in the subsequent steps. The EC₅₀ of photosynthesis inhibition of the reference community (14.6 $\mu\text{g L}^{-1}$) was set as maximal sensitivity threshold for the 25th percentile of the GO processes. After identification of the sensitive biological processes, all responsive contigs belonging to these processes were extracted from both communities (regardless of their BMD) and visualized in heatmaps using the Heatmap () function of the R package ComplexHeatmap v2.6.2 (Gu et al., 2016). In the interest of a clear arrangement, the biological processes were presented in individual panels. Within a panel, the contigs were clustered to generate a logical order of representation.

4.3 Results and discussion

The assembly of the 30 million reads per sample resulted in 3'502'153 contigs in both communities which represent 2'376'397 genes and 1'125'756 isoforms. A total of 66% of the contigs had sizes of less than 500 nucleotides and 12% more than 1000 nucleotides. The contigs were imported in DRomics using the the rlog transformation option and responsive items were picked by a false discovery rate of 0.1. This reduced the amount of contigs to 691 in the reference and 2'804 in contaminated communities. The model fitting further reduced the selection of contigs to 559 for the reference and 2'372 for the contaminated communities. Of the total of 2931 contigs modelled, 547 could be annotated with at least one biological GO process.

4.3.1 Characterization of the meta-transcriptomic fingerprints

The 3'502'153 contigs were rlog transformed and subjected to a principal component analysis. The first principal component (PC) explained 13.7 % of the variance in the data and discriminated between the two communities in their exposure history (**Figure 10**). A total of 3,059,922 contigs were identified that contributed significantly to the first PC. This finding highlights the clear difference in the fingerprints, which rests on the great majority of contigs. The large difference between the meta-transcriptomes of the community could indicate artificially induced variance (e.g. by sample processing), which was addressed by the following steps: I) the initial RNA extracts were compared for significant differences ($p > 0.05$), II) the libraries were pooled equimolar to add the same amount of RNA of each sample, and III) potential sequencing differences in the library size were normalized *in-silico* by the DESeq 2 package. For this reason, the pattern in PCA is considered as a unique meta-transcriptomic fingerprint resulting from chronic exposure.

A subset of 518 contigs was extracted from the data set based on their significant contribution to PC1, which were more than 3000 times higher than average. This subset was aligned to the NCBI nr database, which resulted in 330 protein matches and the results were filtered for biofilm specific organisms. These were subjected to the UniProt database for a functional annotation. Annotation revealed 156 putatively characterized proteins that significantly drive community separation on PC1. Among the characterized proteins 13 were crucial for maintaining protein homeostasis like heat-shock proteins (3) and ubiquitin regulation (10). Others were ribosomal proteins participating in translation (7) or ATP-binding cassette transporters (4) involved in translocation of many substrates such as nutrients, primary- and secondary metabolites or the extrusion of xenobiotics. The large number of unknown (in NCBI: 188) and uncharacterized proteins (in UniProt: 217) suggests that chronic exposure induced changes in transcriptomic fingerprints beyond the extensively studied proteins of the central metabolism which are mostly available in databases for annotation. Another factor explaining this result is that working with biofilms involves many unknown species in addition to the typical model organisms. The large number of contributing contigs indicates that chronic herbicide exposure may have affected large parts of the community apart from the autotrophic species, which might result from indirect effects, e.g. from species interacting with the autotrophs like trophic interactions or usage of algal exudates by bacteria. As the annotated contigs have a

particularly high share in the PCA pattern, these can be assumed to reflect relevant chronic adaptations to the stressor. This proves the effect of the chronic exposure, which shaped the communities in their individual meta-transcriptomic fingerprints.

The second and third PCs explained 7 and 6 % of the variance and the remaining axes did not contribute significantly to the result. The variance explained by PC2 and PC3 was not associated with acute diuron exposure and was therefore not considered in the further analysis. Therefore, the acute gradient exposure of one hour did not induce a systematic variance in transcriptomic fingerprints of the communities. This finding suggests that further analyses must filter for primary effects in the context of the exposure design, as eventually only a few genes were responsive. Trend analysis, e.g. with the DRomics tool, could therefore provide a filter option for responsive genes in terms of gradient exposure.

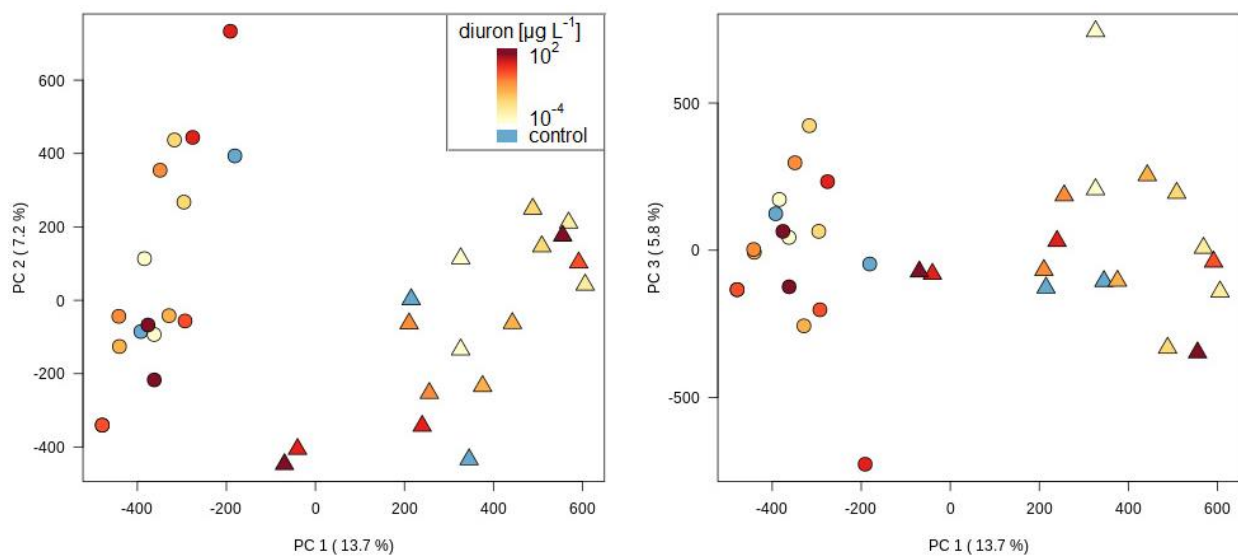


Figure 10 Principal component analysis based on the rlog transformed meta-transcriptome fingerprints ($n = 3'502'153$ contigs). The different concentrations of the acute 1h exposure are presented based on a color gradient ranging from red (high exposure) to yellow (low exposure), whereas blue depicts controls. The contaminated community is marked by the triangle ▲ and the reference community by the filled circle ●.

4.3.2 Insights into community stress response mechanisms using trend analysis (DRomic's)

The inhibited photosynthetic electron transfer by diuron (see **Chapter 2.3.2** for a detailed description of the MoA) can be determined very precisely on the basis of chlorophyll fluorescence using PAM-fluorometry (Schreiber et al., 2007). PAM-fluorescence analysis measures the optimal quantum yield inhibition $\Phi_{II\ max}$ and this revealed a clear increase in the inhibitory concentration in the contaminated communities, which was therefore considered to be more tolerant towards diuron exposure (see **Chapter 3.3.3** for details). To gain insights into the molecular mechanisms leading to community tolerance, the EC_{50} of $\Phi_{II\ max}$ inhibition of the reference communities was set as threshold for functional effects. By filtering the biological processes of the GO annotation, the molecular responses preceding a breakdown in photosynthetic function were prioritized. This linkage to apical functional effects aimed to focus on adaptation mechanisms of the chronic exposure, whereas GO processes with a sensitivity beyond this level were considered less specific. Filtering narrowed down the total of 259 GO processes to a selection of 23 that met the criteria (see **Table 3**). A comparison of the results revealed a higher sensitivity (lower 25th percentile) in the reference biofilms for the majority of GO-processes compared to the contaminated biofilms. This may indicate an adaptation of the contaminated communities after the chronic exposure. However, also a persistent chronic exposure to diuron dissolved in the EPS matrix seems possible, as the acute exposure started directly after the chronic exposure. According to this assumption, an effect would only become detectable at a significantly higher exposure level compared to chronic exposure. Since a respective control without additional diuron addition was included and referenced in each community, an increased adaptation of the contaminated biofilms can be assumed, even though the exact internal exposure concentration remains unclear.

All GO processes were plotted in heatmaps and are discussed below for their similarities and differences. Since there were overlaps between the contigs of some of the GO processes and the assignment of the contigs to a GO processes was ambiguous in some cases, some GO processes were combined into a supergroups and plotted in a joint heatmap (see **Table 3** for details).

The most comprehensive GO process was “translation” featuring 93 unique contigs. However, the contigs mainly comprised the small (40S) and large ribosomal subunit

(60S) expressing a rather non-specific need for acclimation. Both subunits belong to the eukaryotic domain, suggesting that eukaryotic cells had a higher need to acclimate to diuron exposure than other biofilm compartments and is also reflecting the MoA of the stressor. The non-specific assignment of ribosomal subunits did not allow a deep analysis of the differences between the communities. Nevertheless, with regard to the sensitivity the reference communities revealed more sensitive contigs involved in “translation”, which might indicate that they were affected already at lower concentrations (see **Table 3**). Moreover, the responses of the GO-processes “protein-chromophore linkage”, “photosynthesis” and “reductive pentose-phosphate cycle” comprising 33 unique contigs, indicated a high acclimation effort within the autotrophic part of the communities, which is largely composed of eukaryotes. These three GO-processes were summarized into “pooled photosynthesis” and mapped in **Figure 15**. Processes of the carbohydrate and fatty acid metabolism, which are strongly linked to photosynthesis, also proved to be particularly sensitive in this analysis and related GO processes were collectively mapped in **Figure 11**.

Table 3 Results of the sensitivity analysis of the GO processes. The 25th percentile was calculated from all BMD’s assigned to a respective GO process in the reference (Ref.) and contaminated (Conta.) communities. The number of contigs contributing to the respective 25th percentile is listed in last two columns.

Gene Ontology	GO number	25 th perc. Ref. [$\mu\text{g L}^{-1}$]	25 th perc. Conta. [$\mu\text{g L}^{-1}$]	Contigs Ref.	Contigs Conta.
gluconeogenesis	0006094	11.1	26.0	5	1
carboxylic acid metabolic process	0019752	8.0	25.2	6	1
protein-chromophore linkage*	0018298	4.6	33.1	4	11
reductive pentose-phosphate cycle *	0019253	$1.3 \cdot 10^{-4}$	43.5	6	1
lipid metabolic process	0006629	3.8	$1.0 \cdot 10^{-4}$	8	8
ATP synthesis coupled electron transport	0042773	5.25	37.5	5	2
translation	0006412	$2.5 \cdot 10^{-4}$	24.6	12	81
protein folding	0006457	0.6	4.2	6	8
fatty acid biosynthetic process \square	0006633	2.6	1.7	16	6
cell cycle $\#$	0007049	0.5	62.4	4	1
regulation of cell shape $\#$	0008360	0.5	62.9	4	1
peptidoglycan biosynthetic process $\#$	0009252	0.5	62.9	4	1
cell wall organization $\#$	0071555	0.6	62.9	9	1

cell division [‡]	0051301	0.6	36.3	5	4
carbohydrate metabolic process	0005975	9.5	14.0	6	3
tricarboxylic acid cycle	0006099	7.9	47.0	4	4
glutamine metabolic process	0006541	0.1	52.9	24	1
glycolytic process ⁺	0006096	8.0 10 ⁻²	3.0 10 ⁻⁴	7	4
acetyl-CoA biosynthetic process from pyruvate	0006086	2.2	34.2	6	5
photosynthesis [*]	0015979	2.9 10 ⁻⁴	49.7	10	5
glucose metabolic process ⁺	0006006	1.2	15.6	5	1
arginine biosynthetic process	0006526	13.9	2.2 10 ⁻⁴	7	1
malonyl-CoA biosynthetic process [□]	2001295	5.1	12.0	5	2

The biological processes marked were individually pooled to ^{*} pooled photosynthesis, ⁺ pooled glycolysis, [□] pooled fatty acid biosynthesis and [‡] pooled cellular processes based on overlaps in their contigs and a better representation in a heatmap.

Regulated genes showing similar responses in both communities

The gene expression of GO processes ‘pooled glycolysis’, ‘pooled fatty acid biosynthesis’ and ‘lipid metabolic process’ showed very similar patterns in both communities (**Figure 11**). The TaxID’s of the sequences associated with these processes matched diatoms references for a majority of the contigs (> 60 %), but also proteobacteria, ciliophora and cyanobacteria were among the highest matches. Hence, it can be concluded that the gene expression pattern discussed below applies mostly to the autotrophic part of the biofilm.

High diuron concentrations above 10 µg L⁻¹ mostly reduced the gene expression, e.g. of desaturase enzymes, fatty acid elongation enzymes and glycolytic/glyconeogenic enzymes (**Figure 11**, first three panels). The median gene expression for these processes in the 50 and 100 µg L⁻¹ diuron treatments was at a similar level of -2.5 / -2.6 and -3.3 / -4 fold in the reference and contaminated community. This reduction also occurred in the *de novo* fatty acid synthesis from acetyl-CoA via pyruvate dehydrogenase and coincides with a downregulation of contigs involved into ‘ATP synthesis coupled electron transport’ (**Figure 12**, lower panel). The contigs involved in this GO process include NADH dehydrogenases, which are involved in various biochemical processes, such as oxidative phosphorylation or the mitochondrial respiratory chain, which could become co-regulated due to their close biochemical relation to the carbohydrate metabolism. A comparable reduction of genes involved in

the glycolysis and lipid metabolism was also observed in the transcriptome of the marine diatom *P. tricornutum* exposed to 75 $\mu\text{g L}^{-1}$ simazine, another PSII inhibitor (Osborn & Hook, 2013). In addition, some contigs were also induced at high diuron concentrations, such as a contig of glyceraldehyde-3-phosphate dehydrogenase or 1-phosphatidylinositol phosphodiesterase. This may indicate a small proportion of organisms that were oppositely affected by the high diuron concentration.

In contrast to the observed reduction, isocitrate lyase (which occurred in 7 isoforms) and malate synthase were consistently upregulated as soon as most of the other enzymes of the aforementioned processes were downregulated (**Figure 12**, upper and middle panel). The expression level of isocitrate lyase in the 50 and 100 $\mu\text{g L}^{-1}$ diuron treatments ranged from 1.4 to 4.7 in the reference and 0.5 to 4.0 in the contaminated communities. An induction of isocitrate lyase was reported in response to oxidative stress and an increased metabolic fluxes through the so called 'glyoxylate shunt' was anticipated (Ahn et al., 2016). Isocitrate lyase and malate synthase form the backbone of the glyoxylate and dicarboxylate metabolism, which performs the conversion of acetyl-CoA to succinate and thus represents an alternative metabolic pathway for the synthesis of carbohydrates. However, this cycle uses also enzymes associated with the tricarboxylic acid cycle such as aconitate hydratase. This enzyme was also upregulated in contaminated communities at 50 and 100 $\mu\text{g L}^{-1}$. In conclusion, the glyoxylate shunt seems a probable alternative source of carbohydrates for the autotrophic organisms in the biofilm at high diuron concentrations.

Below the 10 $\mu\text{g L}^{-1}$ treatment the reference communities showed a regulation pattern with expression levels ranging from no regulation to a slight induction (**Figure 11**, top three panels). Only enzymes from 'pooled glycolysis' showed a weak reduction in gene expression even at lower diuron concentrations (especially from 0.1 $\mu\text{g L}^{-1}$), which may point on particular sensitive species. The contaminated communities revealed a higher and more consistent induction of gene expression at diuron concentrations below 10 $\mu\text{g L}^{-1}$, which was particularly pronounced in the 'lipid metabolic process', 'pooled glycolysis' (**Figure 11**, top three panels) and 'ATP synthesis coupled electron transport' (**Figure 12**, lower panel). This increased induction in comparison to the control communities could indicate an adaptive mechanism to cope with chronic diuron exposure.

The similarity in the expression pattern of the carbohydrate and fatty acid metabolism might relate to their close metabolic linkage. Glycolysis is the first important step in the conversion of carbohydrates into fatty acids, which in turn are the main component of lipids. The down-regulation of genes involved in fatty acid and lipid anabolism at high diuron concentrations might be related to an energy shortage, which in turn may have triggered a switch from fatty acid anabolism to catabolism by beta-oxidation. Unfortunately, none of the responsive contigs selected by DRomic's relates to beta-oxidation and a specific blasting of a target sequence of acyl-CoA dehydrogenase, which initiates the first step of beta-oxidation merits future consideration to evaluate this hypothesis. In addition, expression analysis of genes involved in carbohydrate metabolism does not provide information about the stock of proteins available to continue catabolism (e.g. glycolysis). Protein synthesis requires an energy input that may exceed the cellular energy budget for *de novo* synthesis (especially at high diuron concentrations), limiting the cell to the available protein stock and reducing transcriptional activities. In conclusion both communities showed comparable patterns at low doses (below the EC_{50} of $\Phi_{II \max}$ inhibition), but at high doses the diuron effect converges to a predominant reduction in gene expression. Moreover, at high doses, an alternative synthesis of carbohydrates could occur via the 'glyoxylate shunt', which bypasses the carbon dioxide-generating steps of the tricarboxylic acid cycle and conserves carbon atoms for gluconeogenesis. The reduction of genes in glycolysis and fatty acid synthesis with simultaneous induction of the glyoxylate cycle could indicate an insufficient carbon supply from the primary metabolic sources (e.g. reductive pentose phosphate pathway), which corresponds to the effect of the herbicide diuron.

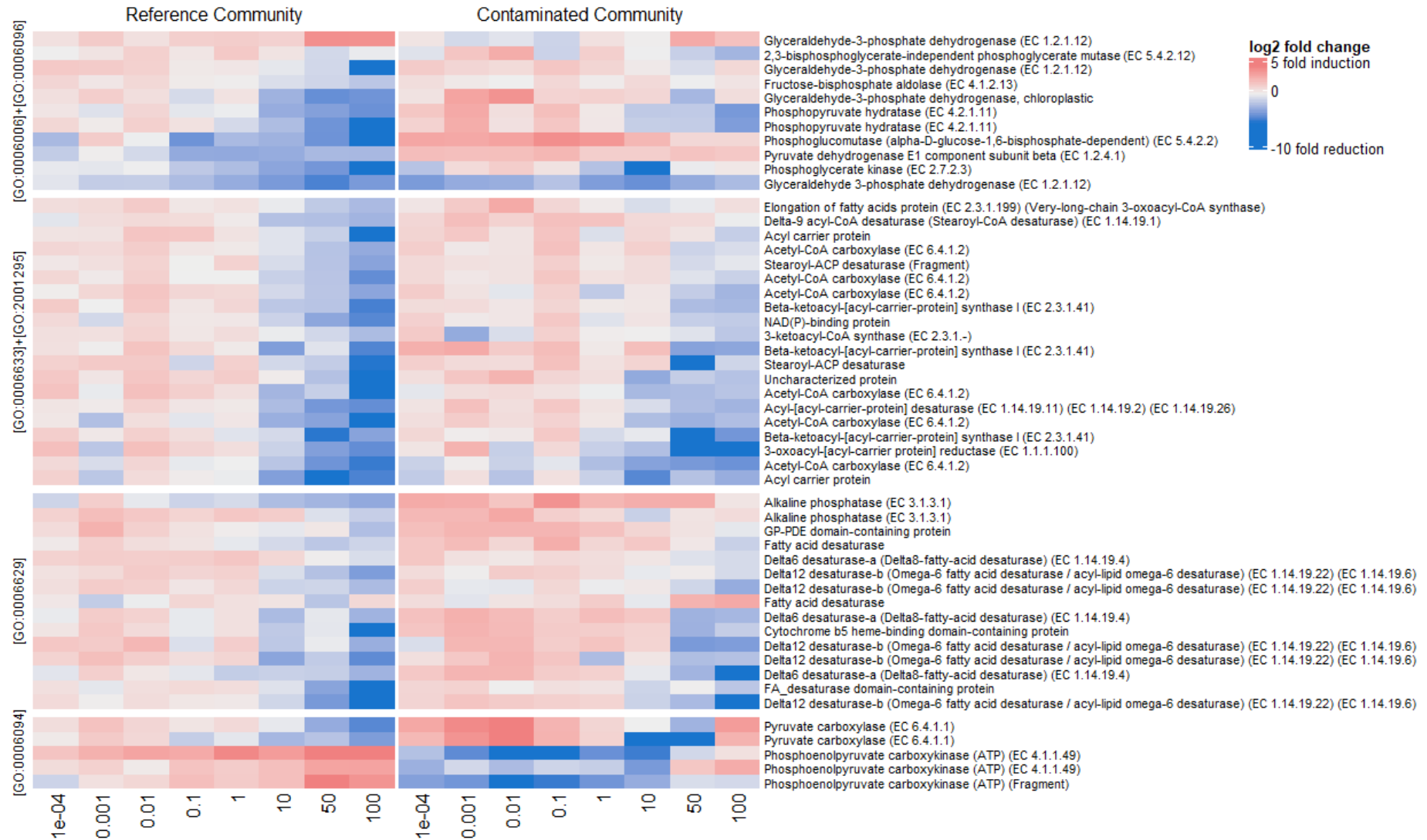


Figure 11 Heatmap of the GO-processes related to the carbohydrate and fatty acid metabolism (pooled glycolysis = 'glycolytic process [GO:0006006]' + 'glucose metabolic process [GO:0006096]'; pooled fatty acid synthesis = 'malonyl-CoA biosynthetic process [GO: 2001295]' + 'fatty acid biosynthetic process [GO:0006633]'; 'lipid metabolic process [GO:0006629]'; 'gluconeogenesis [GO:0006094]').

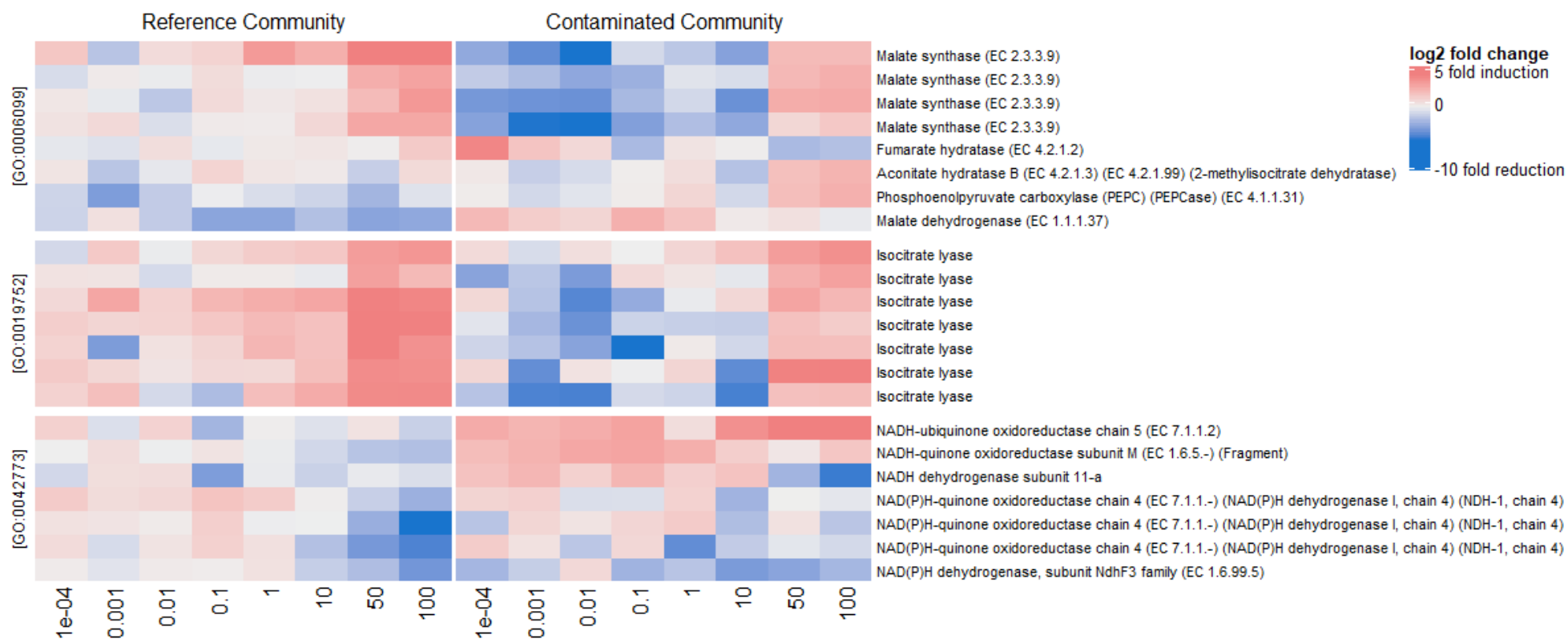


Figure 12 Heatmap of the GO-processes related to the acetyl-CoA metabolism ('tricarboxylic acid cycle [GO: 0006099]', glyoxylate cycle ('carboxylic acid metabolic process [GO:0019752]') and 'ATP synthesis coupled electron transport [GO:0042773]').

Genes differentially regulated in both communities

The clearest difference among the communities was observed in the GO processes related to amino acid metabolism (**Figure 14**) and photosynthesis (**Figure 15**). The reference communities revealed a concentration dependent decline in the expressions of isoforms of the enzyme carbamoyl-phosphate synthase and citrulline – aspartate ligase, while the contaminated communities showed an almost constant high induction pattern. Both enzymes are linked in the synthesis pathway of L-arginine from L-ornithine and carbamoyl phosphate in the chloroplast, which serves as a nitrogen storage, regulates developmental processes, and responses to biotic and abiotic stressors (Winter et al., 2015). Further evidence for L-arginine biosynthesis is the enzyme acetylglutamate synthase (**Figure 14**, lower panel), which facilitates the conversion of glutamate to L-ornithine in the cyclic pathway and shows an analogous expression pattern to the before mentioned enzymes. The role of L-arginine in maintaining homeostasis remains to be clarified, but conversion to other amino acids such as proline, a multifunctional amino acid in stress responses, also seems possible (Verslues & Sharma, 2010).

A reduction of contigs involved into photosystem I (PS I), cytochrome b6f complex and the reductive pentose-phosphate cycle (RPP) was observed in the reference communities (**Figure 15**). In comparison, the contaminated communities showed induction or no expression in the same contigs. Most striking was the difference in the photosystem II (PS II) genes, which were higher expressed in contaminated and barely expressed in the reference communities. The PSII contigs switched from no regulation in the treatments below $10 \mu\text{g L}^{-1}$ to a clear induction of up to 2.8 fold in the 50 and $100 \mu\text{g L}^{-1}$ diuron treatments of the contaminated communities. The expression profile of PS II contigs in reference communities was inconsistent, and a clear trend in regulation across the concentration gradient was not observed. The contigs involved in RPP remained unregulated below $0.01 \mu\text{g L}^{-1}$ diuron treatment in the reference communities, but above this concentration a reduction in gene expression occurred. This may point on the effect progression of diuron in the reference communities, which could limit the energy availability for carbon fixation and the need for further ribulose-bisphosphate carboxylase enzymes. In contrast to this observation, the contaminated community showed an inconsistent expression pattern dominated by a weak induction of the same RPP genes. **Figure 13** schematically illustrates the differential expression profile on genes related to photosynthesis.

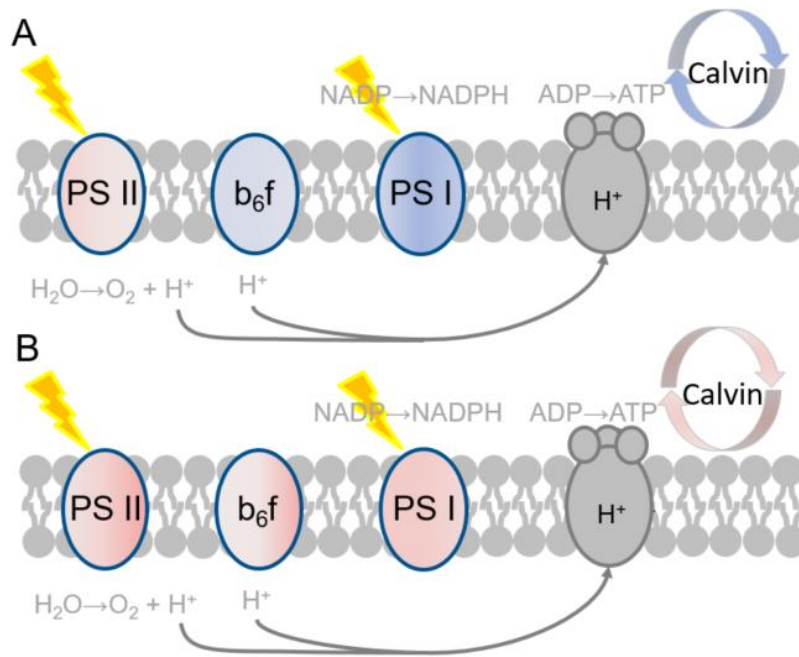


Figure 13 Schematic representation of the expression of genes involved in the photosynthetic apparatus. The expression profile of **A)** the reference community and **B)** the contaminated community is illustrated based on genes related to photosystem I (*PsaA*, *PsaJ*), cytochrome b₆f complex (*petA*, *petN*) and calvin cycle (*rbcL*, *rbcS*), while photosystem II related genes (*PsbA*, *PsbB*, *PsbC*, *PsbZ*). Red color indicates upregulation and blue color downregulation of related genes and the gradient from left to right illustrates their expression pattern along the diuron gradient (see **Figure 15** for a detailed perspective).

Upon the inhibition of PSII, the stoichiometry of the photosynthetic complex and subsequent metabolic processes needs adjustments to maintain homeostasis. In the reference community contigs involved in PSI and the RPP were downregulated in response to diuron, while contigs related to the PSII were barely regulated. This downregulation points to a balancing of the PSI/PSII ratio and the downstream metabolism (e.g. RPP), to adapt to the shortages of PSII under the given exposure. The downregulation of PSI contigs in the presence of diuron is widely documented, and a redox regulation was anticipated in higher plants (Allen et al., 2011; Pfannschmidt et al., 1999), and was now illustrated for microbial autotrophic communities in this study. The PSI and the RPP of the contaminated community responded heterogeneously, but slight upregulation of *PsaJ* in the higher diuron concentrations was observed. Especially the treatments above EC₅₀ of $\Phi_{II\max}$ inhibition

revealed an induction of the majority of the PSI, PSII and RPP contigs. The differences in the expression profile of PS-related contigs in the two communities indicates a potential adaptation to the chronic stressor. In addition to the transcription of PS genes, the posttranscriptional regulation (e.g. splicing and translation), the mRNA half life time (Baginsky & Link, 2008) and the repair of PS proteins (Nishiyama et al., 2006) are also dependent on the redox state of the chloroplast. Thus, adaptations that contribute to the maintenance of the cellular redox state have the potential to maintain photosynthetic activity and related gene expression.

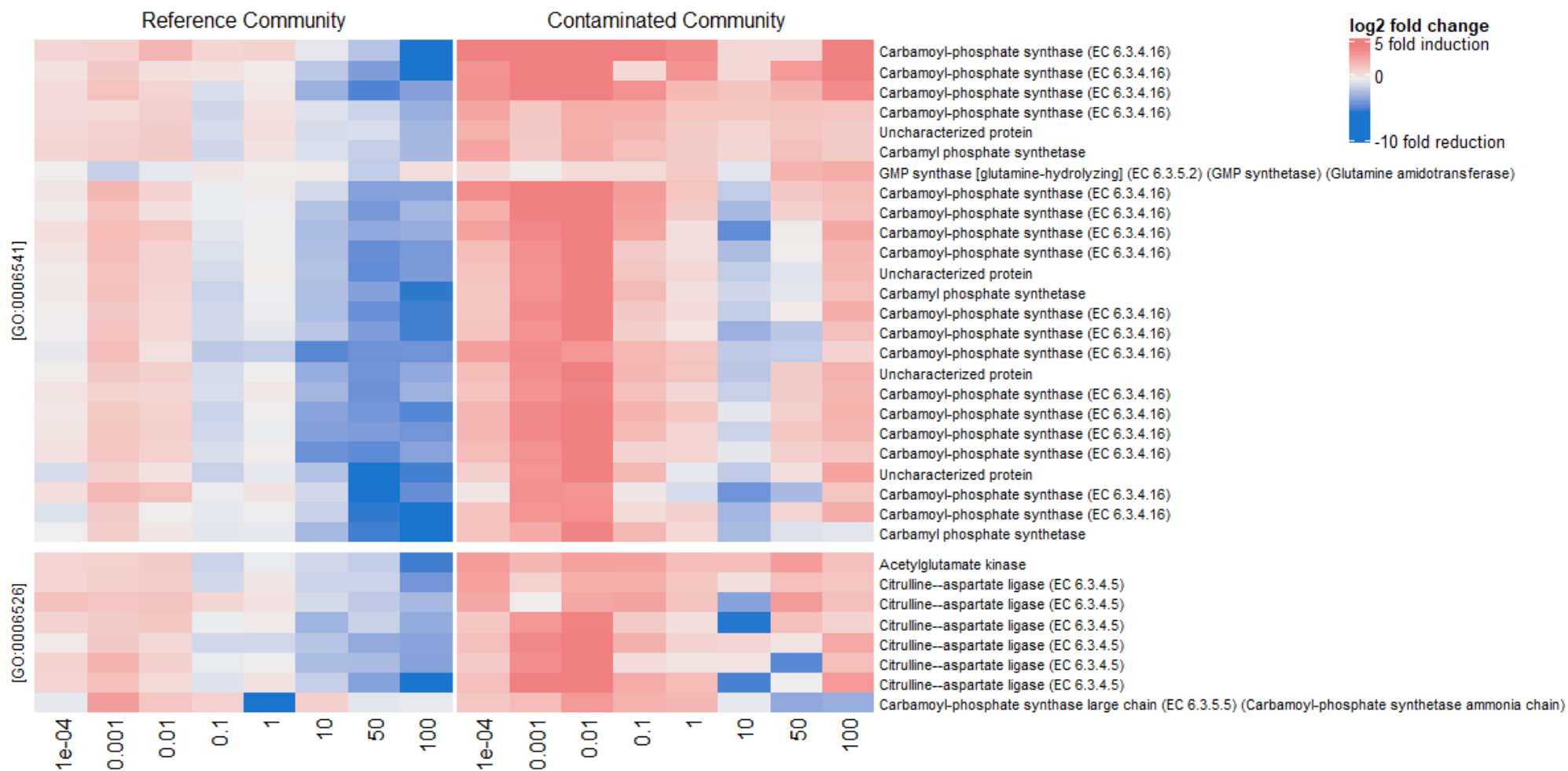


Figure 14 Heatmap of the GO processes related to amino acid metabolism ('glutamine metabolic process [GO:0006541]'; 'arginine biosynthetic process [GO:0006526]').

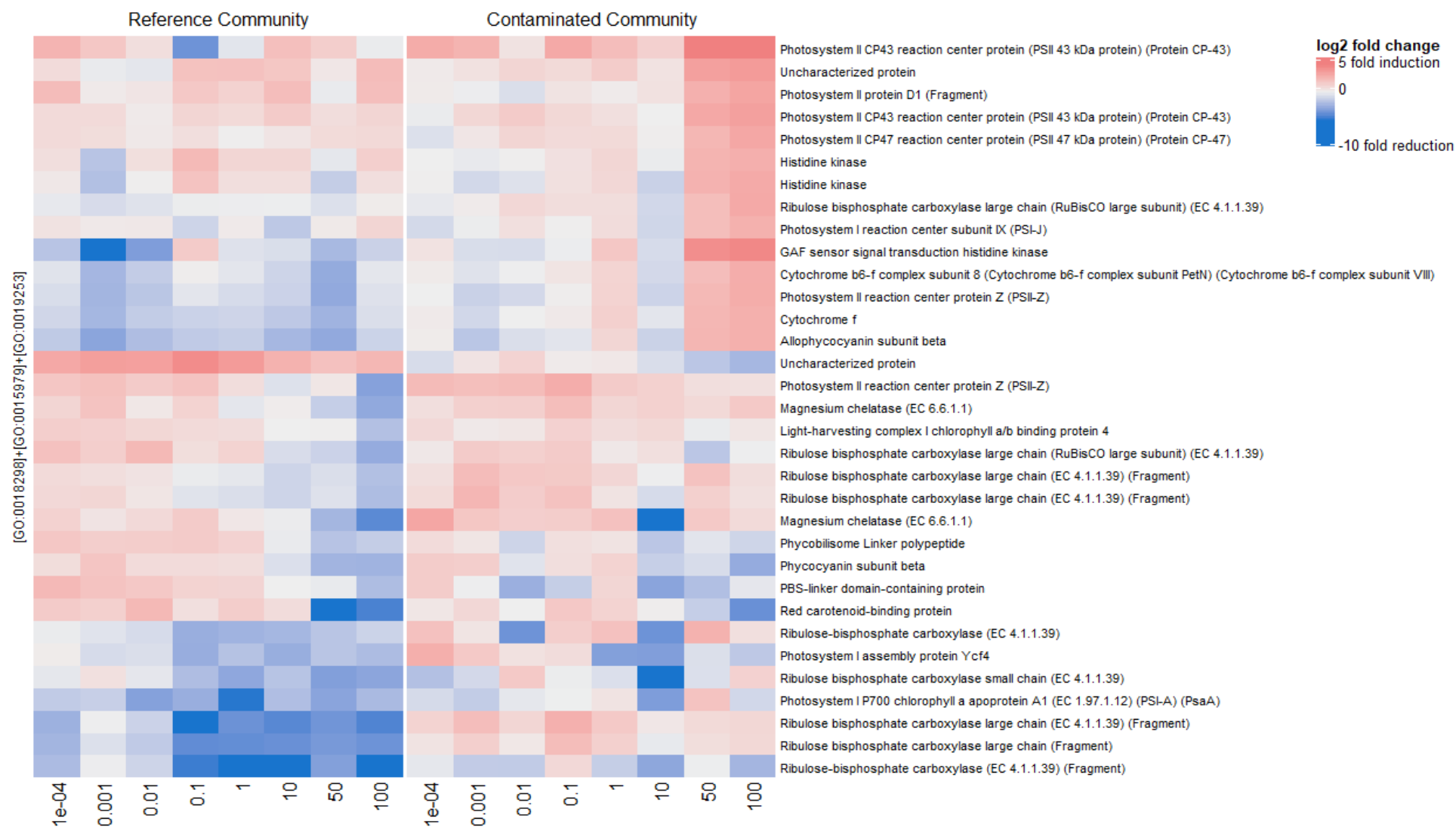


Figure 15 Heatmap of the pooled photosynthetic GO processes (‘protein-chromophore linkage [GO:0018298]’, ‘photosynthesis [GO:0015979]’ and ‘reductive pentose-phosphate cycle [GO:0019253]’).

4.3.3 Response pattern in the isoform PS genes

Filtering with DRomic's selected contigs that match the gradient exposure design. Most of these prioritized contigs had isoforms that were functionally identical, but showed no trend in their expression levels and were thus not recognized by DRomic's. In addition, further contigs related to photosynthesis were identified by annotating suspect genes in the dataset and querying their GO classification. In order to analyze whether the proposed tolerance mechanism (see **chapter 4.3.2**) is restricted to the responsive contigs or whether it can also be observed in the isoforms of the responsive contigs and further photosynthesis related contigs, all contigs belonging to the GO processes 'protein-chromophore linkage', 'photosynthesis' and 'reductive pentose-phosphate cycle' were evaluated using the cross-reference log2 fold change data. Using the cross-reference data, the focus of the analysis was shifted from responsive genes to overall differences in isoform expression between communities resulting from chronic exposure. The log2 fold changes of all treatments were subjected to a boxplot (**Figure 16**) showing higher expression of the isoforms associated with PSI, RPP and PSII in the contaminated community. In particular, contigs related to PSI were expressed up to 4 fold more in the contaminated communities, while the majority of contigs belonging to RPP and PSII were expressed equally in both communities. This observation leads to the conclusion that the regulation pattern shown in **Figure 13** can be extended to the isoform genes. But, instead of being regulated in response to the diuron gradient, these isoforms were already expressed at a consistently higher level in the contaminated communities compared to the reference counterpart. Based on the chronic exposure history, it can be assumed that the contaminated communities had a higher internal exposure to diuron, which might have a long-lasting effect on its gene expression profile. In conclusion, the contaminated communities might have established a balanced PSI / PSII stoichiometry, which remains stable even at an additional diuron exposure. This finding also illustrates that unbiased analysis of the comprehensive data set results in hypothesis which need to be further reflected by targeted approaches.

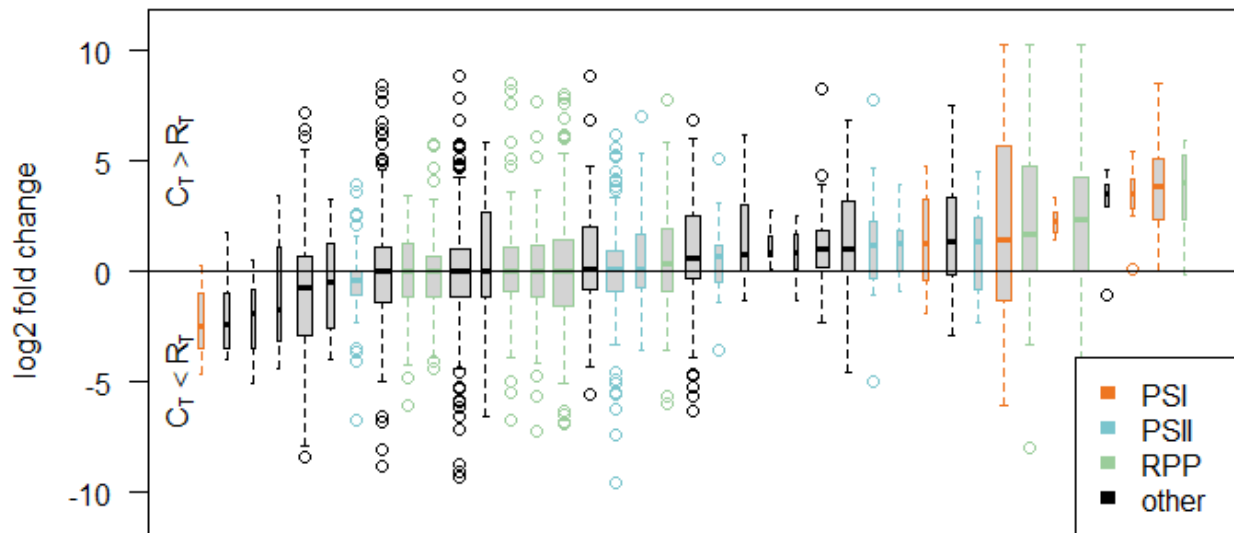


Figure 16 Boxplot of the cross-reference gene expression analysis between the communities of the contigs related to photosynthesis. The cross-reference analysis is based on the ratio of the gene expression of the contaminated (C_T) to the reference community (R_T). Thus, positively regulated contigs were more strongly expressed in the contaminated community.

4.5 Summary and conclusion

Chronic exposure for 5 weeks with 4 $\mu\text{g L}^{-1}$ diuron resulted in the formation of a contaminated community, which differed considerably in its transcriptomic fingerprint from an unexposed reference community. The fingerprints showed large differences, but exposure to a diuron gradient in a short-term response test of 1 h only affected the expression of a small subset of 2'931 genes in both communities. By prioritizing the analysis to regulated contigs and subsequently ranking the sensitivity of the metabolic processes associated with the contigs, photosynthesis, glycolysis, lipid and arginine metabolism were identified as most sensitive pathways affected by the short-term exposure. While the expression of glycolysis, lipid and fatty acid metabolism related contigs similarly declined with increasing diuron concentration, contigs related to the glyoxylate cycle increased in their expression. This pointed to the activation of an alternative pathway for carbohydrate synthesis in both communities. Contigs related to photosynthesis and arginine metabolism showed differential expression in the different communities. The photosynthetic gene regulation involved a reduction of photosystem I in the reference and an induction in the contaminated community. In contrast, the primary target of diuron, photosystem II, remained largely unregulated, and only at high diuron exposure upregulation occurred in the contaminated community. A mechanism for balancing the stoichiometry between the two photosystems is assumed for the reference community, which has already been demonstrated using algal cultures. The up-regulation of photosystem I and also photosystem II at higher diuron concentrations is a potential adaptation resulting from chronic exposure that confers tolerance to diuron in the contaminated community. As the expression of photosystem-related genes depends on the oxidation status of the ubiquinone pool, a deeper analysis of the binding site of diuron at the *psbA* gene needs to be performed to identify potential genetic factors that might favor the observed tolerance mechanism. Furthermore, the different behavior of the arginine metabolism in the different communities could be related to their tolerance. However, further studies particularly addressing the amino acid metabolism are needed to support this finding. Thus, meta-transcriptomics facilitated the identification of photosystem and amino acid metabolism related adaptations to maintain homeostasis under diuron exposure conditions. The use of DRomics enabled the successful prioritization of contigs from the extensive data pool and the formulation of hypotheses that must finally undergo testing in a targeted approach (e.g. using Blast for searching specific genes).

5. Community metabolome analysis

5.1 Introduction to community metabolomics

Chemical pollution drives selection for species while favoring certain physiological traits that enable homeostasis under the given environmental conditions. Identification of these traits can be done at different molecular levels like transcriptomics (see **chapter 4**), proteomics or metabolomics, although integrated analysis of metabolites is the closest molecular readout towards the phenotype and the related ecologic outcome. On the level of the metabolites the activity of 5 million protein coding genes of the earth's proteome (Perez-Iratxeta et al., 2007) converges to changes in the pools of about than 250'000 primary and secondary metabolites (HMDB retrieved 03/2022; Wishart et al., 2021). Hence, metabolites act as an integrating element of the preceding transcription, translation and other regulatory steps. Especially primary metabolites like sugars, amino acids or fatty acids span a range of cellular functions as they control normal growth, development and reproduction in the vast majority of organisms. On the one hand, the integrating character of metabolites in processes of cellular regulation poses a challenge for mechanistic understanding; on the other hand, studying metabolites holds great potential to identify biochemical changes close to the phenotype. Since a single metabolite often has multiple molecular functions in acclimation and overcoming stressful conditions in a cell, it is difficult to assign a protective role to a specific metabolite. Therefore, the interpretation of metabolites must be linked to other physiological data, which is called phenotypic anchoring (Viant, 2007). Only by anchoring molecular patterns in physiological processes it is possible to evaluate metabolite changes in terms of their community function. Another strategy to approach this difficulty is the relative comparison of the metabolome of I) stressed and non-stressed and II) stress-adapted and non-adapted organisms.

The comprehensive analysis of the small biomolecule pools (usually below 1000 Da) synthesized by a biological system is termed metabolomics (Fiehn, 2001). Currently, two complementary approaches – metabolic profiling and -fingerprinting – are in use. Metabolic profiling aims on a quantitative assessment of a selected set of metabolites, while the fingerprinting approach tries to capture as many metabolites as possible regardless their chemical annotation to compare patterns of metabolites that change in response to stress. This unbiased assessment poses a challenge for instrumentation, because of the diverse chemical nature of the metabolite compounds.

So far the application of gas-chromatography coupled to mass spectrometry (GC-MS) covers the widest range of metabolites and is clearly the best platform for untargeted metabolomic fingerprinting (Fiehn, 2016). Combined with a derivatization step, this technique enables the analysis of sugars (mono-, di- and trisaccharides), sugar alcohols/acids, amino and fatty acids, phosphorylated intermediates and many plant secondary metabolites such as phenolics, terpenoids, steroids and alkaloids (Rohloff, 2015).

So far, metabolomics has often been used as a screening tool to investigate adverse effects of chemicals in specific model organisms or to elucidate the mode of action of a chemical (Grossmann et al., 2012). But the vast potential of metabolomics gave rise to novel transdisciplinary fields of application like environmental metabolomics (Bundy et al., 2009; Viant, 2007) or community metabolomics (Jones et al., 2016; Llewellyn et al., 2015). The application of metabolomics in the respective context generally seeks to understand the biochemical mechanisms governing species interactions with their particular environment and its alteration at stressful conditions. Applying metabolomics to communities has the potential to assess their responses in an integrative way, although challenges such as complex data analysis or lower resolution of effects have to be considered. The potential of metabolomics for analyzing aquatic biofilms is rather unexplored. A study of (Gaubert-Boussarie et al., 2020) explored the methodological challenges in metabolic fingerprinting of intertidal mudflat biofilms. The authors proved that metabolomics in biofilms is technically feasible, however, they encountered problems with the annotation of metabolites and the low sensitivity of biofilms in their case study on light exposure. In contrast, a study by Serra-Compte et al. (2018) was able to demonstrate effects of chronic pharmaceutical pollution and desiccation in metabolic fingerprints of Mediterranean biofilms. They identified five respectively seven responsive fatty acids reflecting their exposure history. The most comprehensive metabolomics analysis of biofilms has been carried out by Creusot et al. (2022), who explored the effect of exposure duration and environmental factors such as light, temperature, and flow regime on the metabolic response to the model herbicide diuron. Even though this study does not allow any mechanistic conclusions due to inappropriate quenching during sampling, it could still be shown that biofilms are very sensitive to environmental variables.

In the present thesis, metabolomics was used to characterize the metabolic fingerprint of the reference and contaminated communities and to identify potential adaptations

resulting from chronic exposure. Since the contaminated communities were shown to be more tolerant to diuron (**chapter 3**), and meta-transcriptomics revealed molecular mechanism that supports this tolerance (**chapter 4**), the question arises if these effects also manifest in the metabolome. To reveal such a mechanism, the communities were exposed to diuron in a dose response approach according to the PICT concept and subsequently subjected to a metabolomics workflow.

5.2 Methods

5.2.1 Sampling, metabolite extraction and derivatization

Three colonized slides were quenched directly after acute exposure (see **Annex 1** for details on the cultivation and exposure) in liquid nitrogen and kept at -80°C until further analysis. Then, the slides were freeze dried and alumina cold packs were used to retain the frozen status of samples until completely dry. Dried biomass was homogenized and a 20 mg subsample was transferred into a FastPrep® tube. Then 150 mg of glass beads (5 mm) and 1.2 mL of a solvent mixture containing methanol, chloroform and water (10:5:4, v/v/v) and ribitol as internal standard (10 mg L⁻¹) was added to each sample. Cells were disrupted using a FastPrep®-24 (6.5 m s⁻¹, MP Biomedicals, USA) for 35 sec in three cycles, while the samples were cooled down for two minutes after each run. Cell debris were centrifuged (6 min, 6°C, 20000 × g, r = 10.8 mm) and 1 mL of the supernatant, 0.8 mL milli-Q water and 1.6 mL chloroform were transferred into a 10 mL glass tube. The hydrophilic and lipophilic metabolites were separated by vortexing and a subsequent centrifugation step (10 min, 5°C, 4000 × g, r = 196 mm). One milliliter of the upper hydrophilic methanol/water (=polar) phase was transferred into a 3 mL reaction glass vial and dried at 40°C and gentle nitrogen circulation. The dried sample was incubated with 200 µL MOX™ reagent (2% methoxyamine * HCl in pyridine, PIERCE Biotechnology, USA) for 2 h at 80°C. The methoxaminated samples were dried the same way as before, 100 µL of MSTFA reagent (N-Methyl-N-trimethylsilyltrifluoroacetamide, PIERCE Biotechnology, USA) was added and they were incubated at 90°C for 20 min. Process blanks were included in the metabolite extraction and derivatization step to account and subtract the background contamination of the extraction and derivatization. An aliquot of all samples was pooled into a quality control sample (QC) for the assessment of the instrument performance.

5.2.2 GC-TOF-MS analysis

The samples were randomly analyzed on a gas chromatograph (Agilent 7890, Agilent Technologies, USA) coupled to a time-of-flight mass spectrometer (Pegasus 4D, LECO, USA). The separation was performed with a DB5 column (30m + 10 m DG pre-column, 0.25 mm, 0.25 μ m, Agilent) and helium as carrier gas. A volume of 1 mL was injected in splitless mode and analytes were ionized by electron ionization (see **Annex 6** for instrument settings). Solvent blanks were run every fifth sample, QC samples were placed before and after each sequence and alkane (C7-C30, SIGMA) retention index samples (RI) were analyzed at the end of each sequence.

5.2.3 Data processing and statistical analysis

The chromatograms were aligned using the open source software 'MS-DIAL' version 4.24. (Tsugawa et al., 2015) and the alignment parameters are listed in **Annex 7**. The final alignment of samples contained 1354 peaks which were exported and subsequently corrected by an in-house R-routine. First the alignment was quality checked for peaks that were divided into different alignment ID's. Those peaks were merged if the EI spectrum similarity was above 80 percent, the retention time gap was below 8 seconds and the conflict between the aligned metabolites was below five percent. In total 57 of the 1354 aligned peaks were merged with their corresponding counterpart to correct for peak splitting in the alignment routine. Then the dataset was filtered for artifacts, which were introduced by the MS-DIAL alignment (automatically interpolated peak areas) and sporadically occurring peaks. To this end data were filtered for consistency by requiring a peak to occur at a minimum of 30 percent in the replicates of three subsequent treatments (consistency criterion). The filtering revealed 601 sporadic peaks which were removed from the dataset. In a last filtering step, the blank contamination was removed by setting a five-fold threshold, which the mean peak area must exceed compared to the blank mean. The blank filtering step further reduced the dataset to a final selection of 190 metabolites. This selection was decomposed into sets of common and individual metabolites based on the consistency criterion and plotted in a Venn diagram. The final selection of metabolites was normalized to the internal standard ribitol and the replicates of each treatment were aggregated. The aggregated data was mean centered, auto-scaled and finally subjected to a principal component analysis (PCA). The metabolites were annotated by reference mass spectra of the 'Golm Metabolome Database' (Kopka et al., 2005).

5.3 Results and discussion

5.3.1 Characterization of the metabolic fingerprints

In total 40 % of the 190 metabolites were annotated until the stage of positional isomers and 20 % had a library match of more than 70% and their retention index was within an acceptable range of 15 units. The annotation revealed mono- and disaccharides (13.7 and 5.3 %), amino acids (4.2 %), carboxylic acids (3.7 %), fatty acids (1.6%) and other compounds in smaller quantity. The remaining 60 % of the metabolites were not covered by public libraries and remained unknown in their identity and classification.

A PCA was carried out combining both, communities after succession in the selection phase as well as samples after short-term exposure to structure and prioritize the metabolic features in their response characteristics (**Figure 17**). In total 40 % of the variance of metabolites was explained by the first three principal components (PCs) and 65 % with the first six PCs. PC1 (21.3 %) separated the reference and contaminated communities while the contribution of individual samples to PC1 did not show a distinct pattern. The difference of the metabolic fingerprints of the communities is discussed in **chapter 5.3.2**.

PC2 (8.2 %) and PC3 (7.8%) captured the short-term response to diuron of the two communities in the detection phase. The contribution to PC2 was mainly driven by opposing conditions such as controls and highest diuron treatments, while PC3 represents samples with high diuron concentrations (10, 50 and 100 $\mu\text{g L}^{-1}$). Moreover, PC3 describes a divergent stress response with high diuron stress striving to opposing directions in the PCA. PC2 and PC3 were unable to discriminate diuron treatments below 1 $\mu\text{g L}^{-1}$, which occur close to the controls. The divergent metabolic response is discussed in **chapter 5.3.3** in relation to a potential tolerance mechanism. The subsequent PCs were disregarded in the analysis because their explanatory power dropped to ≤ 5 %.

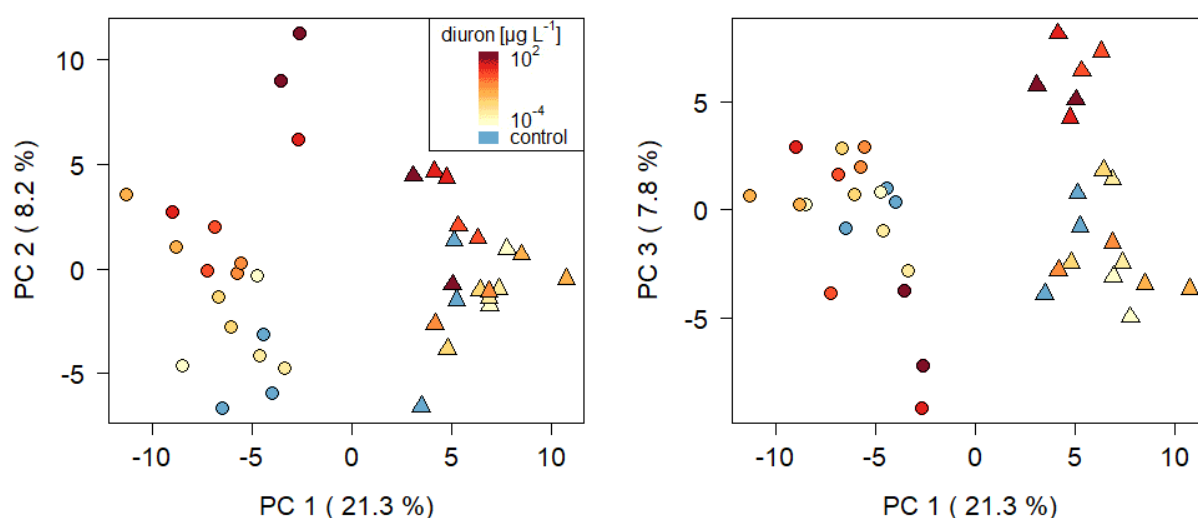


Figure 17 Principal component analysis of the metabolic fingerprints based on the 190 autoscaled metabolites. The different concentrations of the acute 1h exposure are presented based on a color gradient ranging from red (high exposure) to yellow (low exposure), whereas blue depicts controls. The contaminated community is marked by the triangle ▲ and the reference community by the filled circle ●.

5.3.2 Difference in the metabolic fingerprints

The PC1 has revealed a general difference in the metabolic fingerprints of the two communities. This difference was further investigated in a Venn diagram, in which the final selection of metabolites was divided into shared and individual metabolites based on their occurrence (**Figure 18**). About 107 of the 190 metabolites were exclusively found in one of the respective communities (individual metabolites). The remaining 83 metabolites were found in both communities equally (shared metabolites). The proportion of unannotated metabolites was 65% in the contaminated, followed by the reference communities with 57% and lowest in the shared fraction with 49%. Thus, the unknown metabolites were particularly involved in the discrimination of the communities on PC1. Specific marker metabolites were not identified in any of the communities to explain the community difference, but these may exist within the unknowns. A potential exception is the metabolite 785, which was tentatively identified as lumichrome, a photodegradation breakdown product of riboflavin. This metabolite was widespread in the contaminated communities and its content was twice as high as in reference. The vitamin riboflavin is a versatile secondary metabolite involved in regulation of energy metabolism, growth and development (Averianova et al., 2020) and pathogen resistance (Boubakri et al., 2016). Moreover, the unknown metabolites

748, 772 and 895 show a high contribution to community separation and indicate a molecular weight above 250 Dalton based on their retention time and fragmentation pattern. A large fraction of unknown metabolites was also reported by Gaubert-Boussarie et al. (2020), who analyzed microphytobenthic biofilms in intertidal mudflats using a comparable method. Compared to tissues or dense cultures, biofilms have three main differences: I) biofilms contain organisms with different sensitivities and metabolic effects in a small portion of affected species might vanish in the pools of the non-affected ones, II) the diversity in species increases the diversity in metabolites that potentially co-elute and form ambiguous mass spectra, and III) the cellular biomass is low compared to the EPS and detritus. All factors affect the detection of changes in the metabolite pools and the annotation quality.

I) Not all species in a diverse assemblage are equally affected by a stressor, so that small changes in metabolite pools can fall below the detection limit. Furthermore, the high diversity of species within the community brings along an additional variety of metabolites beyond the focus of classical research (such as secondary metabolites). Secondary metabolites of environmental communities have a limited representation in public libraries, as they are non-essential to the life of the producer and are only formed for specific functions such as protection against environmental stressors or competitive interactions.

II) As biodiversity increases, so does biochemical diversity. However, in gas-chromatography, the performance of the separation processes limits the resolution of the individual metabolite spectra. Complex mixtures of structurally similar compounds tend to produce co-eluting substances which affects the annotation based on the spectral identity as well as the quantification.

III) Another factor that can dilute metabolites below the detection limit is the EPS fraction. A review on the poorly studied EPS compartment by Flemming and Wingender (2010) states that active cells in biofilms can have a low content of only 10 % of the total dry weight. In contrast the EPS represents a large exo-metabolome of collectively released polysaccharides and other metabolites with largely unknown chemical composition. Since biofilms are inseparable from the EPS, metabolomics always provides an integrating profile of all compartments. Chronic exposure to pollutants can alter the composition of EPS, which may indicate a protective

mechanism (Gu et al., 2017; Polst et al., 2018) or altered species composition and may be persistent in the metabolic fingerprint even after exposure has subsided.

In conclusion, the chronic exposure resulted in the selection of specific biochemical traits which could be related to changes in the structural composition (see **Chapter 3.3.1**), physiology and EPS composition. Regardless of the different causes, the clear separation of the communities illustrates the strong power of the metabolic fingerprinting approach to detect the effects of chronic diuron exposure at the biochemical level.

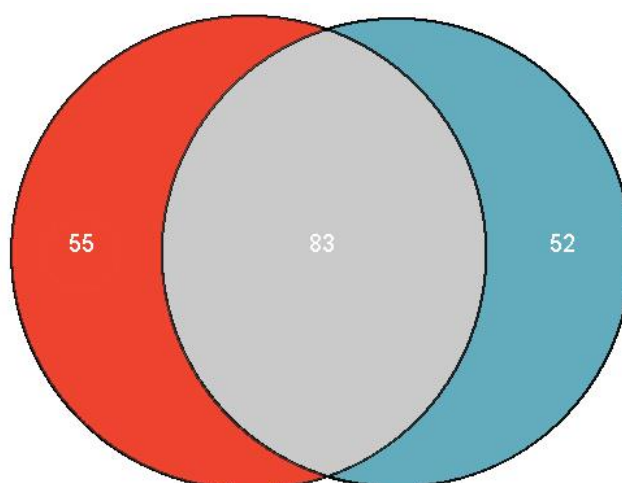


Figure 18 Venn diagram of the 190 metabolites of the final alignment. The red fraction illustrates metabolites that were particularly present in the contaminated communities, while the blue represents the same finding for reference.

5.3.3 Differential metabolic responses of the communities to short-term exposure of diuron

PC3 (**Figure 17**) was associated with a divergent metabolic response, and monosaccharides, sugar alcohols and orthophosphate had a particular high loading. Especially the metabolites 1146, 1100, 675, 1048 and 1113 represented the top 5 with a loading of more than 3%. The metabolites 1146 and 1100 were identified as pentose acid lactones, with lyxonic acid-1,4-lactone (1146; LAL) and arabinonic acid-1,4-lactone (1100; AAL) having the highest library agreement (see **Figure 19** for examples). Since the pentose acid lactones are stereoisomers of a larger group, their

exact annotation cannot be guaranteed without a reference standard. Both metabolites decreased in reference communities by a log2 fold change of 1.3 whereas they increased in contaminated communities by 1.7. A similar pattern was observed for metabolite 1048, which was tentatively identified as threonic acid (TA). Contrary to this observation, the pools of metabolite 675 increased by 4.8 in the reference but decreased by 2.8 in the contaminated communities. The mass spectrum of this metabolite is similar to glycerol (GL) (similarity of 65 %), however some fragments like m/z 148 or 127 did not match the library reference. Other metabolites such as 670 (phosphoric acid; PA), 1285/1286 (glycerolaldopyranosid; GAP) and 1152 (anhydroglycopyranose; AGP) showed a very similar response to metabolite 675, but with a less pronounced fold change.

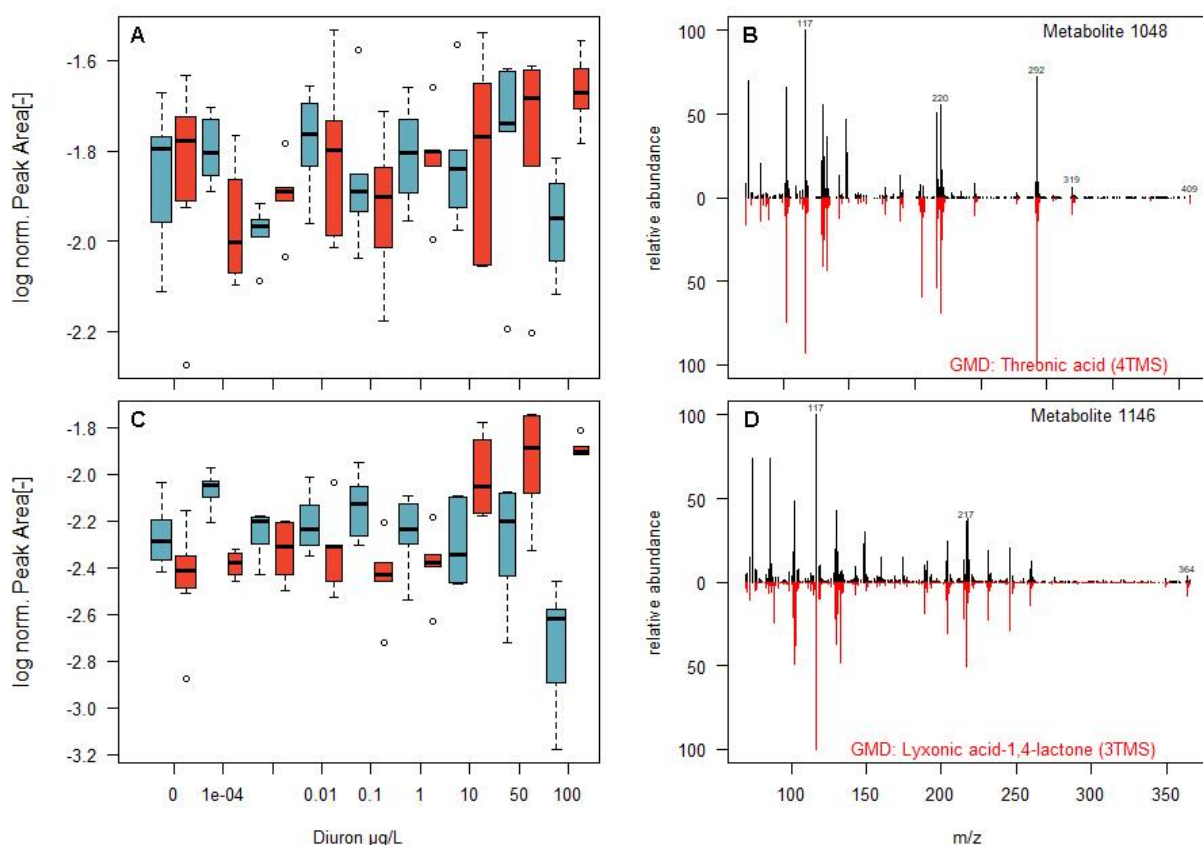


Figure 19 A, C) Boxplot of the normalized peak area of the metabolites 1048 (TA) and 1146 (LAL) with the reference communities in blue and contaminated communities in red. B, D) Spectrum of the metabolites 1048 and 1146 (black) and the highest match of the Golm Metabolome Database (red).

Many carbohydrates switch between cyclic and open chain forms, and each of the various forms would lead to different peaks in gas chromatography. To avoid cyclization, the carbonyl groups of carbohydrates were methoximated, which should give two different peaks in the chromatogram (Engel et al., 2020). However, some of the metabolites were detected in a cyclic structure such as lactones and pyranose sugars. This implies that derivatization may have triggered the formation of multiple peaks from the same precursor due to anomerization (geometric variation in the cyclic molecules). This technical constrain was caused by an incomplete methoximisation step prior to GC analysis, which was also observed in the study by Gaubert-Boussarie et al. (2020). Whether this is an inherent property of the biofilm matrix or due to an unsuitable derivatization reagent remains to be explored. Despite this limitation, the dynamics of these metabolites are not affected by this effect, but some additional peaks may be suspected in the subsequent analysis.

The prominent role of the metabolites LAL, AAL and TA in the differential response of the communities might indicate an adaptation to diuron in the contaminated communities. According to the KEGG PATHWAY database (see **chapter 6.1** for more details) the metabolites LAL and TA are involved in ascorbate and aldarate metabolism (Kanehisa & Goto, 2000), where they are formed as degradation products from ascorbic acid. These products may have formed *in-vitro* (Parsons et al., 2011) or during extraction and derivatization (Dewhirst et al., 2020; Smuda & Glomb, 2013). Ascorbic acid in aqueous extracts undergoes degradation processes in the presence of oxygen atmosphere, pH changes, light and elevated temperature (Deutsch, 1997). Dissolved oxygen triggers the conversion of AA to dehydroascorbic acid (DHA), which in turn may undergo hydrolysis or amine-induced cleavage (Smuda & Glomb, 2013). Derivatization of the metabolite extracts with acidic methoxyamine may have favored the amine-catalyzed breakdown of DHA to carboxylic acid such as threonic acid, lyxonic acid and xylonic acid. In conclusion, there is evidence that the contaminated communities have increased their AA metabolism as a potential defense mechanism to the chronic diuron exposure. The ascorbate-glutathione cycle maintains the ascorbate pool on a stable level of more than 90 % reduced molecules under homeostatic conditions (Smirnoff & Pallanca, 1996). According to the MoA of diuron, the compound primarily suppresses the light-dependent reaction of photosynthesis and the formation of high-energy compounds such as adenosine triphosphate (ATP). Apart from the primary MoA, illumination of the herbicide-inhibited photosystem II

facilitates charge recombination reactions that form singlet oxygen radicals by transferring electrons to O₂ (Krieger-Liszky & Rutherford, 1998; Rutherford & Krieger-Liszky, 2001). The formation of reactive oxygen species (ROS) is part of the natural metabolism of autotrophic cells. Hence, cell compartments like the stroma hold up a pool of 10 to 50 mM of AA to prevent cellular damages (Smirnov & Pallanca, 1996). The elevated amount of LAL, AAL and TA found in the contaminated communities might relate to an adaptation in the ascorbate-glutathione cycle acquired during the chronic exposure with 4 µg L⁻¹ diuron. A diuron concentration of more than 10 µg L⁻¹ may have triggered the formation of AA in the contaminated communities, which was impossible in the reference communities due to diuron related metabolic shortages. In contrast, LAL, AAL and TA in the reference communities even fell below control values at diuron concentrations above 10 µg L⁻¹, which could indicate enhanced catabolic processes due to energy deficiency.

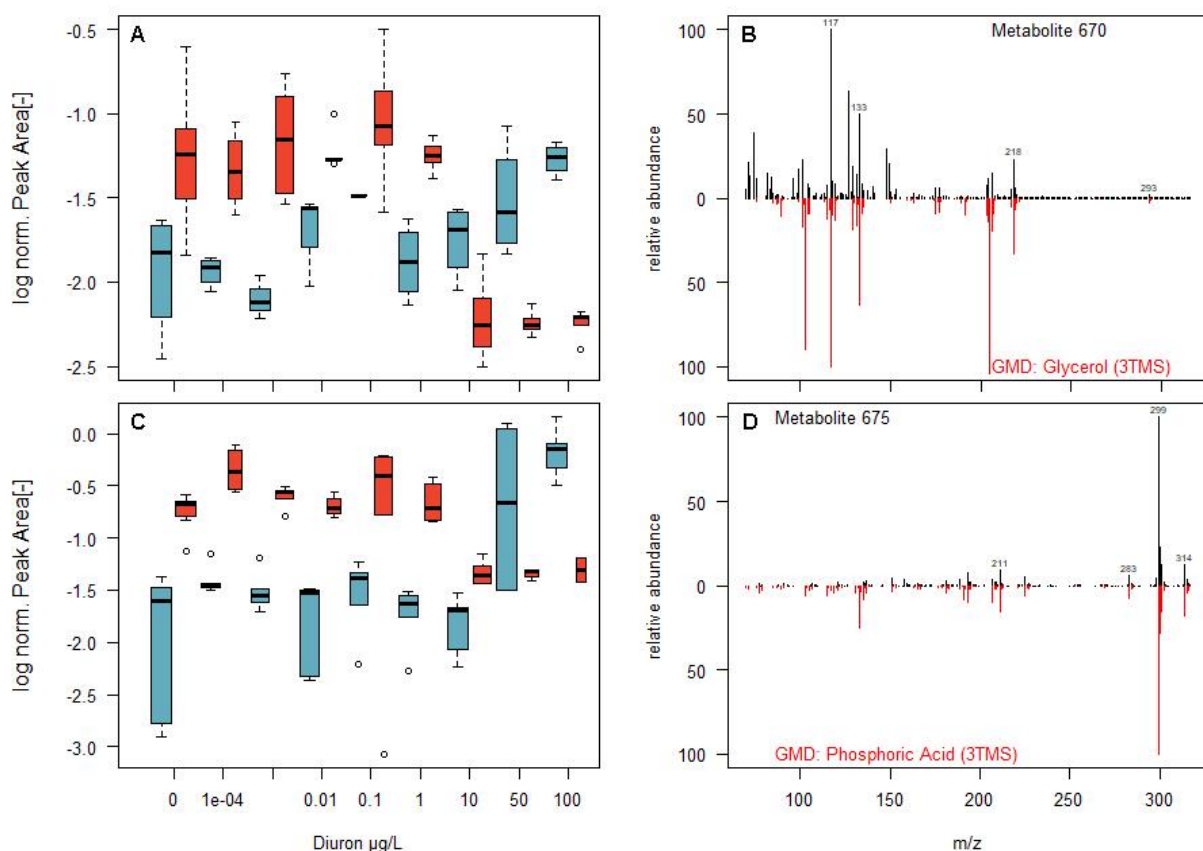


Figure 20 A, C) Boxplot of the normalized peak area of the metabolites 670 (GL) and 675 (PA) with the reference communities in blue and contaminated communities in red. B, D) Spectrum of the metabolites 670 and 675 (black) and the highest match of the Golm Metabolome Database (red).

In addition to the sugar acids, PA, GL, GAP and AGP also showed divergent response tendencies in the communities, with an increase in the reference and decrease in the contaminated communities (see **Figure 20** for examples). The origin of the PA remains unknown, but its central role as an important intermediate metabolite in the energy metabolism points to a clear stress response mechanism. It is possible that a large amount of phosphate was derived from phosphorylation of e.g. sugars, lipids, or nucleotides. Comparable results were found in Kluender et al. (2008), who detected a decrease in phosphorylated sugars, after 4 h of exposure of an algal culture to a PSII inhibiting herbicide. Unfortunately, no phosphorylated compounds were detected in this study, which might result from a low pool size of the phosphorylated forms. Nevertheless, the increase of PA and GL pools in the reference communities indicates an increased sugar and lipid metabolism for reallocation of energy in the cells as a result of their photosynthetic energy shortage. A similar induction of PA and GL pools was observed in the metabolome of the diatom species *Tabellaria flocculosa* re-exposed to 500 $\mu\text{g L}^{-1}$ Zn (Gonçalves et al., 2018). The authors also concluded from the induction that the cells might have reached a low energy status due to catabolic process. In contrast, the abrupt decline in the contaminated communities might relate to their strategy to acquire energy at diuron concentrations above 10 $\mu\text{g L}^{-1}$. Thus, the contaminated communities could invest free PA in their energy metabolism, which could explain the decrease.

5.4 Summary and conclusion

In summary, community metabolomics revealed a distinct molecular fingerprint corresponding to the respective exposure history of the communities and acute exposure revealed a potential mechanism of diuron tolerance in the contaminated communities due to opposing responses in distinct metabolites. The annotation of these metabolites indicated an adaptation in the ascorbate-glutathione cycle, which may support cellular homeostasis against reactive oxygen species. The observed molecular response can be linked to the MoA of the herbicide, because the overproduction of ROS can be considered as a major effect of this PSII-inhibiting herbicide (Rutherford & Krieger-Liszkay, 2001). To confirm the suspected adaptation, the discussed metabolites should be validated with reference material or the structure should be elucidated by GC-APCI-TOF. In conclusion, metabolomics provides insights into molecular stress adaptations at the community level, although the quality and quantity of biogenic metabolites is lower than in tissues or cultures. Due to the higher taxonomic complexity, compound annotation is still a major challenge. Therefore, the mechanistic insight into complex community responses is very limited using untargeted GC-based metabolomics.

6. Synthesis

6.1 Approaches and challenges for linking molecular data to functional measurements

Molecular processes can be described as multidimensional networks of interconnected processes that have proven to be resilient against environmental fluctuations. Unless precise knowledge regarding a molecular endpoint is known, molecular methods are helpful in an integrative analysis (multi-OMICs approaches). However, such analysis generates large amounts of multivariate data and brings along the problem that is paraphrased by the 3 i's - integration, interpretation and insights. **Integration** is the process of analysing multiple molecular and physiological datasets in a synergistic fashion, with the aim of gaining added knowledge from their combination. However, a major weakness of integration tools remains that they do not include higher aggregated measurements such as phenotypic, physiological or functional measurements in their analysis. However, these represent the final manifestation of the molecular changes and should therefore be considered in ecotoxicological studies (e.g. through anchoring approaches). Integration of data can be achieved with different approaches that can be divided into two categories: unsupervised methods such as (multivariate) statistics (e.g. correlation, dimension reduction, clustering) and supervised methods (e.g. pathway analysis). Unsupervised statistical methods remain at the descriptive level of pattern recognition and require annotation of prioritized elements to allow interpretation, whereas supervised methods can only be applied to annotated data. Thus, the **interpretation** is based on the commonalities of the data and requires an annotation of the responsive elements. **Insights**, in turn, can only be derived from the larger context of the data and require relationships to phenotypic, e.g. ecological parameters.

A special form of unsupervised analysis of molecular data is **numerical aggregation**, which does not meet the definition of integration as defined above, but is well suited for a reduction of data complexity to an index value and thus allows a comparison with other univariate measurements. For molecular items this idea was first introduced by Lobenhofer et al. (2004) who summed the number of significantly altered genes, subjected this parameter to dose-response modelling and estimating a No Observed Transcriptional Effect Level (NOTEL), at which the studied estrogenic compound did not alter gene expression in the investigated cells. However, this approach was not

quantitative in terms of the extent to which a gene was altered, and thus, Gou and Gu (2011) adopted their idea and designed a quantitative index, the Transcriptional Effect Level Index (TELI). This index reflects transcriptomic activity compared to a reference condition, assuming that any deviation from the reference conditions triggers gene expression that alters the TELI. The aggregation of gene expression in combination with a dose-response approach allowed Gou and Gu (2011) to compare effect thresholds (EC_x) of gene expression with phenotypic endpoints such as cell growth inhibition. The same approach was transposed to the level of proteins (Proteomic Effect Level Index - PELI; Lan et al., 2016) and metabolites (Metabolic Effect Level Index - MELI; Riedl et al., 2015). However, the applicability of aggregated parameters in complex microbial communities has rarely been studied. To the author's knowledge, the TELI has not been applied in any community approach so far, while the MELI was recently tested in biofilms exposed to diuron (Creusot et al., 2022). The authors proved the MELI can be a sensitive tool to detect molecular changes even at lower concentrations than photosynthetic yield analysis of chlorophyll fluorescence and therewith confirmed the findings of Riedl et al. (2015).

An approach that facilitates unsupervised data integration of different biological level is **sensitivity analysis** combined with the cumulative sensitivity distribution (CSD) analysis. The rationale of this approach is the integration and comparison of different biological entities based on their response sensitivity thresholds (e.g. BMD, EC_x) derived from dose-response analysis. Dose-response analysis from molecular datasets is a challenging task that includes processing of very large datasets, in addition to requiring the implementation of a variety of biological response trends (e.g. linear, sigmoid or Gaussian models). For instance, the meta-transcriptome dataset of this thesis contained 36 treatments with 3.5 million contigs. Recently, these challenges have been addressed by an automated R application 'DRomics' that offers a wide range of different dose-response models for the sensitivity threshold estimation (Larras et al., 2018). Afterwards, the obtained sensitivity thresholds are ranked in into a CSD, which was originally developed to compare species sensitivities towards chemicals (e.g. Fox et al., 2021). In contrast to this original intention, the CSD in this study comprises thresholds of molecular and apical changes as illustrated by Larras et al. (2020). The CSD is classically used to estimate the concentration of a chemical that is hazardous to x percent of all species (HC_x). Since gene regulation or metabolite

changes do not indicate a general hazard, the term molecular regulation concentration (MRC_x) is used in this thesis instead of HC_x . The MRC_x indicates the concentration of a chemical that triggers the regulation of x percent of genes.

However, aggregation to index values and CSD analysis only gives information about a general impact, whereas molecular data can provide insights up to the interpretation of cellular mechanisms. Towards this end molecular data needs to be annotated with respect to the molecular function, which will be addressed in the following and exemplified with the findings of this thesis. In recent years, a variety of integration and mapping tools have been introduced covering the different molecular data types (see Misra et al., 2019 for a recent review). One of the most comprehensive knowledge bases to support annotation, integration and biological interpretation of large molecular data sets across different molecular scales (genes, proteins and metabolites) is the Kyoto Encyclopedia of Genes and Genomes (KEGG) (Kanehisa & Goto, 2000). Compared to the Gene Ontology (see **Chapter 4.2.4**), KEGG combines in a single resource the cross-species annotation of genes and proteins using published complete genomes and links them to the level of metabolites using manually constructed networks of molecular interactions (Aoki-Kinoshita & Kanehisa, 2007). These networks are based on a hierarchical classification system that groups gene catalogues from sequenced genomes into metabolic pathways, which in turn are assigned higher-level systemic functions for the cell, organism and ecosystem. Thus, KEGG enables integration of the transcriptomic and metabolomics data of this thesis into associated molecular functions (e.g. **Table 5** carbohydrate metabolism). This nested approach reduces complexity of datasets of different molecular data types in a similar manner - as a cell converges in its processes towards the phenotype.

The advantage of sensitivity analysis of functional classified molecular data was first demonstrated by Thomas et al. (2007), who explored gene expression changes in rat nasal epithelium following acute formaldehyde exposure from a risk assessment perspective. The rationale behind this approach is to derive a critical concentration for changes in molecular functions that can be used for mechanistic understanding of the MoA of a chemical or risk assessment of molecular impairment. However, not every change at the molecular level testifies an adverse effect on organismal or even community level. Rather, it demonstrates the need for molecular regulation in the face of changing environmental conditions. Therefore, risk assessment of chemicals at the molecular level is only meaningful if it is linked to adverse outcomes, as conceptualized

in the ‘phenotypic anchoring’ approach (see **chapter 1.5**) or the concept of ‘adverse outcome pathways’ (Ankley et al., 2010).

Based on the classification into molecular KEGG functions, the sensitivity analysis in the CSD can be transformed into a functional cumulative sensitivity distribution (CSD_{func}). Thus, a collective sensitivity for each KEGG function need to be computed, ranked and compared. This way, different molecular levels can be integrated and compared with sensitivities derived from traditional phenotypic observations. Larras et al. (2020) illustrated the power of this approach in combining and comparing data from different molecular origins (transcriptomics and metabolomics). Integrating molecular data to KEGG molecular functions allowed the authors to capture the primary MoA of their tested pollutant and to rank the molecular levels in their sensitivity. Through this approach, molecular impairments can be identified, which can be linked to the phenotype or ecologic functions using the same sensitivity threshold. The above-mentioned examples are based on single species cell cultures, whereas integration of molecular data from multi-omics approaches on community level were not done, so far.

In this work, the molecular data is classified according to the KEGG functional classification system, which is linked in a second step to the photosynthetic yield based on the sensitivity distribution analysis. This should facilitate a direct comparability of the different molecular and functional levels and address the following questions: Does a sensitivity-based integration of molecular fingerprinting approaches of freshwater biofilms allows to identify stressor-related adaptations? Is there a relationship between molecular and apical functional parameters in microbial community approaches?

6.2 Methods

6.2.1 Summary on the data

The sensitivity analysis, performed in this study, combines the physiological data from chapter 3 with the molecular data from **chapter 4** (meta-transcriptomics) and **chapter 5** (community metabolomics). To enable comparison, these data were processed by a comparable workflow (DRomics) and BMD-1SD sensitivity thresholds were derived for each item and community. **Table 4** summarizes the data available from the different analysis.

Table 4 Summary on the data collected in the physiological and molecular analysis.

Data type	No. of elements	BMD	KEGG Annotation
Photosynthesis	1	1	1
Meta-Transcriptomics	3'502'153 contigs	2'931	626
Community Metabolomics	190 metabolites	18	6

6.2.2 Aggregation of molecular data to index values (TELI and MELI)

The processed molecular datasets (**Table 4**), which included 3.5 million contigs and 190 metabolites, were each subjected to the aggregation as described by Gou and Gu (2011) and Riedl et al. (2015). In contrast to the Gou and Gu (2011) formula, the logarithm to base 2 was used in this work and normalization to exposure time was not performed, as all communities were exposed to an identical time. Instead, both indices were normalized to the number of aggregated elements. The validation of the indices was carried out manually to guarantee the exclusion of distorting extreme values.

6.2.3 Functional annotation of contigs and metabolites using KEGG

The sequence information of annotated genes helps to assign orthologous genes in non-annotated sequences based on sequence similarity. Towards this end, the filtered subset of 908 responsive and annotated contigs was processed on a web-based server called KEGG Automatic Annotation Server (Moriya et al., 2007), which automated the K number assignment. During data processing a similarity score of the query and the reference sequence set (taken from the KEGG GENES database) is computed, which facilitates to identify homologous genes. These are divided according their KO groups and the K number of the KO group with the highest similarity score is

assigned to the query sequence. KEGG comprises a classification database, called KEGG Orthology (KO) linking annotated genes with their molecular pathway and function (see **Table 5**). The functional annotation was downloaded and the BMDs of each molecular function were aggregated separately for each community using the median. For the calculation of the median, only functions with more than 3 BMD's were considered. The median was chosen to account for the diversity of sensitivities in the biofilm community, instead of prioritizing the most sensitive contigs by e.g. using the 25th percentile. A total of 453 K numbers were assigned, deriving from 114 contigs for the reference communities and 339 from the contaminated communities.

Table 5 Example of the hierarchical classification system of KEGG. There are six top categories (09100 to 09160) covering 34 molecular KEGG functions (e.g. 09101 carbohydrate metabolism) which contain 356 KEGG pathways (e.g. 00010 Glycolysis / Gluconeogenesis).

▼09100 Metabolism

▼09101 Carbohydrate metabolism (KEGG function)

▼00010 Glycolysis / Gluconeogenesis [PATH:ko00010] (KEGG pathway)

- K00844 HK; hexokinase [EC:2.7.1.1]
- ...

►00020 Citrate cycle (TCA cycle) [PATH:ko00020] (KEGG pathway)

►...

►09102 Energy metabolism (KEGG function)

The log transformed dataset covering the final set of 190 metabolites was processed in DRomic's (similar to the meta-transcriptome data described in 4.2.4) using itemselect () with the quadratic trend test option and a false discovery rate of 10 % for selecting responsive elements. Models were fitted with drcfit() using the Akaike information criterion (AIC) and BMD's were determined using bmdcalc() and a z value of 1. A total of 25 BMDs was assigned for 18 metabolites. The discrepancy between the number of BMDs and metabolites results from metabolites where a BMD was derived for both communities. Compared to the automated gene annotation with KAAS, metabolites needed a manual annotation before a KEGG Compound identifier (C number) was assigned. Due to the low annotation depth of the metabolites, only 25 of the 190 metabolites could be assigned to a C number. The intersection of

metabolites with a C number and BMD was 6, which was the final set of metabolites that was joint to the meta-transcriptome data and subjected to the cumulative sensitivity distribution analysis. This involved the metabolites ID's 670 (phosphoric acid (3TMS)), 675 (similar to glycerol (3TMS)), 1100 (arabinonic acid-1,4-lactone (3TMS)), 1146 (lyxonic acid-1,4-lactone (3TMS)), 1147 (putrescine (4TMS)) and 1227 (glucopyranose (5TMS)).

6.3 Results and discussion

6.3.1 Results of aggregation techniques

The molecular data was aggregated into index values representing a quantitative measure of the global transcriptional and metabolic responses to establish comparability with the photosynthesis parameters. The calculation of the transcriptional index TELI revealed a high leverage of extreme values influencing the result (**Annex 9**). Between 9 and 27 extreme values of the 3.5 million contigs accounted for 13 up to 65% of the TELI. These contigs were examined for plausibility by filtering for consistent regulation patterns in the light of the exposure design e.g. by matching their identity to the contigs filtered by DRomics (see **Chapter 4.3.2**) and visual inspection. None of the contigs was included in the DRomics results, and the majority of the contigs only appeared as sporadic signals. Thus, the extreme values were removed and the TELI was re-calculated (**Annex 10**). The TELI does not show a concentration-dependent dynamic, but indicates an overall higher transcriptional activity in contaminated community. The TELI of the contaminated communities was higher than the TELI of reference communities, except for the treatments with 0.001 and 1 $\mu\text{g L}^{-1}$. This underlines the distinct fingerprints of communities revealed by the PCA analysis in **chapter 4.3.1**.

The aggregation of the community metabolome into the MELI revealed the problem of large data gaps of about 20 % missing values in the peak tables. The data was reduced to complete records, leaving 78 and 87 metabolites for the reference and contaminated communities, respectively, for the calculation of the MELI. However, the MELI was also dominated by extreme values (cf. **Annex 11 A and B**), which were removed after a visual inspection. After removal of the extreme values, no concentration-dependent dynamics was found in the communities (**Annex 11, B**). Generally, the reference communities had a higher MELI than the contaminated in the low concentration range,

but at 10, 50 and 100 $\mu\text{g L}^{-1}$ diuron treatment, the contaminated community exceeded the reference MELI. As the MELI does not provide any information about the type of change (i.e. increase or decrease of a metabolite), only a general metabolic activity can be deduced from this rise in MELI.

In summary, aggregating community omics data is a delicate task that requires manual data curation and quality control. In particular, dealing with extreme values complicates application of aggregation approaches, as extreme values may indicate I) potential biomarkers or II) represent technical artefacts of the bioinformatic pipeline. Verification of extreme values is not in line with the goals of aggregation, which should enable a rapid assessment of effects. Aggregation techniques may have advantages when dealing with uniform responses of identical organisms e.g. in cultures or if the application is focused on the raw data before processing e.g. the use of fragments instead of peaks in mass spectrometry of metabolites (Creusot et al., 2022; Riedl et al., 2015). Similar to the results of the PCA (see **Figure 10, Chapter 4.3.1**), the TELI also failed to reveal the effect of the short-term exposure on the autotrophic part of the communities. This highlights the weaknesses of global unfiltered analysis of meta-transcriptome data and reinforces the sensitivity-based approach as a viable way for prioritization and comparison of responsive items. The MELI performed slightly better, which may be due to the methodological focus on primary metabolites (e.g. sugars). Due to the methodological difficulties and the limited significance, the aggregation methods are not considered further in the following.

6.3.2 Sensitivity analysis of the different molecular approaches and endpoints

The BMD values of the different molecular approaches were ranked in a global cumulative sensitivity distribution (CSD) (**Figure 21**) according to their sensitivity in the different communities. The sensitivity distributions of both communities clearly differed in their pattern with the reference communities showing a steeper increase of responsive contigs with increasing diuron concentration. In contrast, the contaminated communities revealed a much weaker increase in activated molecular responses, which is also reflected in the molecular regulation concentration that affects 20% of genes (MRC_{20}). The MRC_{20} differed between the communities by a factor of 1000 ($\text{MRC}_{20 \text{ conta}} = 8.2 \mu\text{g L}^{-1}$; $\text{MRC}_{20 \text{ ref}} = 8 \cdot 10^{-3} \mu\text{g L}^{-1}$). The initial steep increase in the CSD's represents contigs that already showed a difference from the controls at the

lowest diuron concentrations. Another phase of steep increase in the CSD's occurred above the diuron concentration that inhibits 50% of the photosystems (EC_{50}). This phase is also characterized by detectable changes in the majority of the metabolites. One metabolite in each community had a higher sensitivity than the majority of all others. However, their annotation remained unsettled and the BMD's of these metabolites were uncertain due to visual inconsistencies of the data and the modelled curve. Therefore, these metabolites were disregarded in the further consideration. The different response characteristics of the CSD's and especially the different dynamics found in the range of the EC_{50} of photosynthesis inhibition with the remarkable increase in transcript and metabolite changes illustrates the difference in adaptation of the communities after chronic exposure. The sharp increase in responses occurred in the contaminated communities at higher concentrations compared to the reference communities, indicating their adaptation to chronic diuron exposure. This adaptation has already been identified in photosynthetic tolerance (see **chapter 3.3.3**) and could be confirmed here using molecular methods. The coincidence of the EC_{50} of photosynthesis inhibition and the strong increase in molecular regulation opens up the potential to use CSD curves and MRC thresholds as a molecular marker for PICT.

Although the CSD's revealed molecular regulation up to the $ng\ L^{-1}$ range, this cannot be supported by apical effects in this study nor literature. A study of Nestler et al. (2012) confirmed regulation in the proteome of the microalgae *C. reinhardtii* exposed to $769\ ng\ L^{-1}$ diuron, with a majority of altered protein found in the photosystem and protein synthesis. In this study regulation in gene expression was revealed by modelling even at $0.1\ ng\ L^{-1}$, which corresponds to a total of $51\ 10^9$ diuron molecules in the solution. Even though this seems an appropriate amount for cellular effects, apical effects have not been reported so far. A query of the ECOTOX knowledgebase (keywords: diuron, aquatic, algae; date: 13.11.2021) yielded in lowest observed effect concentrations (LOEC) for photosynthesis between 0.1 and $5\ \mu g\ L^{-1}$. As apical effects of diuron at the primary site of action occurred beyond a BMD of $1.7\ \mu g\ L^{-1}$ in this thesis, molecular regulation at lower concentrations is considered effective in restoring homeostasis and no immediate impairment can be inferred. Thus, interpretation of molecular responses below the BMD may provide mechanistic insights into cellular regulation, but is not appropriate in the context of risk assessment.

Before interpreting the sensitivity distribution with respect to cellular regulation, it is important to be aware of the sensitivity bias of the two molecular methods. Both, meta-

transcriptomics and community metabolomics integrate the effects in the different organisms of the biofilm, but at a different resolution. Meta-transcriptomics allows differentiation of responses down to isoform genes, while metabolomics also incorporates changes (in small molecules) in the EPS matrix. This may reduce the sensitivity to small scale effects imposed to a subset of the biofilm species at acute exposure. Therefore, no mechanistic comparison of the sensitivity of stress responses at the different biological levels can be made, but the general sensitivity of each method for detecting effects in a complex biofilm community can be illustrated. Metabolomics has been shown to be very sensitive to detect effects in cultures of the chlorophyte *Scenedesmus vacuolatus* (Sans-Piché et al., 2010) or the macrophyte *Myriophyllum spicatum* (Riedl et al., 2015) even at sub-inhibitory concentrations of endpoints, close to the MoA of the toxicant. Creusot et al. (2022) argued that this sensitivity can also be transferred to biofilms communities under diuron exposure. The authors showed that at the BMD_{1SD} value of the photosynthesis inhibition ($1.13 \mu\text{g L}^{-1}$), already around 45 % of the metabolites have been altered. However, the annotation of their responsive metabolites revealed mostly fatty acid metabolism related compounds, but no relation to the MoA of diuron. Obtaining sensitive responses beyond the primary effect of the chemical raises methodological questions, which the authors discussed in relation to improper quenching during sampling. Thus, a direct comparison of the results remains challenging. Regarding methodology, there are two major differences: firstly Creusot et al. (2022) used ultra-performance liquid chromatography system coupled to high-resolution mass spectrometry (UPLC-HRMS) and secondly their acute exposure time was twice as long. Using UPLC-HRMS allowed the authors to analyze underivatized samples, which on one hand narrows down the spectrum of potential analytes but on the other hand also reduces the interfering influence of EPS, which is partly dissolved by derivatization. The interfering properties of EPS in derivatization of GC-TOF samples and the abundance of the potential target organisms as a decisive factor for the sensitivity of community metabolomics were discussed in detail in **chapter 5.3.2**. In conclusion, the methodological differences between the studies do not allow for comparability and thus the lower sensitivity of the metabolome in this study needs to be validated in future studies.

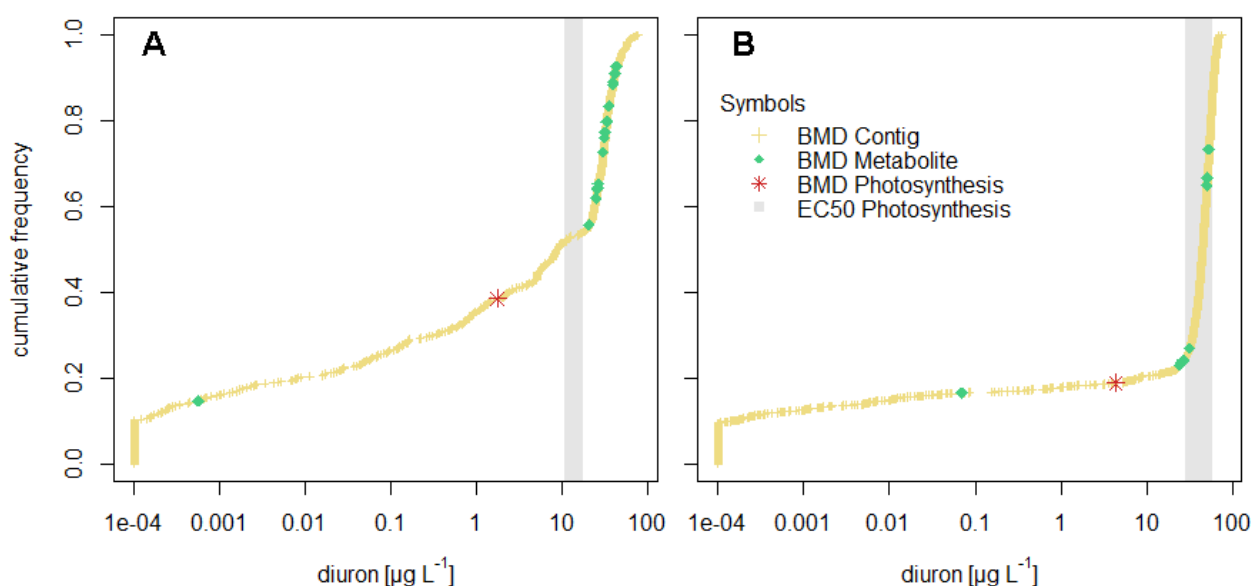


Figure 21 Global cumulative sensitivity distribution of the contigs, metabolites and inhibition of the photosynthetic yield along the diuron gradient of the reference communities **A)** and the contaminated communities **(B)**. The grey-shaded area illustrates the concentration range when 50 % of the photosynthetic yield is inhibited.

6.3.3 Mechanistic view of the molecular stress responses based on KEGG functions

The global CSD allows insights into the cascaded efforts of exposed organisms to maintain cellular homeostasis. However, this approach does not allow a mechanistic perspective on the maintenance of homeostasis with increasing exposure concentration, because they are not related to molecular functions. For this reason, the elements of the global CSD were translated to their molecular functions using KEGG and a median BMD was assigned to each function. Filtering and aggregating BMD's to KEGG functions reduced the complexity of incoherently regulated contigs and allowed to focus on general patterns and affected functions.

The resulting functional cumulative sensitivity distribution (CSD_{func}) (**Figure 22**) confirms the characteristic curves of the communities of the global analysis in **Figure 21**. The reference communities showed a broad range of molecular KEGG functions regulated in response to increasing diuron concentration starting at $0.001 \mu\text{g L}^{-1}$ and ending at $31 \mu\text{g L}^{-1}$. In contrast, the molecular response in the contaminated communities occurred within a small concentration range of 27 to $51 \mu\text{g L}^{-1}$, which overlaps EC_{50} of photosynthesis inhibition. As the plotted thresholds for the molecular

functions are median values of the associated BMDs, a broader distribution of the underlying BMD's is conceivable. This is underlined by the standard distribution for the median BMD's which ranged from 12 to 21 $\mu\text{g L}^{-1}$ in the reference and 18 to 28 $\mu\text{g L}^{-1}$ in the contaminated communities. Taking together the large range of medians and the high standard deviation in the responses of the reference communities, it can be concluded that they reacted very variably with respect to their molecular functions, while the contaminated communities responded rather homogeneously. Comparing the reference and the contaminated communities with respect to their median BMDs of a KEGG function ($\text{BMD}_{\text{ref}} / \text{BMD}_{\text{conta}}$), the reference communities were particularly sensitive in transport and catabolism ($\log_{10} = -4.5$), membrane transport ($\log_{10} = -2.9$), folding, sorting and degradation ($\log_{10} = -2.4$), energy metabolism ($\log_{10} = -2.3$), cell growth and death ($\log_{10} = -2.1$), nucleotide metabolism ($\log_{10} = -1.7$) and amino acid metabolism ($\log_{10} = -1.1$). This sequence of molecular functions could indicate the effect of diuron in the reference communities. As a primary effect these communities adjusted cellular transport and protein homeostasis to protect against diuron actions like increasing ROS formation due to disrupted electron transfer. Subsequently, energy metabolism is regulated as diuron increasingly reaches the receptor and inhibits photosynthesis. Moreover, growth and other metabolic pathways (e.g. nitrogen metabolism) were adapted to the novel cellular state as secondary effects. In contrast, transcription, lipid metabolism and nucleotide metabolism were the most sensitive KEGG functions in the contaminated communities. However, their responses were within a small concentration range, which does not imply a sequence in regulation given the small differences between thresholds. Rather, all molecular functions in the contaminated communities occurred immediately upon exceeding the EC_{50} for photosynthesis inhibition. This indicates a tipping point, where molecular responses of the contaminated communities were triggered.

The reduced sensitivity of the contaminated communities could indicate both adaptation as well as a remaining internal exposure concentration lasting from the previous chronic exposure, rendering lower diuron applications meaningless compared to prevailing levels. The biofilms were taken immediately from chronic exposure and transferred to the gradient exposure, suggesting elevated diuron residues in cells and EPS. Therefore, a persistent effect of diuron residues seems likely, which combines with the acutely administered amount. Adaptations in the contaminated communities might offer a sufficient protection against internal concentrations and insignificant

diuron additions, which reduces the need for further gene regulation beyond established homeostasis during chronic exposure. These adaptations at low concentrations could already be present in the protein pool or occur via permanently highly expressed (non-responsive) genes and therefore do not fall within the focus of this work. Based on this assumption, non-responsive adaptations could be sufficient to maintain cellular homeostasis against increasing diuron exposure until the EC₅₀ value of photosynthesis inhibition is reached. At this stage, an increasing amount of potential antioxidant degradation products was detected in the metabolome of the contaminated communities, which could indicate their adaptation to maintain cellular homeostasis at higher diuron levels. However, **Figure 21** showed 445 regulated contigs with BMD's below 4 µg L⁻¹ in the contaminated communities, suggesting that gene regulation also occurred below the chronic exposure concentration. The majority (95 %) of these contigs were modelled with biphasic concentration response curves, for which two BMDs can be determined (Larras et al., 2018). How the biphasic responses were obtained, given the hypothesis of increased internal concentration in the contaminated communities, remains a future perspective. Dealing with biphasic responses such as bell-shaped and U-shaped models (which were equally represented in this study) in sensitivity analysis is controversial, as there are different opinions on which BMD better represents the cellular response. DRomic's uses the lower BMD, which forces a higher sensitivity in the global cumulative sensitivity distribution. Instead, the higher BMD threshold of the biphasic models could have been used for this analysis. To avoid skewing the sensitivity of the KEGG functions by a proportion of extreme values, the median was used as a robust method for data aggregation. The choice of BMD did not affect the focus of cellular regulation in the contaminated communities, which was robustly determined by the median at higher concentrations compared to the reference biofilms. In the absence of data on the internal concentration, there is no certainty on the acute exposure concentration that poses a relevant additional burden on the cell. However, each community was compared with controls from the respective culturing conditions, which includes possible residues in the assessment. Thus, any deviation from the control is considered an effect of acute exposure, and the potential residues from chronic exposure are considered part of the adaptation.

In conclusion, reference communities were more sensitive in functions related to the MoA of diuron, whereas contaminated communities were less sensitive and responded abruptly when the EC₅₀ of photosynthesis inhibition was reached. Even though the

diuron residues in the contaminated biofilms were not quantified, it can be said on the basis of this analysis that the contaminated communities were physiologically adapted to tolerate elevated diuron concentrations. However, not every molecular change correlates with an adverse outcome, and changes in transport and catabolism, membrane transport or folding, sorting and degradation may indicate successful acclimation to ambient diuron concentrations (see also **chapter 6.3.2**). Thus, anchoring the molecular data to apical effects in photosynthetic efficiency allows to compare the different sensitivities with respect to the primary effect of diuron and presents a first step towards an ecophysiologic interpretation of molecular data. Molecular responses that occur without measurable effect at the primary site of action fall in the homeostatic range, in which the acclimation of communities occurs without triggering stress. In conclusion, sensitive molecular responses can reveal the MoA of a chemical or the mechanism of tolerance, although they cannot prove efficacy.

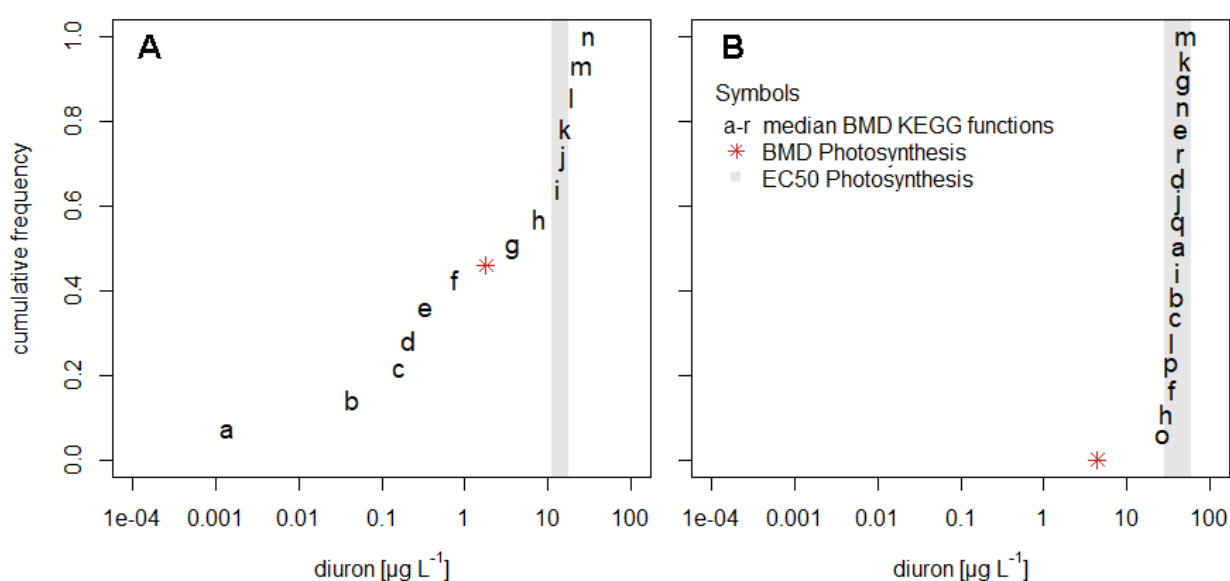


Figure 22 Cumulative sensitivity distribution of molecular KEGG functions (contigs and metabolites) in the reference community (A) and the contaminated community (B). The BMD's of each KEGG function were aggregated using the median, thus only functions with more than 3 BMDs were considered. The letters code for: **a** Transport and catabolism; **b** Membrane transport; **c** Folding, sorting and degradation; **d** Energy metabolism; **e** Cell growth and death; **f** Nucleotide metabolism; **g** Amino acid metabolism; **h** Lipid metabolism; **i** Carbohydrate metabolism; **j** Translation; **k** Glycan biosynthesis and metabolism; **l** Signal transduction; **m** Metabolism of cofactors and vitamins; **n** Biosynthesis of other secondary metabolites; **o** Transcription; **p** Xenobiotics biodegradation and metabolism; **q** Metabolism of other amino acids; **r** Cellular community - prokaryotes.

6.4 Consolidation of the results – holistic interpretation and discussion

6.4.1 Adaptation to chronic diuron exposure - from molecular changes to community effects

Exposure to herbicides poses a threat to aquatic biofilms by affecting their community structure, physiology and functioning. On the other hand, biofilms adapt to herbicide exposure, causing PICT. In this chapter, the adaptive processes of chronic diuron exposure are outlined from the molecular level to the effects on the community.

For this purpose, the acclimatory responses of the communities were compared under the assumption that any difference in the acclimation behavior derived from adaptation (as defined in **chapter 2.3.3**). At the molecular level, divergent patterns in photosynthesis and arginine metabolism related genes were identified. The contaminated communities increased their expression of photosystem-related genes at high diuron concentrations, whereas reference communities reduced the expression of genes involved in photosystem I, in order to balance the output of both photosystems (see **Chapter 4.3.2**). The expression of PS genes, the post-transcriptional regulation, the mRNA half life time (Baginsky & Link, 2008) and the repair of PS proteins (Nishiyama et al., 2006) depends on the redox state of the chloroplast. Community metabolomics indicated an increased amount of breakdown products of ascorbic acid in the contaminated community (see **Chapter 5.3.3**), which might indicate an adaptation to compensate ROS generated from the inhibition of the photosystem and maintaining the redox state of the cell even at elevated diuron concentrations. As the gene expression is based on the redox status, the observed transcription of PS genes in the contaminated community may have resulted from the protective mechanism of ascorbic acid, which attenuated the diuron effect on the redox state of the cell. Another mechanism that depends on the ascorbic acid pool is the photoprotective xanthophyll cycle, which controls the amount of energy reaching the reaction center by converting the pigment violaxanthin to zeaxanthin (Goss & Jakob, 2010). The contaminated communities held a higher pool of violaxanthin and its ratio to zeaxanthin was much higher compared to the reference communities (see **chapter 3.3.1; Annex 8**), which also indicates an improved control of the redox state of the cells. Thus, the evidence regarding an adaptation in redox maintenance is high and ascorbic acid, one of the major antioxidant metabolites (in algae) is a very likely candidate. It has a central role in redox signaling, which controls cell growth up to the light-dependent regulation of photosynthesis. However, maintaining the cellular redox state of the cell via increased

ascorbic acid production is a costly adaptation that takes its toll. Chronic exposure to diuron might have selected for species capable of paying the price of adaptation, which on the other hand impaired the biofilms in their biomass accrual. The chronically exposed communities particularly lost autotrophic biomass, reflected by the decreasing specific chlorophyll content. Selection for adapted biochemical traits largely affected the molecular fingerprint, and the contaminated communities diverged from the reference communities in both their transcriptomic and metabolic fingerprints. As a result of the extensive adaptation processes of the contaminated biofilms, their diuron tolerance increased threefold, thus providing evidence of PICT.

The sensitivity-based analysis of the fingerprints used in this thesis results in blind spots in the evaluation of potential adaptations, which can be addressed in future studies. Microevolutionary processes are particularly relevant in this respect, which might, for example, lead to a decrease in the receptor binding of diuron and thus to a reaction that is decoupled from the acute exposure. A first insight into microevolutionary processes was summarized in **chapter 6.5**.

6.4.2 Assessment of the ecological costs of Pollution-induced community tolerance based on primary production

Adaptations to pollutants serve as the basis for maintaining ecologic functions at chemical exposure. A trait that arises from adaptations is tolerance, which can be quantified according to the concept of pollution induced community tolerance (PICT; Blanck & Wängberg, 1988). In this study, PICT was detected in a contaminated biofilm that grew under diuron exposure for 5 weeks. This tolerance was also indicated in primary production, as the specific production per chlorophyll a was increased in the contaminated community. However, the tolerant community showed a reduced total net primary production and productivity (NPP/R ratio), compared to an unexposed reference community. This impairment persisted even under repeated short-term exposure, demonstrating that PICT cannot safeguard net primary production. On the contrary, the selection process associated with PICT decreased autotrophic biomass in the contaminated community and affected autotrophic diversity indicated by changes in the pigment pattern. The tolerance mechanisms described above, which involve the production of ascorbic acid, are associated with increased metabolic costs (Mouneyrac et al., 2011) that can lead to a further decline in metabolically susceptible organisms. The cost of compensating for oxidative stress, in addition to the energy shortages due

to inhibited photosynthesis, most likely reduced the productivity and ultimately the biomass of the contaminated community during the selection phase. The loss of autotrophic biomass is the main reason for the reduced productivity even during re-occurring exposure. In contrast the reference community featured a higher autotrophic biomass, which compensated for the greater inhibitory effect. In summary, PICT was associated with ecological adaptation costs, and the price is reflected in the decline in function and biomass. These findings do not confirm the hypothesis of Tlili et al. (2016, p. 2144) who stated “...*chemical-induced loss of the most sensitive species, one of the processes underpinning PICT, should not affect ecosystem functions, while PICT predicts community tolerance to increase...*”. In line with the findings of this thesis PICT in sediment associated biofilms exposed to Cu was associated with a species shift and a decline in provision of functions (Ahmed et al., 2020; Mahamoud Ahmed et al., 2018). Moreover, also marine biofilms exposed to Cu for 18 days showed a similar increase in PICT, whereas autotrophic biomass and photosynthetic yield was decreased (Corcoll et al., 2019). In this context, the stressor intensity of the chronic exposure phase is particularly relevant, as a low intensity promotes a low PICT at a high structural diversity, while a high intensity promotes the opposite. Having this in mind, any exposure that stimulates PICT will affect the functional capacity of a community (Pesce et al., 2020).

Given that PICT cannot safeguard function, the recovery potential of biofilms after chronic exposure is of crucial importance. A laboratory recovery experiment of Cu tolerant biofilms revealed, that biomass of exposed biofilms did not recover within a 6 week absence of exposure (Lambert et al., 2012). Nevertheless, the authors also found that the presence of unexposed biofilms improved the recovery of diatom species, which immigrated into the previously exposed community. Thus, in the environment, the structural and functional recovery of biofilms after a certain duration of pollution (e.g. the herbicide application season) could be faster at a large inoculum for re-colonization. This was tested in several translocation experiments in rivers, e.g. by Rotter et al. (2011) who found a recovery in community structure after 24 days, while the community tolerance did not recover within this time. Unfortunately, the authors did not address functional parameters such as primary production or the associated biomass. Translocation studies by Dorigo, Bérard, Bouchez, et al. (2010) and Dorigo, Bérard, Rimet, et al. (2010) in a stream contaminated with Cu and diuron yielded ambiguous results, as in one experiment recovery in structure and function was

observed within 5 weeks, while in another recovery was not yet complete after 9 weeks. The recovery process depends on external and internal factors, such as the flow regime or nutrient content, which can alter the trajectory of recovery, or internal exposure to EPS-adsorbed pollutants, which prologs the recovery phase (Dorigo, Bérard, Rimet, et al., 2010). In the light of multiple-stressors interactions (e.g. Romero et al., 2020), the loss of sensitive species poses a risk to community functions as the stabilizing aspect of diversity fades (Yachi & Loreau, 1999). Therefore, chemical exposure may not only alter functions, but also increase the vulnerability of microbial communities to further environmental disturbances.

In summary, PICT does not protect primary production at diuron exposure and the decline of sensitive species may outweigh the tolerance benefit. However, due to the short generation time and the immigration of organisms, biofilms have a high recovery potential, allowing fast regeneration of structure and function at favorable environmental conditions. In combination with other stressors, a fast regeneration of biofilm structure and function remains to be demonstrated.

6.5 Outlook

Pesticides can directly affect **trophic interaction** top down (e.g. by affecting a predator Foit et al., 2010) or bottom up by affecting the prey. This thesis has revealed a structural and functional decline in aquatic biofilms after chronic diuron exposure, which are the major prey in freshwater streams for e.g. grazing macroinvertebrates and gastropods. A decline in autotrophic species can alter the food quality of biofilms for grazers. An upscaling study exploring the effects of chronic diuron exposure of biofilms on primary consumers (represented by the gastropod *Physella acuta*) found that changes in the composition of biofilms and their fatty acid profile may also alter the fatty acid profile of the grazer and thus possibly its grazing behavior (Konschak et al., 2021). Given the decrease in autotrophic biomass and the metabolite alterations in the contaminated communities detected in this thesis a potential hazard for primary consumers was identified. Moreover, also symbiotic interactions might be affected by chronic exposure. Species that benefit from the provision of algal exudates might lose their food source and their decline could have promoted the strong deviation of the molecular fingerprints. A co-correspondence analysis of metagenome data could shed light on this aspect of interaction.

In addition, the potential of Pollution-Induced Community Tolerance to maintain **ecological functioning** upon re-exposure to diuron was explored. It was found that the gain in tolerance does not outweigh the loss of autotrophic biomass and thus a reduction in net primary production of the contaminated biofilm occurred as a result of PICT. A reduction in net primary production can affect stream metabolism (e.g. increase the need for external carbon sources), but other stressors such as eutrophication, climate change or hydromorphological degradation must also be considered for a meaningful prediction.

In addition, the **molecular mechanisms underlying PICT** were investigated and stimulated ascorbate metabolism and xanthophyll cycle were postulated in the contaminated communities. A further analysis of the gene expression related to the ascorbate and aldarate metabolism (such as ascorbate peroxidase (APX), dehydroascorbate reductase (DHAR) or glutathione reductase (GR)) may shed light on this hypothesis. Moreover, the meta-transcriptome dataset offers the opportunity to analyze genetic adaptations from a **microevolutionary perspective**. The tolerance detected by chlorophyll fluorescence analysis could also have a genetic origin, such

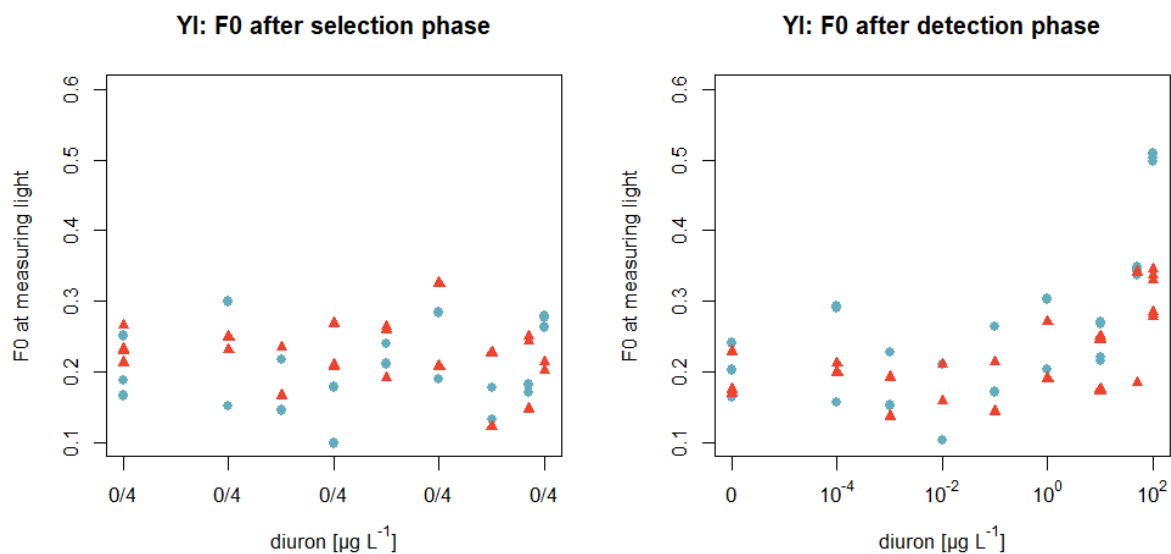
as adaptations that reduces diuron binding efficiency. The evolutionary perspective of diuron exposure can be studied by blasting a sequence of the diuron target (*psbA*) against the non-annotated contigs of this experiment. A preliminary amount of more than 7 gene clusters was identified by this approach. Aligning these and evaluating the amino acid region 197 to 291 containing the herbicide-binding niche revealed two aspects for future evaluation. First, the PEST region (from Arg₂₂₅ to Arg₂₃₈), which is typically associated with protein turnover contained up to 5 individual amino acid variants. Secondly, 6 other amino acid variants outside the PEST region were identified within the binding pocket. However, these differ from described ones (e.g. Val₂₁₉ or Phe₂₇₄) and a potential function is not known (Lu et al., 2019; Mengistu et al., 2000). Towards this end, a functional analysis is needed, e.g. by comparing expression level of certain variants at diuron stress.

Appendix

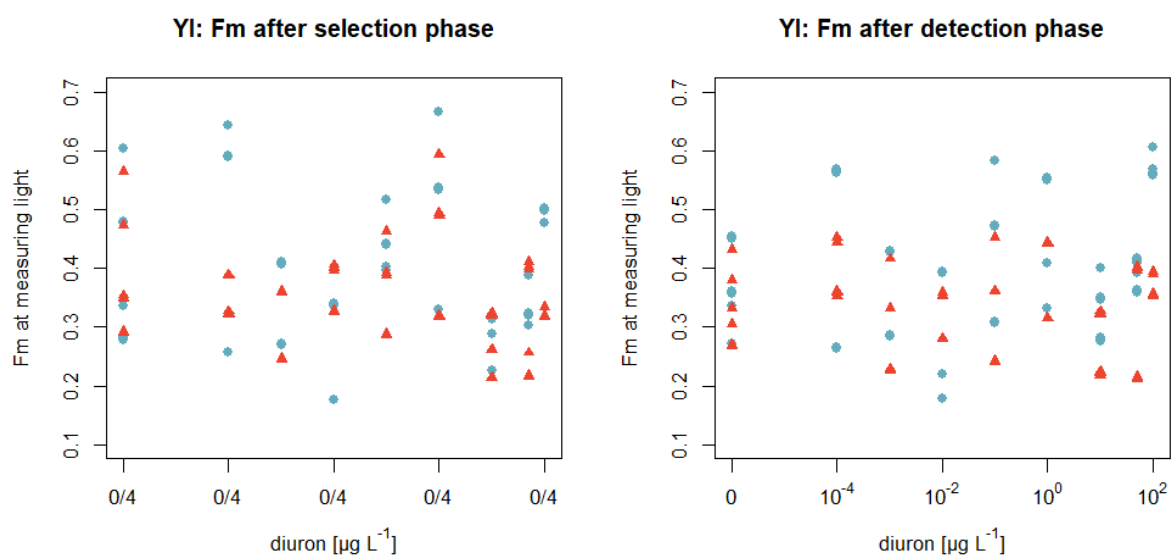
Annex 1 Details on biofilm cultivation and exposure.

Selection Phase Glass slides (15.25 cm²) were placed as artificial substrate in 20 L glass tanks and unfiltered river water from the Parthe river, a local stream (sampling point: 51°22'18.5"N 12°25'07.7"E) served as inoculum for biofilm growth. The inoculation started on 27.04.2018 and ended on 04/05.06.2018 with the detection phase of the respective communities. The slides were placed in holders with varying spatial position (up, mid, low), which were approximately 10 cm, 13 cm and 16 cm below water surface. Water was stirred permanently and exchanged weekly to guarantee sufficient supply of nutrients and a near-natural inoculum of species. Oxygen saturation, pH and temperature were monitored at each water exchange (data not shown). Water temperature was maintained at 22±1°C and the light cycle was set to 14/10 hours light/dark cycle. The photon yield of the LED plant lamps (C-series, Valoya, Helsinki, Finland) above the water surface was approximately 150 µmol photons m⁻² s⁻¹. Half of the microcosms were contaminated with 4 µg L⁻¹ diuron, starting from the second week of cultivation. The addition of diuron should induce the growth of contaminated communities, whereas the uncontaminated microcosms represent reference communities.

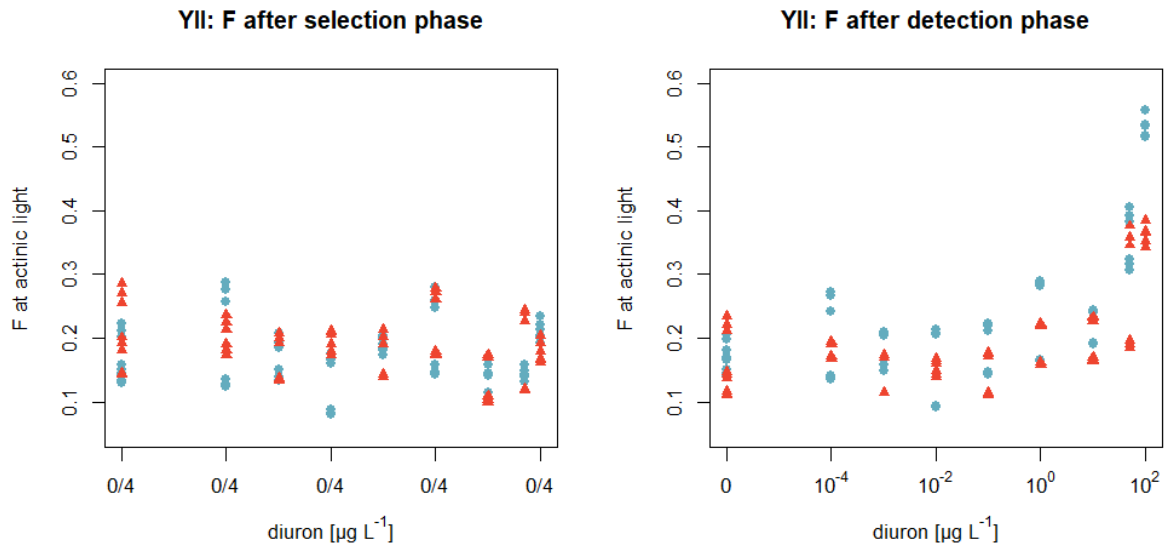
Detection Phase After the selection phase the slides were randomly sampled from the different tanks at varying spatial position (up, mid, low) to avoid a spatial bias in the microbial community. The slides were exposed for a second time in a controlled environment using a phytotron (MultitronPro, IFORS, Einsbach, Germany). Petri dishes were slightly agitated at 30 RPM and illuminated by LEDs. The temperature and light intensity were kept consistent to the selection phase.



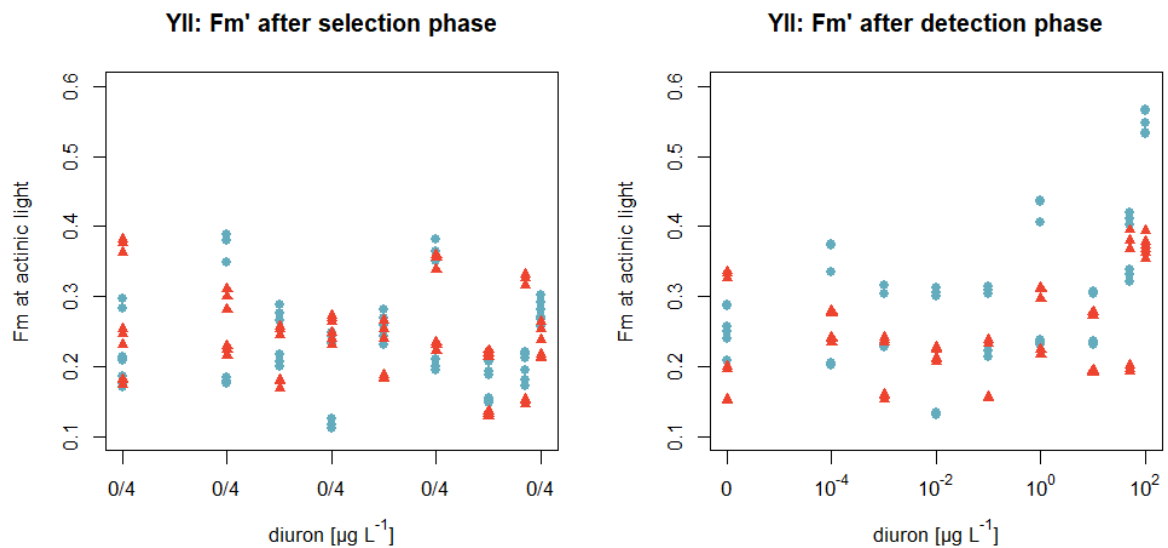
Annex 2 Basal fluorescence (F_0) of chlorophyll of the contaminated (▲) and reference community (●) at dark adapted state. The left plot shows F_0 after selection phase and on the right the same communities are displayed after the detection phase. The analysis was conducted using an Imaging PAM (Heinz WALZ GmbH, Effeltrich, Germany).



Annex 3 Maximum fluorescence (F_m) of chlorophyll of the contaminated (▲) and reference community (●) at dark adapted state. The left plot shows F_m after selection phase and on the right the same communities are displayed after the detection phase. The analysis was conducted using an Imaging PAM (Heinz WALZ GmbH, Effeltrich, Germany).



Annex 5 Basal fluorescence (F) of chlorophyll of the contaminated (\blacktriangle) and reference community (\bullet) after light adaptation. The left plot shows F after selection phase and on the right the same communities are displayed after the detection phase. The analysis was conducted using an Imaging PAM (Heinz WALZ GmbH, Effeltrich, Germany).



Annex 4 Maximum fluorescence (F_m') of chlorophyll of the contaminated (\blacktriangle) and reference community (\bullet) after light adaptation. The left plot shows F_m' after selection phase and on the right the same communities are displayed after the detection phase. The analysis was conducted using an Imaging PAM (Heinz WALZ GmbH, Effeltrich, Germany).

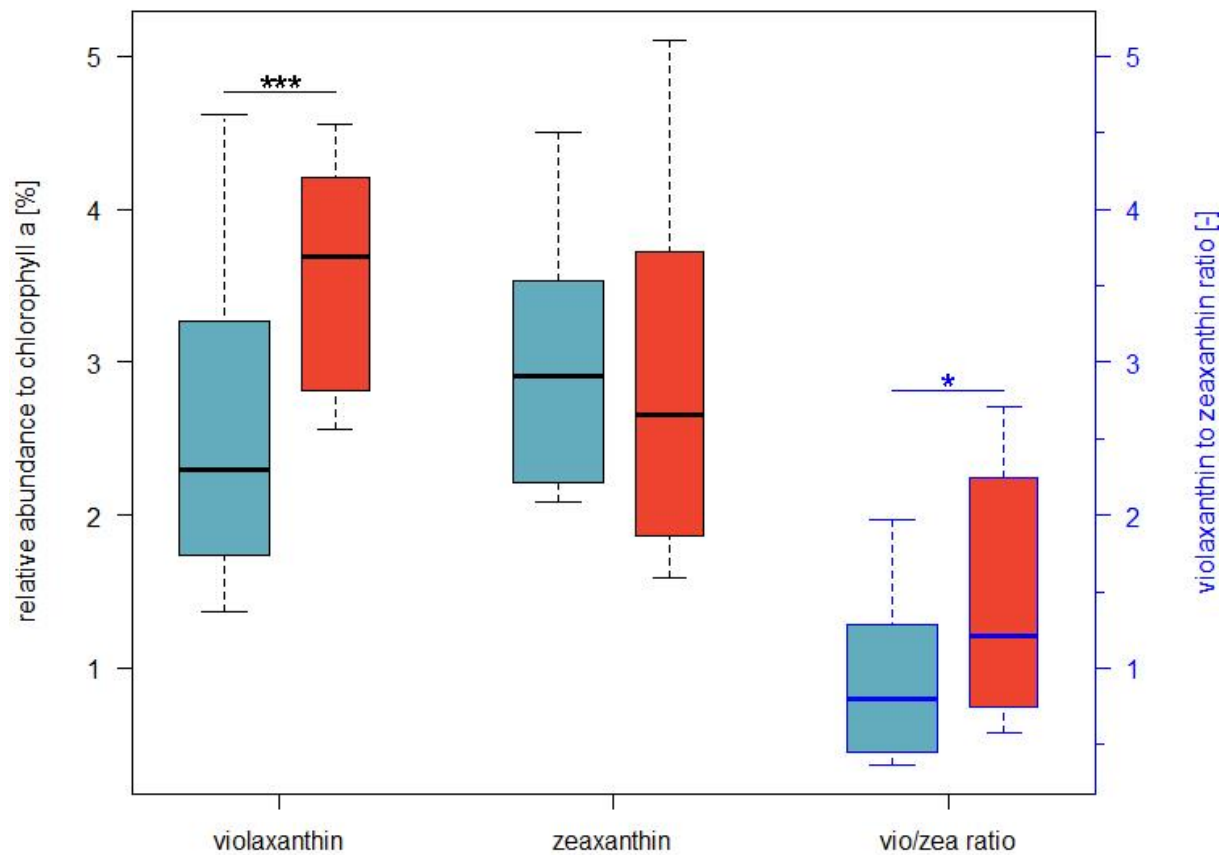
Annex 6 GC-TOF/MS and CTC autosampler settings for the community metabolomics analysis.

Autosampler-Parameters	CTC PAL Dual Head Autosampler			
Sample Volume	1 µL			
Solvent A/B Post Wash	5 (n-hexane, isopropanol)			
GC-Parameters	Agilent® 7890 Gas Chromatograph			
Column	DB5-DG (30 m + 10 m DG, 0.25 mm, 0.25 µm, Agilent)			
Front Inlet Mode	Splitless			
Front Inlet & Transfer Line Temp.	250 °C			
Front Inlet Septum Purge Flow	3 mL min ⁻¹			
Front Inlet Purge Time	1 min			
Front Inlet Purge Flow	40 mL min ⁻¹			
Front Inlet Total Flow	42.2 mL min ⁻¹			
Target Flow	2.2 mL min ⁻¹ (Constant Flow)			
Oven Temperature Ramp	Rate [°C min ⁻¹]	Target [°C]	Temp	Duration [min]
	Initial	60		1.00
	10.00	325		10.00
GC Method Total Time	37.5 min			
MS-Parameters	Pegasus 4D, LECO			
Acquisition Delay	5.5 min			
Scan-Range	50 – 600 m/z			
Acquisition Rate	10 spectra second ⁻¹			
Electron Energy	-70 Volts			
Ion Source	250 °C			

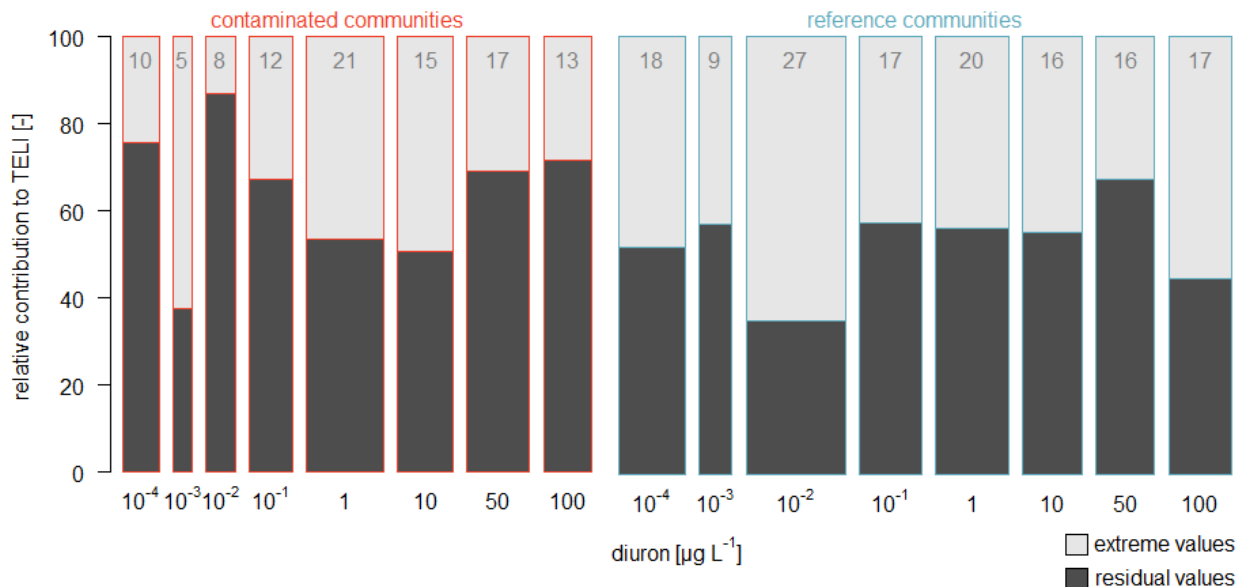
Annex 7 MS-DIAL data alignment settings of the community metabolome data.

Data Processing Parameters	MS-DIAL version 4.24
Data type	
Data type	Centroid
Ion mode	Positive
Accuracy type	IsNominal
Data collection parameters	
Retention time begin	5.833 min
Retention time end	37.5 min
Mass range	70 – 600 m/z
Peak detection parameters	
Minimum Peak Height	1000 amplitude
Smoothing Method	Linear weighted moving average
Smoothing Level	2 scan
Average Peak Width	30 scan
Mass slice width	0.5
Mass accuracy	0.5

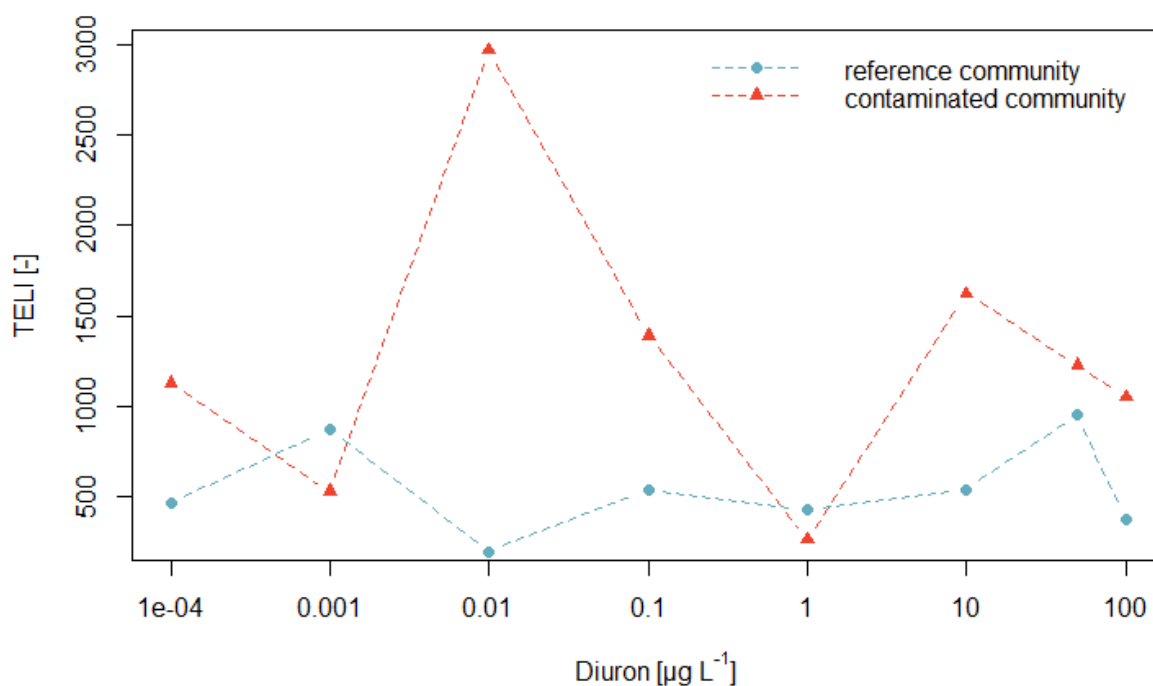
Mass Exclusion List	73, 75, 89, 103, 116, 147, 205 (Mass Tolerance 0.005 Da)
MS1Dec Parameters	
Sigma Window Value	0.4
El spectra cut off	1 amplitude
Identification	
Retention Type	RI (Index Type = Alkanes)
Retention Index Tolerance	20
m/z Tolerance	0.5 Da
El similarity library tolerance	70 %
Identification score cut off	70 %
Use retention info for scoring	TRUE
Use retention info for filtering	FALSE
Use quant masses defined in ...	FALSE
Only report the top hit	TRUE
Alignment Parameter Setting	
Reference file	20191108_C0_1_C7_1_3.abf
RI or RT	RI
MSP file (library)	GMD_20111121_VAR5_ALK_MSP_RI_corr.msp
Retention index tolerance	5
El similarity tolerance	70 %
Retention time factor	0.5
El similarity factor	0.5
Identification after alignment	TRUE
Gap filling by compulsion	FALSE
Choose base peaks m/z for ...	FALSE
Filtering setting	
Peak count filter	0 %
Remove features based on blank	FALSE
Keep identified/annotated...	FALSE
Keep removable features...	FALSE



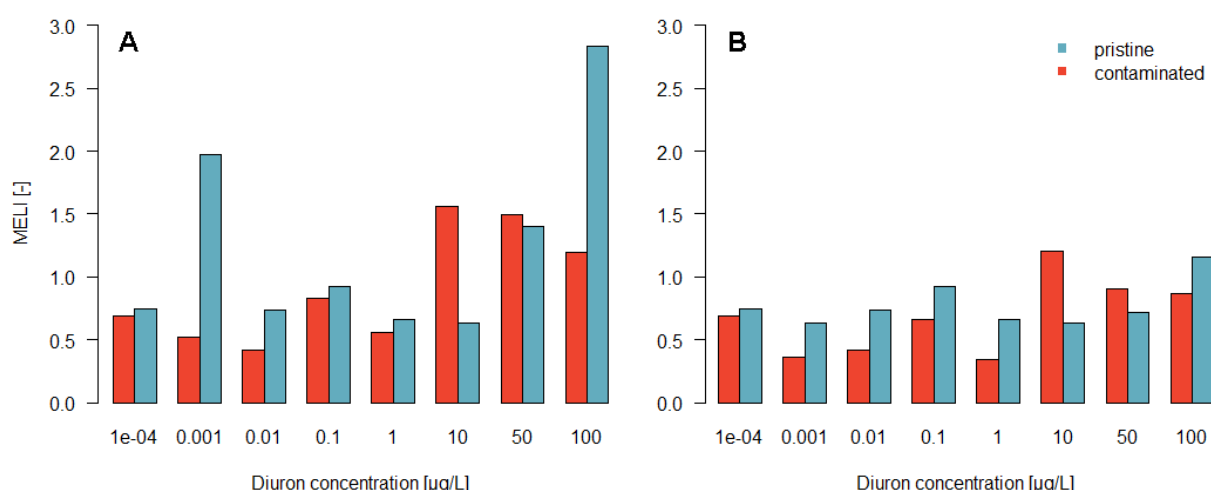
Annex 8 Comparison of the normalized pigment content of violaxanthin and zeaxanthin, the crucial pigments of the photoprotective xanthophyll cycle. The contaminated community is colored red, the reference community blue, and significant differences have been marked with asterisks (* < 0.05; *** < 0.001). The ratio of violaxanthin to zeaxanthin is illustrated on the right, indicated by a blue outline.



Annex 9 Contribution of extreme values to the Transcriptional Effect Level Index (TELI). The upper light grey bars show the contribution of extreme values to the TELI. The number of extreme values is indicated by the bar width and the grey value in upper part of the bar (n_{extr}). The lower bars represent the contribution of the remaining contigs ($3502153 - n_{\text{extr}}$) to the TELI.



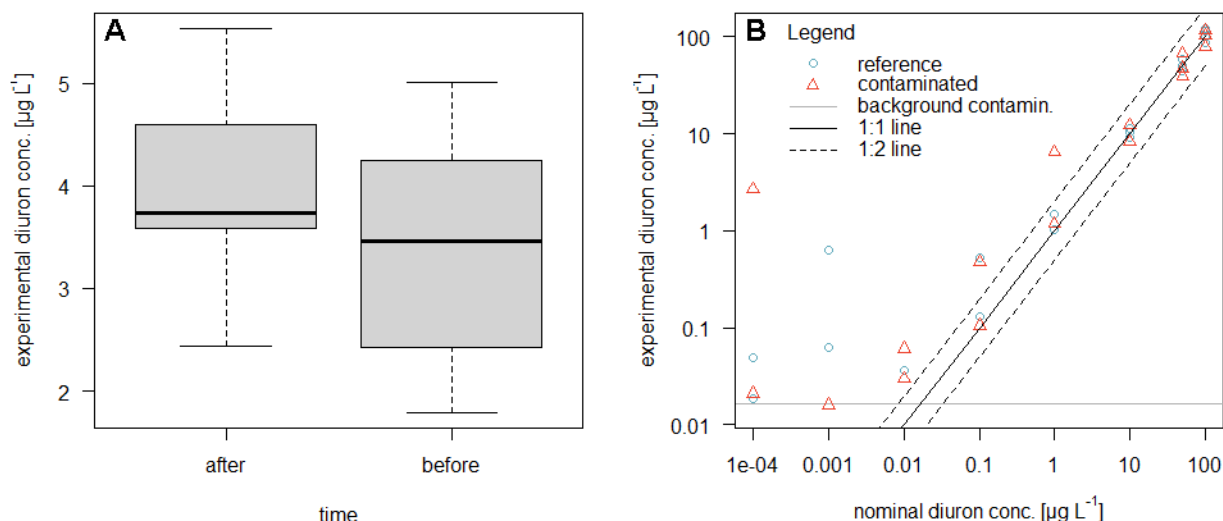
Annex 10 Transcriptional Effect Level Index (TELI) after removal of extreme values (see Annex 1, upper lightgrey bars).



Annex 11 Aggregation of the community metabolomics data to Metabolic Effect Level Index (MELI). **A)** MELI without removal of extreme values. **B)** MELI after visual inspection and removal of sporadic occurring extreme values ($n_{\text{conta}} = 10$; $n_{\text{ref}} = 13$).

Annex 12 Summary of the most abundant pigments in algal lineages of typical biofilm taxa. The symbols represent + present, + major pigment and v variable occurrence. Grey highlighted pigments were used as marker pigments in this study. The table was adapted after Werner (2022).

Lineage		blue	green	red
Division		Cyanophyta	Chlorophyta	Heterokontophyta
carotenoids	19'-butanoyloxyfucoxanthin			v
	diadinoxanthin			+
	diatoxanthin			v
	echinenon	v	+	
	fucoxanthin			+
	lutein		+	
	neoxanthin		+	
	violaxanthin		+	+
	zeaxanthin	+	v	v
	alpha-Carotene			
	beta-Carotene	+	+	+
chlorophylls	chlorophyll a	+	+	+
	chlorophyll b		+	
	chlorophyll c1			+
	chlorophyll c2			+
	chlorophyll c3			+



Annex 13 A) LC-MS/MS results of the chronic exposure (selection phase) with a nominal concentration of 4 µg L⁻¹ diuron. The measured diuron concentration is subdivided according to the exposure time. The box 'before' presents the diuron concentration in the microcosms before the renewal of water, while 'after' shows the exposure concentrations after the inoculation water was refreshed and new diuron was spiked. **B)** 1:1 Plot of the expected and measured exposure concentrations during the acute exposure (detection phase). The background contamination was assessed from the three control samples of the reference communities. The lower acute exposure concentrations (0.0001, 0.001 and 0.01) were affected by background levels of diuron, but also showed a high variation in concentration. The settings of the LC – MS/MS can be found in the following:

Autosampler	Agilent 1260 HiP Bio ALS		
Column compartment	Agilent 1260 TCC		
Pump	Agilent 1260 Bio Quat Pump		
Thermostat	Agilent 1290 Thermostat		
Eluent A (<i>water (HPLC-grade) + 0.1% formic acid</i>) Eluent B (<i>methanol (LC-grade) + 0.1% formic acid</i>)	Time [min]	Eluent A	Eluent B
	1	95	5
	8	10	90
	16	5	95
	16.4	95	5
	16.5	Acquisition Off	
Flow rate	350 µL min ⁻¹		
Injection volume	25 µL		
Column temperature	30 °C		

Turbo VTM Ion Source			
Ion Source	ESI (positive ion mode)		
Curtain gas	25 psi		
Ion Spray Voltage	4500 V		
Temperature	400 °C		
Ion source gas (GS1 & GS2)	50 psi		
AB Sciex 6500 (Qtrap) MRM			
MRM method for diuron	Fragment [m/z]	Collision Energy [V]	Collision cell exit potential [V]
Parent mass = 232.935 [m/z]	71.9	47	8
Declustering potential = 96 [V]	46.1	39	12
Entrance potential = 10 [V]	159.9	35	18
Scan time = 100 [ms]	132.9	51	54

References

- Agathokleous, E., Wang, Q., Iavicoli, I., & Calabrese, E. J. (2021)** The relevance of hormesis at higher levels of biological organization: Hormesis in microorganisms. *Current Opinion in Toxicology*.
- Ahmed, A. M., Tardy, V., Bonnineau, C., Billard, P., Pesce, S., & Lyautey, E. (2020)** Changes in sediment microbial diversity following chronic copper-exposure induce community copper-tolerance without increasing sensitivity to arsenic. *Journal of Hazardous Materials*, 391, 122197.
- Ahn, S., Jung, J., Jang, I.-A., Madsen, E. L., & Park, W. (2016)** Role of Glyoxylate Shunt in Oxidative Stress Response. *Journal of Biological Chemistry*, 291(22), 11928-11938.
- Allen, J. F., Santabarbara, S., Allen, C. A., & Puthiyaveetil, S. (2011)** Discrete redox signaling pathways regulate photosynthetic light-harvesting and chloroplast gene transcription. *PLoS One*, 6(10), e26372.
- Allison, S. D., & Martiny, J. B. H. (2008)** Resistance, resilience, and redundancy in microbial communities. *Proceedings of the National Academy of Sciences*, 105, 11512-11519.
- Ankley, G. T., Bennett, R. S., Erickson, R. J., Hoff, D. J., Hornung, M. W., Johnson, R. D., Mount, D. R., Nichols, J. W., Russom, C. L., Schmieder, P. K., Serrano, J. A., Tietge, J. E., & Villeneuve, D. L. (2010)** Adverse outcome pathways: A conceptual framework to support ecotoxicology research and risk assessment. *Environmental Toxicology and Chemistry*, 29(3), 730-741.
- Aoki-Kinoshita, K. F., & Kanehisa, M. (2007)** Gene annotation and pathway mapping in KEGG. In *Comparative genomics* (pp. 71-91). Springer.
- Auletta, G., Ellis, G. F., & Jaeger, L. (2008)** Top-down causation by information control: from a philosophical problem to a scientific research programme. *Journal of the Royal Society Interface*, 5(27), 1159-1172.
- Averianova, L. A., Balabanova, L. A., Son, O. M., Podvolotskaya, A. B., & Tekutyeva, L. A. (2020)** Production of Vitamin B2 (Riboflavin) by Microorganisms: An Overview [Review]. *Frontiers in Bioengineering and Biotechnology*, 8.
- Baginsky, S., & Link, G. (2008)** Redox regulation of chloroplast gene expression. In *Photoprotection, Photoinhibition, Gene Regulation, and Environment* (pp. 269-287). Springer.
- Baker, N. R. (2008)** Chlorophyll Fluorescence: A Probe of Photosynthesis In Vivo. *Annual Review of Plant Biology*, 59(1), 89-113.
- Bashiardes, S., Zilberman-Schapira, G., & Elinav, E. (2016)** Use of metatranscriptomics in microbiome research. *Bioinformatics and biology insights*, 10, BBI. S34610.
- Battaglino, B., Grinzato, A., & Pagliano, C. (2021)** Binding Properties of Photosynthetic Herbicides with the QB Site of the D1 Protein in Plant Photosystem II: A Combined Functional and Molecular Docking Study. *Plants*, 10(8), 1501.
- Battin, T. J., Besemer, K., Bengtsson, M. M., Romani, A. M., & Packmann, A. I. (2016)** The ecology and biogeochemistry of stream biofilms. *Nature Reviews Microbiology*, 14(4), 251-263.
- Bergsveinson, J., Roy, J., Maynard, C., Sanschagrin, S., Freeman, C. N., Swerhone, G. D. W., Dynes, J. J., Tremblay, J., Greer, C. W., Korber, D. R., & Lawrence, J. R. (2020)** Metatranscriptomic Insights Into the Response of

- River Biofilm Communities to Ionic and Nano-Zinc Oxide Exposures [Original Research]. *Frontiers in Microbiology*, 11.
- Bettin, C., Oehlmann, J., & Stroben, E. (1996)** TBT-induced imposex in marine neogastropods is mediated by an increasing androgen level. *Helgoländer Meeresuntersuchungen*, 50(3), 299-317.
- Bikel, S., Valdez-Lara, A., Cornejo-Granados, F., Rico, K., Canizales-Quinteros, S., Soberón, X., Del Pozo-Yauner, L., & Ochoa-Leyva, A. (2015)** Combining metagenomics, metatranscriptomics and viromics to explore novel microbial interactions: towards a systems-level understanding of human microbiome. *Computational and Structural Biotechnology Journal*, 13, 390-401.
- Blanck, H. (2002)** A Critical Review of Procedures and Approaches Used for Assessing Pollution-Induced Community Tolerance (PICT) in Biotic Communities. *Human and Ecological Risk Assessment: An International Journal*, 8(5), 1003-1034.
- Blanck, H., & Wängberg, S. (1988)** Pollution-induced community tolerance: A new ecotoxicological tool. *Functional Testing of Aquatic Biota for Estimating Hazards of Chemicals*, (ASTM International)(988), 219.
- Bonny, S. (2016)** Genetically Modified Herbicide-Tolerant Crops, Weeds, and Herbicides: Overview and Impact. *Environmental Management*, 57(1), 31-48.
- Borowitzka, M. A. (2018)** The 'stress' concept in microalgal biology—homeostasis, acclimation and adaptation. *Journal of Applied Phycology*, 30(5), 2815-2825.
- Boubakri, H., Gargouri, M., Mliki, A., Brini, F., Chong, J., & Jbara, M. (2016)** Vitamins for enhancing plant resistance. *Planta*, 244(3), 529-543.
- Brack, W., Escher, B. I., Müller, E., Schmitt-Jansen, M., Schulze, T., Slobodnik, J., & Hollert, H. (2018)** Towards a holistic and solution-oriented monitoring of chemical status of European water bodies: how to support the EU strategy for a non-toxic environment? *Environmental Sciences Europe*, 30(1), 33.
- Buchfink, B., Xie, C., & Huson, D. H. (2015)** Fast and sensitive protein alignment using DIAMOND. *Nature methods*, 12(1), 59-60.
- Bundy, J. G., Davey, M. P., & Viant, M. R. (2009)** Environmental metabolomics: a critical review and future perspectives. *Metabolomics*, 5(1), 3-21.
- Busch, W., Schmidt, S., Kühne, R., Schulze, T., Krauss, M., & Altenburger, R. (2016)** Micropollutants in European rivers: A mode of action survey to support the development of effect-based tools for water monitoring. *Environmental Toxicology and Chemistry*, 35(8), 1887-1899.
- Calow, P. (1991)** Physiological costs of combating chemical toxicants: ecological implications. *Comparative biochemistry and physiology. C, Comparative pharmacology and toxicology*, 100(1-2), 3-6.
- Carles, L., Wullschleger, S., Joss, A., Eggen, R. I. L., Schirmer, K., Schuwirth, N., Stamm, C., & Tlili, A. (2021)** Impact of wastewater on the microbial diversity of periphyton and its tolerance to micropollutants in an engineered flow-through channel system. *Water research*, 203, 117486.
- Ceballos, G., Ehrlich, P. R., Barnosky, A. D., García, A., Pringle, R. M., & Palmer, T. M. (2015)** Accelerated modern human-induced species losses: Entering the sixth mass extinction. *Science Advances*, 1(5), e1400253.
- Charif, D., Lobry, J. R., Necsulea, A., Palmeira, L., Penel, S., Perriere, G., & Penel, M. S. (2021)** Package 'seqinr'.
- Clements, W. H., & Rohr, J. R. (2009)** Community responses to contaminants: using basic ecological principles to predict ecotoxicological effects. *Environmental Toxicology and Chemistry: An International Journal*, 28(9), 1789-1800.

- Consortium, T. G. O. (2021)** The Gene Ontology resource: enriching a GOld mine. *Nucleic Acids Research*, 49(D1), D325-D334.
- Consortium, T. U. (2020)** UniProt: the universal protein knowledgebase in 2021. *Nucleic Acids Research*, 49(D1), D480-D489.
- Corcoll, N., Acuña, V., Barceló, D., Casellas, M., Guasch, H., Huerta, B., Petrovic, M., Ponsatí, L., Rodríguez-Mozaz, S., & Sabater, S. (2014)** Pollution-induced community tolerance to non-steroidal anti-inflammatory drugs (NSAIDs) in fluvial biofilm communities affected by WWTP effluents. *Chemosphere*, 112, 185-193.
- Corcoll, N., Yang, J., Backhaus, T., Zhang, X., & Eriksson, K. M. (2019)** Copper Affects Composition and Functioning of Microbial Communities in Marine Biofilms at Environmentally Relevant Concentrations. *Frontiers in Microbiology*, 9.
- Creusot, N., Chaumet, B., Eon, M., Mazzella, N., Moreira, A., & Morin, S. (2022)** Metabolomics insight into the influence of environmental factors in responses of freshwater biofilms to the model herbicide diuron. *Environmental Science and Pollution Research*, 29(20), 29332-29347.
- Crump, B. C., Wojahn, J. M., Tomas, F., & Mueller, R. S. (2018)** Metatranscriptomics and Amplicon Sequencing Reveal Mutualisms in Seagrass Microbiomes. *Frontiers in Microbiology*, 9.
- Davies, K. J. A. (2016)** Adaptive homeostasis. *Molecular Aspects of Medicine*, 49,1-7
- Deutsch, J. C. (1997)** [2] Gas chromatographic/mass spectrometric measurement of ascorbic acid and analysis of ascorbic acid degradation in solution. *Methods in enzymology*, 279, 13-24.
- Dewhirst, R. A., Murray, L., Mackay, C. L., Sadler, I. H., & Fry, S. C. (2020)** Characterisation of the non-oxidative degradation pathway of dehydroascorbic acid in slightly acidic aqueous solution. *Archives of Biochemistry and Biophysics*, 681,108240.
- Dopheide, A., Lear, G., He, Z., Zhou, J., & Lewis, G. D. (2015)** Functional gene composition, diversity and redundancy in microbial stream biofilm communities. *PLoS One*, 10(4), e0123179.
- Dorigo, U., Bérard, A., Bouchez, A., Rimet, F., & Montuelle, B. (2010)** Transplantation of microbenthic algal assemblages to assess structural and functional recovery after diuron exposure. *Archives of environmental contamination and toxicology*, 59(4), 555-563.
- Dorigo, U., Bérard, A., Rimet, F., Bouchez, A., & Montuelle, B. (2010)** In situ assessment of periphyton recovery in a river contaminated by pesticides. *Aquatic Toxicology*, 98(4), 396-406.
- Dorigo, U., Leboulanger, C., Bérard, A., Bouchez, A., Humbert, J.-F., & Montuelle, B. (2007)** Lotic biofilm community structure and pesticide tolerance along a contamination gradient in a vineyard area. *Aquatic microbial ecology*, 50(1), 91-102.
- Drakvik, E., Altenburger, R., Aoki, Y., Backhaus, T., Bahadori, T., Barouki, R., Brack, W., Cronin, M. T. D., Demeneix, B., Hougaard Bennekou, S., van Klaveren, J., Kneuer, C., Kolossa-Gehring, M., Lebre, E., Posthuma, L., Reiber, L., Rider, C., Rügge, J., Testa, G., . . . Bergman, Å. (2020)** Statement on advancing the assessment of chemical mixtures and their risks for human health and the environment. *Environment International*, 134, 105267.
- Engel, B., Suralik, P., & Marchetti-Deschmann, M. (2020)** Critical considerations for trimethylsilyl derivatives of 24 primary metabolites measured by gas

- chromatography–tandem mass spectrometry. *Separation Science Plus*, 3(9), 407-418.
- Eriksson, K., Antonelli, A., Nilsson, R., Clarke, A., & Blanck, H. (2009)** A phylogenetic approach to detect selection on the target site of the antifouling compound irgarol in tolerant periphyton communities. *Environmental microbiology*, 11(8), 2065-2077.
- Eriksson, K., Clarke, A., Franzen, L.-G., Kuylenstierna, M., Martinez, K., & Blanck, H. (2009)** Community-level analysis of psbA gene sequences and irgarol tolerance in marine periphyton. *Applied and Environmental Microbiology*, 75(4), 897-906.
- Farnsworth, K. D., Albantakis, L., & Caruso, T. (2017)** Unifying concepts of biological function from molecules to ecosystems. *Oikos*, 126(10), 1367-1376.
- Fasching, C., Akotoye, C., Bižić, M., Fonvielle, J., Ionescu, D., Mathavarajah, S., Zoccarato, L., Walsh, D. A., Grossart, H.-P., & Xenopoulos, M. A. (2020)** Linking stream microbial community functional genes to dissolved organic matter and inorganic nutrients. *Limnology and Oceanography*, 65(S1), S71-S87.
- Federhen, S. (2011)** The NCBI Taxonomy database. *Nucleic Acids Research*, 40(D1), D136-D143.
- Feio, M., Alves, T., Boavida, M., Medeiros, A., & Graça, M. (2010)** Functional indicators of stream health: A river-basin approach. *Freshwater Biology*, 55(5), 1050-1065.
- Fiehn, O. (2001)** Combining Genomics, Metabolome Analysis, and Biochemical Modelling to Understand Metabolic Networks. *Comparative and Functional Genomics*, 2, 914970.
- Fiehn, O. (2016)** Metabolomics by gas chromatography–mass spectrometry: Combined targeted and untargeted profiling. *Current protocols in molecular biology*, 114(1), 30.34. 31-30.34. 32.
- Flemming, H.-C., & Wingender, J. (2010)** The biofilm matrix. *Nature Reviews Microbiology*, 8(9), 623-633.
- Foit, K., Chatzinotas, A., & Liess, M. (2010)** Short-term disturbance of a grazer has long-term effects on bacterial communities—Relevance of trophic interactions for recovery from pesticide effects. *Aquatic Toxicology*, 99(2), 205-211.
- Fox, D. R., van Dam, R. A., Fisher, R., Batley, G. E., Tillmanns, A. R., Thorley, J., Schwarz, C. J., Spry, D. J., & McTavish, K. (2021)** Recent Developments in Species Sensitivity Distribution Modeling. *Environmental Toxicology and Chemistry*, 40(2), 293-308.
- Fryer, M. J., Andrews, J. R., Oxborough, K., Blowers, D. A., & Baker, N. R. (1998)** Relationship between CO₂ assimilation, photosynthetic electron transport, and active O₂ metabolism in leaves of maize in the field during periods of low temperature. *Plant physiology*, 116(2), 571-580.
- Gaubert-Boussarie, J., Prado, S., & Hubas, C. (2020)** An untargeted metabolomic approach for microphytobenthic biofilms in intertidal mudflats. *Frontiers in Marine Science*, 250.
- Genty, B., Briantais, J.-M., & Baker, N. R. (1989)** The relationship between the quantum yield of photosynthetic electron transport and quenching of chlorophyll fluorescence. *Biochimica et Biophysica Acta (BBA) - General Subjects*, 990(1), 87-92.
- Gianessi, L. P. (2013)** The increasing importance of herbicides in worldwide crop production. *Pest Management Science*, 69(10), 1099-1105.

- Giordano, M. (2013)** Homeostasis: an underestimated focal point of ecology and evolution. *Plant Science*, 211, 92-101.
- Gonçalves, S., Kahlert, M., Almeida, S. F. P., & Figueira, E. (2018)** A freshwater diatom challenged by Zn: Biochemical, physiological and metabolomic responses of *Tabellaria flocculosa*(Roth) Kützing. *Environmental Pollution*, 238, 959-971.
- Goss, R., & Jakob, T. (2010)** Regulation and function of xanthophyll cycle-dependent photoprotection in algae. *Photosynthesis Research*, 106(1), 103-122.
- Gou, N., & Gu, A. Z. (2011)** A new transcriptional effect level index (TELI) for toxicogenomics-based toxicity assessment. *Environmental Science & Technology*, 45(12), 5410-5417.
- Grabherr, M. G., Haas, B. J., Yassour, M., Levin, J. Z., Thompson, D. A., Amit, I., Adiconis, X., Fan, L., Raychowdhury, R., & Zeng, Q. (2011)** Full-length transcriptome assembly from RNA-Seq data without a reference genome. *Nature biotechnology*, 29(7), 644-652.
- Grant, A. (2002)** Pollution-Tolerant Species and Communities: Intriguing Toys or Invaluable Monitoring Tools? *Human and Ecological Risk Assessment: An International Journal*, 8(5), 955-970.
- Grossmann, K., Christiansen, N., Looser, R., Tresch, S., Hutzler, J., Pollmann, S., & Ehrhardt, T. (2012)** Physionomics and metabolomics—two key approaches in herbicidal mode of action discovery. *Pest Management Science*, 68(4), 494-504.
- Gu, C., Gao, P., Yang, F., An, D., Munir, M., Jia, H., Xue, G., & Ma, C. (2017)** Characterization of extracellular polymeric substances in biofilms under long-term exposure to ciprofloxacin antibiotic using fluorescence excitation-emission matrix and parallel factor analysis. *Environmental Science and Pollution Research*, 24(15), 13536-13545.
- Gu, Z., Eils, R., & Schlesner, M. (2016)** Complex heatmaps reveal patterns and correlations in multidimensional genomic data. *Bioinformatics*, 32(18), 2847-2849.
- Guasch, H., Artigas, J., Bonet, B., Bonnineau, C., Canals, O., Corcoll, N., Foulquier, A., López-Doval, J., Kim-Tiam, S., & Morin, S. (2016)** The use of biofilms to assess the effects of chemicals on freshwater ecosystems. *Aquatic Biofilms: Ecology Water Quality and Wastewater Treatment; Caister Academic Press: Rofo, UK*, 125-144.
- Hager, A. (1969)** Lichtbedingte pH-erniedrigung in einem chloroplasten-kompartiment als ursache der enzymatischen violaxanthin→ zeaxanthin-umwandlung; beziehungen zur photophosphorylierung. *Planta*, 224-243.
- Hollingsworth, P. M., Forrest, L. L., Spouge, J. L., Hajibabaei, M., Ratnasingham, S., Bank, M. v. d., Chase, M. W., Cowan, R. S., Erickson, D. L., Fazekas, A. J., Graham, S. W., James, K. E., Kim, K.-J., Kress, W. J., Schneider, H., AlphenStahl, J. v., Barrett, S. C. H., Berg, C. v. d., . . Little, D. P. (2009)** A DNA barcode for land plants. *Proceedings of the National Academy of Sciences*, 106(31), 12794-12797.
- Hultman, J., Waldrop, M. P., Mackelprang, R., David, M. M., McFarland, J., Blazewicz, S. J., Harden, J., Turetsky, M. R., McGuire, A. D., & Shah, M. B. (2015)** Multi-omics of permafrost, active layer and thermokarst bog soil microbiomes. *Nature*, 521(7551), 208-212.
- Jax, K. (2005)** Function and “functioning” in ecology: what does it mean? *Oikos*, 111(3), 641-648.

- Jeffrey, S. W., Wright, S. W., & Zapata, M. (2011)** Microalgal classes and their signature pigments. In C. A. Llewellyn, E. S. Egeland, G. Johnsen, & S. Roy (Eds.), *Phytoplankton Pigments: Characterization, Chemotaxonomy and Applications in Oceanography* (pp. 3-77). Cambridge University Press.
- Johnston, E. L., Mayer-Pinto, M., & Crowe, T. P. (2015)** Chemical contaminant effects on marine ecosystem functioning. *Journal of Applied Ecology*, 52(1), 140-149.
- Jones, O. A., Lear, G., Welji, A. M., Collins, G., & Quince, C. (2016)** Community metabolomics in environmental microbiology. In *Microbial Metabolomics* (pp. 199-224). Springer.
- Kanehisa, M., & Goto, S. (2000)** KEGG: Kyoto Encyclopedia of Genes and Genomes. *Nucleic Acids Research*, 28(1), 27-30.
- Kassambara, A., & Mundt, F. (2017)** Package 'factoextra'. *Extract and visualize the results of multivariate data analyses*, 76.
- Kautsky, H. (1931)** Neue Versuche zur Kohlensäureassimilation. *Naturwissenschaften*, 19, 964.
- Kim Tiam, S., Laviale, M., Feurtet-Mazel, A., Jan, G., Gonzalez, P., Mazzella, N., & Morin, S. (2015)** Herbicide toxicity on river biofilms assessed by pulse amplitude modulated (PAM) fluorometry. *Aquatic Toxicology*, 165, 160-171.
- Kluender, C., Sans-Piché, F., Riedl, J., Altenburger, R., Härtig, C., Laue, G., & Schmitt-Jansen, M. (2008)** A metabolomics approach to assessing phytotoxic effects on the green alga *Scenedesmus vacuolatus*. *Metabolomics*, 5(1), 59.
- Köhler, H.-R., & Triebkorn, R. (2013)** Wildlife ecotoxicology of pesticides: can we track effects to the population level and beyond? *Science*, 341(6147), 759-765.
- Konschak, M., Zubrod, J. P., Duque Acosta, T. S., Bouchez, A., Kroll, A., Feckler, A., Röder, N., Baudy, P., Schulz, R., & Bundschuh, M. (2021)** Herbicide-Induced Shifts in the Periphyton Community Composition Indirectly Affect Feeding Activity and Physiology of the Gastropod Grazer *Physella acuta*. *Environmental Science & Technology*, 55(21), 14699-14709.
- Kopka, J., Schauer, N., Krueger, S., Birkemeyer, C., Usadel, B., Bergmüller, E., Dörmann, P., Weckwerth, W., Gibon, Y., & Stitt, M. (2005)** GMD@ CSB. DB: the Golm metabolome database. *Bioinformatics*, 21(8), 1635-1638.
- Kortenkamp, A., Faust, M., Backhaus, T., Altenburger, R., Scholze, M., Müller, C., Ermler, S., Posthuma, L., & Brack, W. (2019)** Mixture risks threaten water quality: the European Collaborative Project SOLUTIONS recommends changes to the WFD and better coordination across all pieces of European chemicals legislation to improve protection from exposure of the aquatic environment to multiple pollutants. *Environmental Sciences Europe*, 31(1), 69.
- Krause, S., Le Roux, X., Niklaus, P. A., Van Bodegom, P. M., Lennon, J. T., Bertilsson, S., Grossart, H.-P., Philippot, L., & Bodelier, P. L. (2014)** Trait-based approaches for understanding microbial biodiversity and ecosystem functioning. *Frontiers in Microbiology*, 5, 251.
- Kreyling, J., Schweiger, A. H., Bahn, M., Ineson, P., Migliavacca, M., Morel-Journel, T., Christiansen, J. R., Schtickzelle, N., & Larsen, K. S. (2018)** To replicate, or not to replicate—that is the question: how to tackle nonlinear responses in ecological experiments. *Ecology Letters*, 21(11), 1629-1638.
- Krieger-Liszkay, A., & Rutherford, A. W. (1998)** Influence of herbicide binding on the redox potential of the quinone acceptor in photosystem II: relevance to photodamage and phytotoxicity. *Biochemistry*, 37(50), 17339-17344.
- Kültz, D. (2005)** Molecular and evolutionary basis of the cellular stress response. *Annu. Rev. Physiol.*, 67, 225-257.

- Lambert, A.-S., Morin, S., Artigas, J., Volat, B., Coquery, M., Neyra, M., & Pesce, S. (2012)** Structural and functional recovery of microbial biofilms after a decrease in copper exposure: influence of the presence of pristine communities. *Aquatic Toxicology*, 109, 118-126.
- Lan, J., Gou, N., Rahman, S. M., Gao, C., He, M., & Gu, A. Z. (2016)** A Quantitative Toxicogenomics Assay for High-throughput and Mechanistic Genotoxicity Assessment and Screening of Environmental Pollutants. *Environmental Science & Technology*, 50(6), 3202-3214.
- Larras, F., Billoir, E., Baillard, V., Siberchicot, A., Scholz, S., Wubet, T., Tarkka, M., Schmitt-Jansen, M., & Delignette-Muller, M.-L. (2018)** DRomics: a Turnkey Tool to support the use of the dose–response framework for omics data in ecological risk assessment. *Environmental Science & Technology*, 52(24), 14461-14468.
- Larras, F., Billoir, E., Scholz, S., Tarkka, M., Wubet, T., Delignette-Muller, M.-L., & Schmitt-Jansen, M. (2020)** A multi-omics concentration-response framework uncovers novel understanding of triclosan effects in the chlorophyte *Scenedesmus vacuolatus*. *Journal of Hazardous Materials*, 397, 122727.
- Latowski, D., Kuczyńska, P., & Strzałka, K. (2011)** Xanthophyll cycle – a mechanism protecting plants against oxidative stress. *Redox Report*, 16(2), 78-90.
- Lavergne, J., & Briantais, J.-M. (1996)** Photosystem II Heterogeneity. In D. R. Ort, C. F. Yocum, & I. F. Heichel (Eds.), *Oxygenic Photosynthesis: The Light Reactions* (pp. 265-287). Springer Netherlands.
- Llewellyn, C. A., Sommer, U., Dupont, C. L., Allen, A. E., & Viant, M. R. (2015)** Using community metabolomics as a new approach to discriminate marine microbial particulate organic matter in the western English Channel. *Progress in Oceanography*, 137, 421-433.
- Lobenhofer, E. K., Cui, X., Bennett, L., Cable, P. L., Merrick, B. A., Churchill, G. A., & Afshari, C. A. (2004)** Exploration of low-dose estrogen effects: identification of No Observed Transcriptional Effect Level (NOTEL). *Toxicologic pathology*, 32(4), 482-492.
- Locey, K. J., & Lennon, J. T. (2016)** Scaling laws predict global microbial diversity. *Proceedings of the National Academy of Sciences*, 113(21), 5970-5975.
- Louca, S., Jacques, S. M. S., Pires, A. P. F., Leal, J. S., Srivastava, D. S., Parfrey, L. W., Farjalla, V. F., & Doebeli, M. (2016)** High taxonomic variability despite stable functional structure across microbial communities. *Nature Ecology & Evolution*, 1(1), 0015.
- Louca, S., Polz, M. F., Mazel, F., Albright, M. B. N., Huber, J. A., O'Connor, M. I., Ackermann, M., Hahn, A. S., Srivastava, D. S., Crowe, S. A., Doebeli, M., & Parfrey, L. W. (2018)** Function and functional redundancy in microbial systems. *Nature Ecology & Evolution*, 2(6), 936-943.
- Love, M. I., Huber, W., & Anders, S. (2014)** Moderated estimation of fold change and dispersion for RNA-seq data with DESeq2. *Genome biology*, 15(12), 1-21.
- Lu, H., Yu, Q., Han, H., Owen, M. J., & Powles, S. B. (2019)** A novel psbA mutation (Phe274–Val) confers resistance to PSII herbicides in wild radish (*Raphanus raphanistrum*). *Pest Management Science*, 75(1), 144-151.
- Magnusson, M., Heimann, K., & Negri, A. P. (2008)** Comparative effects of herbicides on photosynthesis and growth of tropical estuarine microalgae. *Marine Pollution Bulletin*, 56(9), 1545-1552.
- Mahamoud Ahmed, A., Lyautey, E., Bonnineau, C., Dabrin, A., & Pesce, S. (2018)** Environmental Concentrations of Copper, Alone or in Mixture With Arsenic, Can

- Impact River Sediment Microbial Community Structure and Functions. *Frontiers in Microbiology*, 9.
- Malaj, E., Ohe, P. C. v. d., Grote, M., Kühne, R., Mondy, C. P., Usseglio-Polatera, P., Brack, W., & Schäfer, R. B. (2014)** Organic chemicals jeopardize the health of freshwater ecosystems on the continental scale. *Proceedings of the National Academy of Sciences*, 111(26), 9549-9554.
- Maxwell, K., & Johnson, G. N. (2000)** Chlorophyll fluorescence—a practical guide. *Journal of Experimental Botany*, 51(345), 659-668.
- McCann, K. S. (2000).** The diversity–stability debate. *Nature*, 405(6783), 228-233.
- McClellan, K., Altenburger, R., & Schmitt-Jansen, M. (2008)** Pollution-induced community tolerance as a measure of species interaction in toxicity assessment. *Journal of Applied Ecology*, 45(5), 1514-1522.
- McMahon, T. A., Halstead, N. T., Johnson, S., Raffel, T. R., Romansic, J. M., Crumrine, P. W., & Rohr, J. R. (2012)** Fungicide-induced declines of freshwater biodiversity modify ecosystem functions and services. *Ecology Letters*, 15(7), 714-722.
- Medina, M. H., Correa, J. A., & Barata, C. (2007)** Micro-evolution due to pollution: possible consequences for ecosystem responses to toxic stress. *Chemosphere*, 67(11), 2105-2114.
- Mengistu, L. W., Mueller-Warrant, G. W., Liston, A., & Barker, R. E. (2000)** psbA mutation (valine219 to isoleucine) in *Poa annua* resistant to metribuzin and diuron. *Pest Management Science: formerly Pesticide Science*, 56(3), 209-217.
- Meyer, J. N., & Di Giulio, R. T. (2003)** Heritable adaptation and fitness costs in killifish (*Fundulus heteroclitus*) inhabiting a polluted estuary. *Ecological Applications*, 13(2), 490-503.
- Misra, B. B., Langefeld, C., Olivier, M., & Cox, L. A. (2019)** Integrated omics: tools, advances and future approaches. *Journal of molecular endocrinology*, 62(1), R21-R45.
- Molander, S., & Blanck, H. (1992)** Detection of pollution-induced community tolerance (PICT) in marine periphyton communities established under diuron exposure. *Aquatic Toxicology*, 22(2), 129-143.
- Morin, S., Chaumet, B., & Mazzella, N. (2018)** A time-dose response model to assess diuron-induced photosynthesis inhibition in freshwater biofilms. *Frontiers in Environmental Science*, 131.
- Moriya, Y., Itoh, M., Okuda, S., Yoshizawa, A. C., & Kanehisa, M. (2007)** KAAS: an automatic genome annotation and pathway reconstruction server. *Nucleic Acids Research*, 35, W182-W185.
- Mouneyrac, C., Leung, P. T., & Leung, K. M. (2011)** Cost of tolerance. In *Tolerance to environmental contaminants* (pp. 265-298). CRC Press.
- Muller, M. L. D., Billoir, E., & Larras, F. (2021)** Overview of the DRomics package.
- Mulligan, B., Schultes, N., Chen, L., & Bogorad, L. (1984)** Nucleotide sequence of a multiple-copy gene for the B protein of photosystem II of a cyanobacterium. *Proceedings of the National Academy of Sciences*, 81(9), 2693-2697.
- Naeem, S. (1998)** Species Redundancy and Ecosystem Reliability. *Conservation Biology*, 12(1), 39-45.
- Nakamura, Y., Yamamoto, N., Kino, Y., Yamamoto, N., Kamei, S., Mori, H., Kurokawa, K., & Nakashima, N. (2016)** Establishment of a multi-species biofilm model and metatranscriptomic analysis of biofilm and planktonic cell communities. *Applied microbiology and biotechnology*, 100(16), 7263-7279.
- Nestler, H., Groh, K. J., Schönenberger, R., Eggen, R. I., & Suter, M. J.-F. (2012)** Linking proteome responses with physiological and biochemical effects in

- herbicide-exposed *Chlamydomonas reinhardtii*. *Journal of proteomics*, 75(17), 5370-5385.
- Nishiyama, Y., Allakhverdiev, S. I., & Murata, N. (2006)** A new paradigm for the action of reactive oxygen species in the photoinhibition of photosystem II. *Biochimica et Biophysica Acta (BBA)-Bioenergetics*, 1757(7), 742-749.
- Oaks, J. L., Gilbert, M., Virani, M. Z., Watson, R. T., Meteyer, C. U., Rideout, B. A., Shivaprasad, H. L., Ahmed, S., Iqbal Chaudhry, M. J., Arshad, M., Mahmood, S., Ali, A., & Ahmed Khan, A. (2004)** Diclofenac residues as the cause of vulture population decline in Pakistan. *Nature*, 427(6975), 630-633.
- Oksanen, J., Blanchet, F. G., Kindt, R., Legendre, P., Minchin, P. R., O'hara, R., Simpson, G. L., Solymos, P., Stevens, M. H. H., & Wagner, H. (2013)** Package 'vegan'. *Community ecology package, version*, 2(9), 1-295.
- Osborn, H. L., & Hook, S. E. (2013)** Using transcriptomic profiles in the diatom *Phaeodactylum tricornutum* to identify and prioritize stressors. *Aquatic Toxicology*, 138-139, 12-25.
- Parsons, H. T., Yasmin, T., & Fry, S. C. (2011)** Alternative pathways of dehydroascorbic acid degradation in vitro and in plant cell cultures: novel insights into vitamin C catabolism. *Biochemical Journal*, 440(3), 375-385.
- Parte, A. C., Carbasse, J. S., Meier-Kolthoff, J. P., Reimer, L. C., & Göker, M. (2020)** List of Prokaryotic names with Standing in Nomenclature (LPSN) moves to the DSMZ. *International Journal of Systematic and Evolutionary Microbiology*, 70(11), 5607.
- Perez-Iratxeta, C., Palidwor, G., & Andrade-Navarro, M. A. (2007)** Towards completion of the Earth's proteome. *EMBO reports*, 8(12), 1135-1141.
- Persson, L., Carney Almroth, B. M., Collins, C. D., Cornell, S., de Wit, C. A., Diamond, M. L., Fantke, P., Hassellöv, M., MacLeod, M., Ryberg, M. W., Søgaard Jørgensen, P., Villarrubia-Gómez, P., Wang, Z., & Hauschild, M. Z. (2022)** Outside the Safe Operating Space of the Planetary Boundary for Novel Entities. *Environmental Science & Technology*, 56(3), 1510-1521.
- Pesce, S., Bérard, A., Coutellec, M.-A., Langlais-Hesse, A., Hedde, M., Larras, F., Leenhardt, S., Mongruel, R., Munaron, D., & Sabater, S. (2022)** Linking the effects of plant protection products on biodiversity and ecological processes to potential impairment of ecosystem functions and services—A multidisciplinary conceptual framework.
- Pesce, S., Fajon, C., Bardot, C., Bonnemoy, F., Portelli, C., & Bohatier, J. (2006)** Effects of the phenylurea herbicide diuron on natural riverine microbial communities in an experimental study. *Aquatic Toxicology*, 78(4), 303-314.
- Pesce, S., Ghiglione, J.-F., Topp, E., & Martin-Laurent, F. (2020)** Microbial Ecotoxicology. *Frontiers in Microbiology*, 1342.
- Pesce, S., Margoum, C., & Montuelle, B. (2010)** In situ relationships between spatio-temporal variations in diuron concentrations and phototrophic biofilm tolerance in a contaminated river. *Water research*, 44(6), 1941-1949.
- Peters, K., Bundschuh, M., & Schäfer, R. B. (2013)** Review on the effects of toxicants on freshwater ecosystem functions. *Environmental Pollution*, 180, 324-329.
- Pfannschmidt, T., Nilsson, A., & Allen, J. F. (1999)** Photosynthetic control of chloroplast gene expression. *Nature*, 397(6720), 625-628.
- Polst, B. H., Anlanger, C., Risse-Buhl, U., Larras, F., Hein, T., Weitere, M., & Schmitt-Jansen, M. (2018)** Hydrodynamics Alter the Tolerance of Autotrophic Biofilm Communities Toward Herbicides. *Frontiers in Microbiology*, 9.
- Porsbring, T., Arrhenius, Å., Backhaus, T., Kuylénstierna, M., Scholze, M., & Blanck, H. (2007)** The SWIFT periphyton test for high-capacity assessments of

- toxicant effects on microalgal community development. *Journal of experimental marine biology and ecology*, 349(2), 299-312.
- Porter, R. D., & Wiemeyer, S. N. (1969)** Dieldrin and DDT: Effects on Sparrow Hawk Eggshells and Reproduction. *Science*, 165(3889), 199-200.
- Proia, L., Morin, S., Peipoch, M., Romaní, A., & Sabater, S. (2011)** Resistance and recovery of river biofilms receiving short pulses of Triclosan and Diuron. *Science of the total environment*, 409(17), 3129-3137.
- Pu, Y., Pan, J., Yao, Y., Ngan, W. Y., Yang, Y., Li, M., & Habimana, O. (2021)** Ecotoxicological effects of erythromycin on a multispecies biofilm model, revealed by metagenomic and metabolomic approaches. *Environmental Pollution*, 276, 116737.
- Purdum, C. E., Hardiman, P. A., Bye, V. V. J., Eno, N. C., Tyler, C. R., & Sumpter, J. P. (1994)** Estrogenic Effects of Effluents from Sewage Treatment Works. *Chemistry and Ecology*, 8(4), 275-285.
- Quackenbush, J. (2002)** Microarray data normalization and transformation. *Nature genetics*, 32(4), 496-501.
- Ricart, M., Barceló, D., Geiszinger, A., Guasch, H., de Alda, M. L., Romaní, A. M., Vidal, G., Villagrassa, M., & Sabater, S. (2009)** Effects of low concentrations of the phenylurea herbicide diuron on biofilm algae and bacteria. *Chemosphere*, 76(10), 1392-1401.
- Riedl, J., Schreiber, R., Otto, M., Heilmeyer, H., Altenburger, R., & Schmitt-Jansen, M. (2015)** Metabolic Effect Level Index Links Multivariate Metabolic Fingerprints to Ecotoxicological Effect Assessment. *Environmental Science & Technology*, 49(13), 8096-8104.
- Rockström, J., Steffen, W., Noone, K., Persson, Å., Chapin, F. S., Lambin, E. F., Lenton, T. M., Scheffer, M., Folke, C., Schellnhuber, H. J., Nykvist, B., de Wit, C. A., Hughes, T., van der Leeuw, S., Rodhe, H., Sörlin, S., Snyder, P. K., Costanza, R., Svedin, U., . . . Foley, J. A. (2009)** A safe operating space for humanity. *Nature*, 461(7263), 472-475.
- Rohloff, J. (2015)** Analysis of phenolic and cyclic compounds in plants using derivatization techniques in combination with GC-MS-based metabolite profiling. *Molecules*, 20(2), 3431-3462.
- Romero, F., Acuña, V., Sabater, S., & Schaffner, D. W. (2020)** Multiple Stressors Determine Community Structure and Estimated Function of River Biofilm Bacteria. *Applied and Environmental Microbiology*, 86(12), e00291-00220.
- Rotter, S., Sans-Piché, F., Streck, G., Altenburger, R., & Schmitt-Jansen, M. (2011)** Active bio-monitoring of contamination in aquatic systems—An in situ translocation experiment applying the PICT concept. *Aquatic Toxicology*, 101(1), 228-236.
- Rutherford, A. W., & Krieger-Liszkay, A. (2001)** Herbicide-induced oxidative stress in photosystem II. *Trends in biochemical sciences*, 26(11), 648-653.
- Sabater, S., Guasch, H., Ricart, M., Romaní, A., Vidal, G., Klünder, C., & Schmitt-Jansen, M. (2007)** Monitoring the effect of chemicals on biological communities. The biofilm as an interface. *Analytical and bioanalytical chemistry*, 387(4), 1425-1434.
- Sandom, C., Faurby, S., Sandel, B., & Svenning, J.-C. (2014)** Global late Quaternary megafauna extinctions linked to humans, not climate change. *Proceedings of the Royal Society B: Biological Sciences*, 281(1787), 20133254.
- Sanli, K., Bengtsson-Palme, J., Nilsson, R. H., Kristiansson, E., Alm Rosenblad, M., Blanck, H., & Eriksson, K. M. (2015)** Metagenomic sequencing of marine

- periphyton: taxonomic and functional insights into biofilm communities. *Frontiers in Microbiology*, 6, 1192.
- Sans-Piché, F., Kluender, C., Altenburger, R., & Schmitt-Jansen, M. (2010)** Anchoring metabolic changes to phenotypic effects in the chlorophyte *Scenedesmus vacuolatus* under chemical exposure. *Marine environmental research*, 69, S28-S30.
- Schlüter, L., Møhlenberg, F., Havskum, H., & Larsen, S. (2000)** The use of phytoplankton pigments for identifying and quantifying phytoplankton groups in coastal areas: testing the influence of light and nutrients on pigment/chlorophyll a ratios. *Marine Ecology progress series*, 192, 49-63.
- Schmitt-Jansen, M., & Altenburger, R. (2005)** Predicting and observing responses of algal communities to photosystem ii-herbicide exposure using pollution-induced community tolerance and species-sensitivity distributions. *Environmental Toxicology and Chemistry*, 24(2), 304-312.
- Schmitt-Jansen, M., Bley, L. M., Krumbiegel, M. L., & Rotter, S. (2016)** Induced community tolerance of periphyton towards combined salt and toxic stress. *Freshwater Biology*, 61(12), 2152-2161.
- Schreiber, U. (2004)** Pulse-Amplitude-Modulation (PAM) Fluorometry and Saturation Pulse Method: An Overview. In G. C. Papageorgiou & Govindjee (Eds.), *Chlorophyll a Fluorescence: A Signature of Photosynthesis* (pp. 279-319). Springer Netherlands.
- Schreiber, U., Quayle, P., Schmidt, S., Escher, B. I., & Mueller, J. F. (2007)** Methodology and evaluation of a highly sensitive algae toxicity test based on multiwell chlorophyll fluorescence imaging. *Biosensors and Bioelectronics*, 22(11), 2554-2563.
- Schreiber, U., Schliwa, U., & Bilger, W. (1986)** Continuous recording of photochemical and non-photochemical chlorophyll fluorescence quenching with a new type of modulation fluorometer. *Photosynthesis Research*, 10(1), 51-62.
- Serra-Compte, A., Corcoll, N., Huerta, B., Rodríguez-Mozaz, S., Sabater, S., Barceló, D., & Álvarez-Muñoz, D. (2018)** Fluvial biofilms exposed to desiccation and pharmaceutical pollution: New insights using metabolomics. *Science of the total environment*, 618, 1382-1388.
- Shakya, M., Lo, C.-C., & Chain, P. S. (2019)** Advances and challenges in metatranscriptomic analysis. *Frontiers in genetics*, 904.
- Sjollema, S. B., van Beusekom, S. A., van der Geest, H. G., Booij, P., de Zwart, D., Vethaak, A. D., & Admiraal, W. (2014)** Laboratory algal bioassays using PAM fluorometry: Effects of test conditions on the determination of herbicide and field sample toxicity. *Environmental Toxicology and Chemistry*, 33(5), 1017-1022.
- Smetanová, S., Riedl, J., Zitzkat, D., Altenburger, R., & Busch, W. (2015)** High-throughput concentration–response analysis for omics datasets. *Environmental Toxicology and Chemistry*, 34(9), 2167-2180.
- Smirnoff, N., & Pallanca, J. E. (1996)** Ascorbate metabolism in relation to oxidative stress. *Biochemical Society Transactions*, 24(2), 472-478.
- Smuda, M., & Glomb, M. A. (2013)** Maillard degradation pathways of vitamin C. *Angewandte Chemie International Edition*, 52(18), 4887-4891.
- Southerland, H. A., & Lewitus, A. J. (2004)** Physiological responses of estuarine phytoplankton to ultraviolet light-induced fluoranthene toxicity. *Journal of experimental marine biology and ecology*, 298(2), 303-322.
- Steffen, W., Richardson, K., Rockström, J., Cornell, S. E., Fetzer, I., Bennett, E. M., Biggs, R., Carpenter, S. R., Vries, W. d., Wit, C. A. d., Folke, C., Gerten,**

- D., Heinke, J., Mace, G. M., Persson, L. M., Ramanathan, V., Reyers, B., & Sörlin, S. (2015) Planetary boundaries: Guiding human development on a changing planet. *Science*, 347(6223), 1259855.
- Stitt, M., & Gibon, Y. (2014) Why measure enzyme activities in the era of systems biology? *Trends in Plant Science*, 19(4), 256-265.
- Störmer, R., Wichels, A., & Gerdts, G. (2013) Geo-Chip analysis reveals reduced functional diversity of the bacterial community at a dumping site for dredged Elbe sediment. *Marine Pollution Bulletin*, 77(1), 113-122.
- Strzepek, R., Nunn, B., Bach, L., Berges, J., Young, E., & Boyd, P. (2021) The ongoing need for rates: can physiology and omics come together to co-design the measurements needed to understand complex ocean biogeochemistry? *Journal of Plankton Research*, 22.
- Taylor, M., & Feyereisen, R. (1996) Molecular biology and evolution of resistance of toxicants. *Molecular Biology and Evolution*, 13(6), 719-734.
- Thomas, R. S., Allen, B. C., Nong, A., Yang, L., Bermudez, E., Clewell, H. J., III, & Andersen, M. E. (2007) A Method to Integrate Benchmark Dose Estimates with Genomic Data to Assess the Functional Effects of Chemical Exposure. *Toxicological Sciences*, 98(1), 240-248.
- Tian, Z., Zhao, H., Peter, K. T., Gonzalez, M., Wetzel, J., Wu, C., Hu, X., Prat, J., Mudrock, E., Hettinger, R., Cortina, A. E., Biswas, R. G., Kock, F. V. C., Soong, R., Jenne, A., Du, B., Hou, F., He, H., Lundeen, R., . . . Kolodziej, E. P. (2021) A ubiquitous tire rubber-derived chemical induces acute mortality in coho salmon. *Science*, 371(6525), 185-189.
- Tlili, A., Berard, A., Blanck, H., Bouchez, A., Cássio, F., Eriksson, K. M., Morin, S., Montuelle, B., Navarro, E., & Pascoal, C. (2016) Pollution-induced community tolerance (PICT): towards an ecologically relevant risk assessment of chemicals in aquatic systems. *Freshwater Biology*, 61(12), 2141-2151.
- Tlili, A., Bérard, A., Roulier, J.-L., Volat, B., & Montuelle, B. (2010) PO43-dependence of the tolerance of autotrophic and heterotrophic biofilm communities to copper and diuron. *Aquatic Toxicology*, 98(2), 165-177.
- Tlili, A., Corcoll, N., Arrhenius, Å., Backhaus, T., Hollender, J., Creusot, N., Wagner, B., & Behra, R. (2020) Tolerance patterns in stream biofilms link complex chemical pollution to ecological impacts. *Environmental Science & Technology*, 54(17), 10745-10753.
- Tlili, A., Dorigo, U., Montuelle, B., Margoum, C., Carluer, N., Gouy, V., Bouchez, A., & Bérard, A. (2008) Responses of chronically contaminated biofilms to short pulses of diuron: an experimental study simulating flooding events in a small river. *Aquatic Toxicology*, 87(4), 252-263.
- Tlili, A., Marechal, M., Montuelle, B., Volat, B., Dorigo, U., & Berard, A. (2011) Use of the MicroResp™ method to assess pollution-induced community tolerance to metals for lotic biofilms. *Environmental Pollution*, 159(1), 18-24.
- Tsugawa, H., Cajka, T., Kind, T., Ma, Y., Higgins, B., Ikeda, K., Kanazawa, M., VanderGheynst, J., Fiehn, O., & Arita, M. (2015) MS-DIAL: data-independent MS/MS deconvolution for comprehensive metabolome analysis. *Nature methods*, 12(6), 523-526.
- van Straalen, N. M., & Timmermans, M. J. T. N. (2002) Genetic Variation in Toxicant-Stressed Populations: An Evaluation of the “Genetic Erosion” Hypothesis. *Human and Ecological Risk Assessment: An International Journal*, 8(5), 983-1002.

- Verslues, P. E., & Sharma, S. (2010)** Proline metabolism and its implications for plant-environment interaction. *The Arabidopsis Book/American Society of Plant Biologists*, 8.
- Viant, M. R. (2007)** Metabolomics of aquatic organisms: the new 'omics' on the block. *Marine Ecology progress series*, 332, 301-306.
- Villeneuve, A., Larroudé, S., & Humbert, J.-F. (2011)** Herbicide contamination of freshwater ecosystems: impact on microbial communities. *Pesticides-Formulations, effects, fate*, 285.
- Vrba, J. M., & Curtis, S. E. (1990)** Characterization of a four-member psbA gene family from the cyanobacterium *Anabaena* PCC 7120. *Plant Molecular Biology*, 14(1), 81-92.
- Walter, H., Consolaro, F., Gramatica, P., Scholze, M., & Altenburger, R. (2002)** Mixture Toxicity of Priority Pollutants at No Observed Effect Concentrations (NOECs). *Ecotoxicology*, 11(5), 299-310.
- Wang, Z., Walker, G. W., Muir, D. C. G., & Nagatani-Yoshida, K. (2020)** Toward a Global Understanding of Chemical Pollution: A First Comprehensive Analysis of National and Regional Chemical Inventories. *Environmental Science & Technology*, 54(5), 2575-2584.
- Werner, J. (2022)** *Structural analysis of autotrophic 'plastisphere' communities from the 'Great Pacific Garbage Patch' by HPLC pigment analysis* [Master Thesis, Johannes Gutenberg-Universität, Mainz].
- White, R. A., Bottos, E. M., Chowdhury, T. R., Zucker, J. D., Brislawn, C. J., Nicora, C. D., Fansler, S. J., Glaesemann, K. R., Glass, K., Jansson, J. K., & Langille, M. (2016)** Molecule Long-Read Sequencing Facilitates Assembly and Genomic Binning from Complex Soil Metagenomes. *mSystems*, 1(3), e00045-00016.
- Winter, G., Todd, C. D., Trovato, M., Forlani, G., & Funck, D. (2015)** Physiological implications of arginine metabolism in plants [Review]. *Frontiers in Plant Science*, 6.
- Wishart, D. S., Guo, A., Oler, E., Wang, F., Anjum, A., Peters, H., Dizon, R., Sayeeda, Z., Tian, S., Lee, Brian L., Berjanskii, M., Mah, R., Yamamoto, M., Jovel, J., Torres-Calzada, C., Hiebert-Giesbrecht, M., Lui, Vicki W., Varshavi, D., Varshavi, D., . . . Gautam, V. (2021)** HMDB 5.0: the Human Metabolome Database for 2022. *Nucleic Acids Research*, 50(D1), D622-D631.
- Woese, C. R., & Fox, G. E. (1977)** Phylogenetic structure of the prokaryotic domain: The primary kingdoms. *Proceedings of the National Academy of Sciences*, 74(11), 5088-5090.
- Woitke, P., Martin, C.-D., Nicklisch, S., & Kohl, J.-G. (1994)** HPLC determination of lipophilic photosynthetic pigments in algal cultures and lake water samples using a non-endcapped C18-RP-column. *Fresenius' journal of analytical chemistry*, 348(11), 762-768.
- Wolf, D. I., & Vis, M. L. (2020)** Stream Algal Biofilm Community Diversity Along An Acid Mine Drainage Recovery Gradient Using Multimarker Metabarcoding. *Journal of Phycology*, 56(1), 11-22.
- Yachi, S., & Loreau, M. (1999)** Biodiversity and ecosystem productivity in a fluctuating environment: The insurance hypothesis. *Proceedings of the National Academy of Sciences*, 96(4), 1463-1468.
- Yang, L., Li, H., Zhang, Y., & Jiao, N. (2019)** Environmental risk assessment of triazine herbicides in the Bohai Sea and the Yellow Sea and their toxicity to phytoplankton at environmental concentrations. *Environment International*, 133, 105175.

- Yao, Y., Pan, J., Pu, Y., Kan, K., Li, M., & Habimana, O. (2022)** The response of a freshwater biofilm model to a sub-inhibitory concentration of erythromycin: A metatranscriptomic study. *Journal of Environmental Chemical Engineering*, 10(2), 107248.
- Yergeau, E., Sanschagrin, S., Waiser, M. J., Lawrence, J. R., & Greer, C. W. (2012)** Sub-inhibitory concentrations of different pharmaceutical products affect the meta-transcriptome of river biofilm communities cultivated in rotating annular reactors. *Environmental Microbiology Reports*, 4(3), 350-359.
- Young, R. G., Matthaei, C. D., & Townsend, C. R. (2008)** Organic matter breakdown and ecosystem metabolism: functional indicators for assessing river ecosystem health. *Journal of the North American Benthological Society*, 27(3), 605-625.

Thesis publications and manuscripts

Lips, S., Larras, F., & Schmitt-Jansen, M. (2022) Community metabolomics provides insights into mechanisms of pollution-induced community tolerance of periphyton. *Science of The Total Environment*, 824, 153777.

Larras, F., Lips, S., Veber, P., Schreiber, S., Billoir, E., Delignette-Muller, M. L., Schmitt-Jansen, M. (in prep.) Metatranscriptomics reveals stress adaptation processes in microbial communities differing in exposure history.